FACULTY OF SCIENCES

# A RECONSTRUCTION OF MIOCENE SEDIMENT WAVE DYNAMICS IN THE PORCUPINE SEABIGHT, OFFSHORE IRELAND

Kimberley Bossée
Student number: 01605961

Promotor: Prof. dr. David Van Rooij

Jury: Prof. dr. Maarten Van Daele, dr. Marta Ribó

Master's dissertation submitted in partial fulfilment of the requirements for the degree of master in geology

Academic year: 2020-2021

GHENT UNIVERSITY

KU LEUVEN

# 1 ACKNOWLEDGEMENTS

Foremost, I would like to start by thanking the whole Department of Geology and the University of Ghent for giving me 5 years full of knowledge, lovely excursions and fun times. I would like to express my sincere and deep gratitude for my promotor professor Van Rooij, not only for the opportunity of working on this subject, but also for guiding me through a long thesis year (filled with many online meetings). I want to thank you for your support and insights, which made this thesis far more interesting. You have taught me many great things throughout my thesis, and I am very grateful for that! (You were a true "Gandalf" 😉)

I also want to thank Alice Matossian for her guidance through the RadExPro and IHS Kingdom softwares. Obviously, also for your many help and support throughout this year (on campus and online), which was very much appreciated. You were always there when I needed you! At last, I want to thank you for reviewing my dissertation.

Additionally, I would like to thank everyone from the RCMG department. Special thanks to Lotte Verweirder, Stijn Albers and Katleen Wils for the many support and solutions to the occasional computer problem. My sincere thanks also goes to the people that were involved in the RV Belgica cruise 2019/16 for gathering the data I used. Without them this thesis dissertation could not have taken place. I would also like to thank professor De Batist for the quick approvals every time I wanted to be on campus in these corona times.

A special thanks goes out to Morgan Vervoort, Sharmaine Verhaert and Sarah Stammen! You were of great support throughout the 5 years of university. We had our laughs, some to many drinks, awesome evenings packed with so much joy, lovely diner dates, enjoyable lectures, fun breaks and much more… Although we have been limited to do those things over the last year due to corona, you all still made my year so memorable! Thanks to you I had the best university experience I could get, and I hope that you will stay in my life forever 😉! I would also like to thank my very good friend Nathan De Kerpel for all the support and always being there for me! I would like to thank many more people and could probably fill my whole thesis with thanking you all, but the easiest way to do this is to thank Geologica! Thanks to the Praesidium for organizing many great events throughout the year, although online… And thanks to all the alumni, honour members and members!

I cannot express enough thanks to my whole family (including my boyfriends' family) for all the support they gave me. A special thanks goes to my mom, dad, brother and mitsy (my cat) for being there for me during this though period, cooking for me and giving me some well deserved breaks (from working in the garden to movie nights).

And last, but very much not least, I would like to thank my boyfriend! Thank you for supporting me, loving me and encouraging me! I couldn't have finished this without you. Thank you for the awesome breaks, the lovely and supporting gifts, for the much needed 'study-budy', thank you for always being there for me! And thank you for reviewing my dissertation all these times to make sure as little as possible errors would be left. Lots of love for everything you have done for me!

Big thanks to you all!

# 2 TABLE OF CONTENTS

# 3 TABLE OF FIGURES

# 4 ABBREVIATION LIST

| | |
|---|---|
| BMP | Belgica Mound Province |
| CWC mounds | Cold-Water Coral mounds |
| CTD | Conductivity, Temperature and Depth |
| ENAW | Eastern North Atlantic Water |
| GEBCO | GEneral Bathymetric Chart of the Oceans |
| IRD | Ice Rafted Debris |
| LSW | Labrador Sea Water |
| mbsl | Meters Below Sea Level |
| MOW | Mediterranean Outflow Water |
| NAC | North Atlantic Current |
| NEADW | North East Atlantic Deep Water |
| nm | Nautical Mile (1 nm = 1.85 km) |
| NSW | Norwegian Sea Water |
| PSB | Porcupine SeaBight |
| SEC | Shelf Edge Current |
| SF | SeaFloor |
| TWT | Two-Way Travel time |

# 5 THE STORY OF MY RESEARCH

Unfortunately, I had to make my thesis during a worldwide Covid-19 pandemic. It impacted a lot of things and of course also my research. All began with choosing the topic for my dissertation, two subjects immediately stood out for me. One was the study of microplastics in deep-see sediment drifts offshore Ireland, but the samples could not be taken due to the corona measures. A second topic that piqued my interest was quite similar to my bachelor project. It was about the influence of internal waves on the formation of Miocene sediment waves in the Porcupine Seabight, offshore Ireland, which lead to this dissertation. I am glad to have chosen this subject because it was a real learning experience.

Already in the first semester, I started processing my data and studying many papers. Eventually, in February, the real work started with examining my data further and writing the first texts. I expanded my knowledge on interpreting seismic profiles, learned much more about sediment waves and gained some basic understanding of gridding and mapping. After some last stressful weeks, my dissertation was finally completed, although I personally think a thesis is never finished.

I really enjoyed working with sediment waves and exploring the many possibilities of their origin. Even though they were sometimes a real botheration. It was definitely not easy to work on Palaeo-sediment waves of which the hydrographic origin was not known. But I learned a lot in the process of this dissertation and feel like I have matured scientifically.

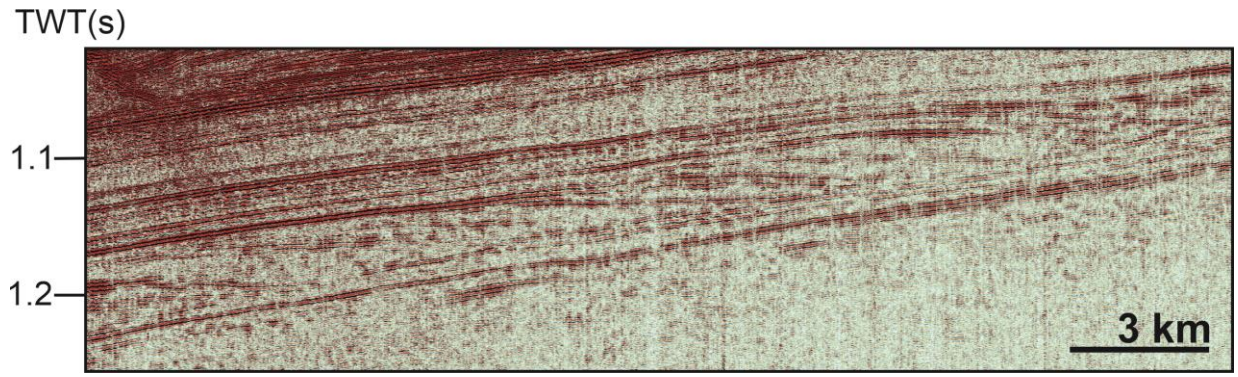


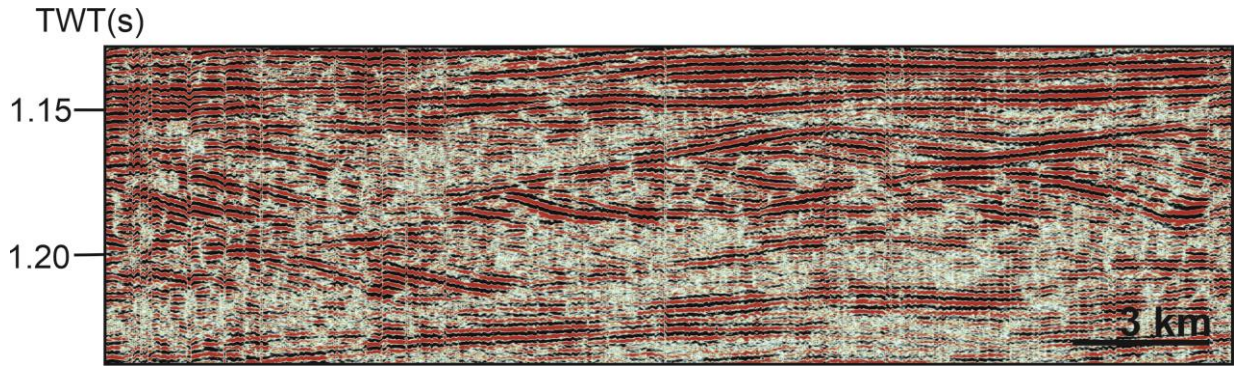

# 6 INTRODUCTION

Large-scale depositional bedforms, among which sediment waves, have been recognized both in passive and active continental margins (Symons et al., 2016; Ribó et al., 2018). They have been documented at various depths and settings among which the slopes of volcanic islands, submarine canyons and channels, continental shelves, continental slopes, continental rises and abyssal plains (Gonthier et al., 2002; Gong et al., 2012; Baldwin et al., 2017; Belde et al., 2017; Pope et al., 2018; Ribó et al., 2018). Their sedimentary structures can have a wide variety in lithology, morphology and dimensions (Ribó et al., 2018). They mostly, but not exclusively, form in fine-grained sediments such as silt and clay (Faugères et al., 2002a). The mechanisms behind these sediment waves have been discussed for a long time, because many sediment dynamic processes can lead to their formation (Karl et al., 1986; Wynn and Stow, 2002; Li et al., 2019). It is generally accepted that generating deep-water sediment waves involves flows at or close to the sea floor (Cartigny et al., 2011). However, there are four dynamic systems that are most prominent in generating deep-water sediment waves being: turbidity currents (Fig. 1A), gravity-controlled mass transport (Fig. 1B), internal wave dynamics (Fig. 1C) and contour currents(Fig. 1D; Li et al., 2019).

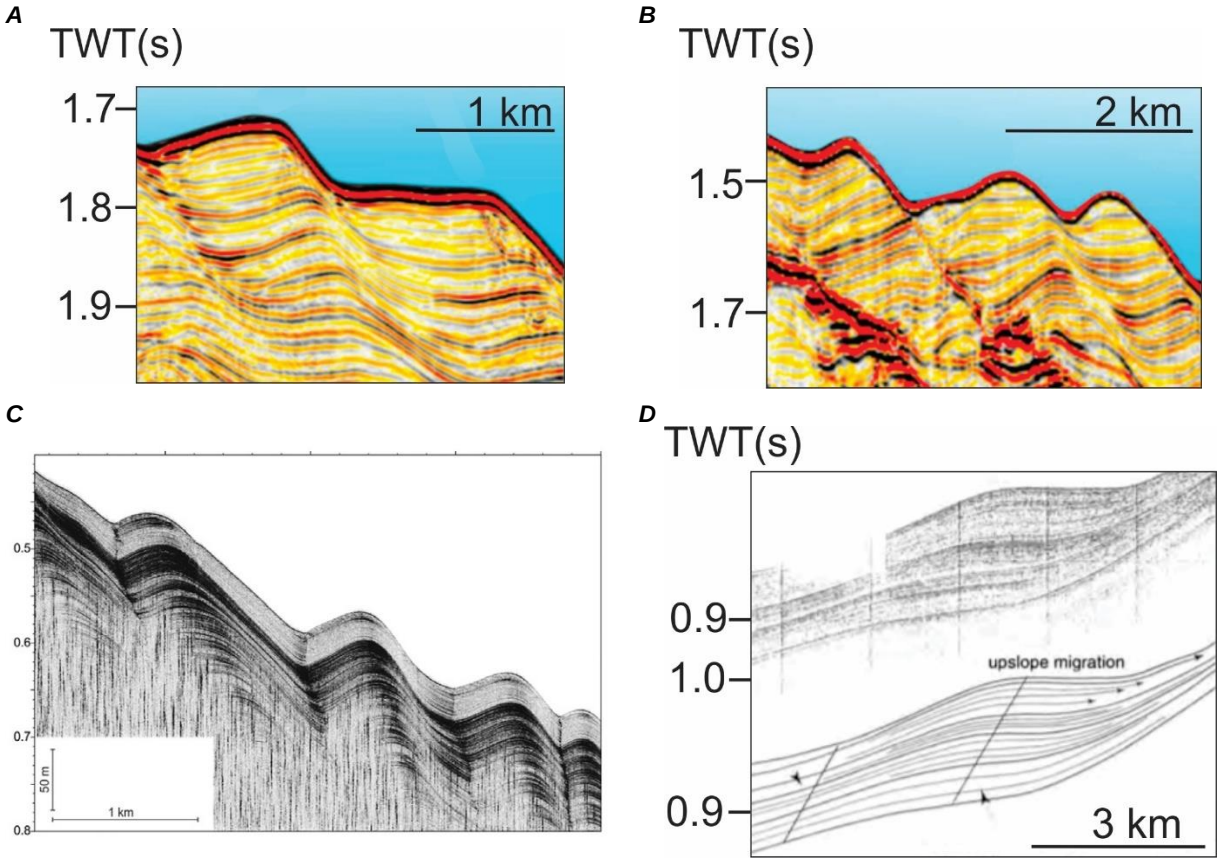


*Fig. 1: A composite figure of the seismic expression of the different wave dynamics. A) Sediment waves generated by turbidity currents in the canyon area of the northern South China Sea; modified after Li et al. (2019). B) Sediment waves generated by gravity-driven submarine creep in the canyon areas of the northern South China Sea; modified after Li et al. (2019). C) Sediment waves formed by the interaction of internal waves; modified after Ribó et al. (2016). D) An elongate drift deposit with a sigmoidal character on P67 in the study of the Corsica Channel by Roveri (2002).*

The sediment waves formed by turbidity currents frequently occur on the back side of levees, close to canyon and channel systems on the continental slope (Lee et al., 2002). These have been documented in many places as for example in the northern South China Sea (Gong et al., 2012), on the South Iberian Margin (Perez-Hernandez et al., 2014) and in the Monterey Fan channel (Normark et al., 1980). This dynamic system only occurs with a downslope flow, creating sediment waves whereof their crests align perpendicular to the slope (Wynn and Stow, 2002). In seismic profiles they commonly show as gently undulating and slightly climbing bedforms (Cartigny et al., 2011). Turbidity current formed sediment waves can have wavelengths up to 7 km and a wave hight up to 80 m in fine-grained sediments. In coarse grained sediments, the dimensions are smaller. Here, the wavelengths of the sediment waves can go up to 1 km and can have a wave height up to 10 m (Wynn and Stow, 2002). Sediment waves formed by turbidity currents can show a cyclic step, where the step refers to the slowly upstream migrating bedforms (Fig.2A). The downward step is formed due to the steeply dropping flow passing through a hydraulic jump. This process is extensively explained by Cartigny et al. (2011).

Sediment waves can also be formed due to gravity-driven mass transport such as submarine creep, sliding or slumping (Faugères et al., 2002a). Examples are slump structures in the Porcupine basin, offshore Ireland (Moore and Shannon, 1991), submarine creep on the northern South China Sea (Li et al., 2019) and sediment waves formed by cascading dense shelf waters in the Gulf of Roses (Ribó et al., 2018). However, these are not sediment waves in the strict definition due to their synsedimentary origin (Faugères et al., 2002a). These undulations are formed when higher up the slope extension or sliding occurs, which will cause a compression lower on the slope. In that way sediment accumulations and deformations are formed, aligning perpendicular to the slope. Gravity-driven formed sediment waves mostly occur on a moderate to steep continental slope, but can also occur on seamounts. The waves are characterized by the presence of extension and compression related elements (Fig. 2B). Examples of the first are detachment faults, rotated blocks, faults, etc. Examples of compression related elements are folds, faults, compressional edges, etc. (Faugères et al., 2002b).

The third type of hydrodynamic process, forming sediment waves, are internal waves. These waves exist at interfaces between water masses with a high contrast in density and temperature (Cullen and Ivanov, 2020). Examples are the interface of the Western Mediterranean Intermediate Waters and the Levantine Intermediate Waters influencing the Gulf of Valencia (Ribó et al., 2016a) and the interface of the Northern Pacific Intermediate and Deep Water manipulating the northern South China Sea (Li et al., 2019). They manifest as large vertical fluctuations within the water column and are associated with strong horizontal currents (Yuan et al., 2020). When the internal waves coincide with the tidal cyclicity, they are called internal tides. Whenever these internal waves or tides interact with the continental slope, sediment waves can form. However, this can only occur under a critical angle, where the slope of the path ray of the internal waves exceeds the slope of the seafloor (Rice et al., 1990). The breaking of these internal waves on the slope can generate local intense bottom currents which can transport and redeposit sediment (Fig. 2C) (Bogucki and Redekopp, 1999; Ribbe and Holloway, 2001; Reeder et al., 2011). The seafloor-fluid mixtures, created in this process, have a repeated upslope and downslope movement (Hotchkiss and Wunsch, 1982; Karl et al., 1986; Pomar et al., 2012). This can create sediment waves with their crests parallel to the isobaths (Ma et al., 2016).

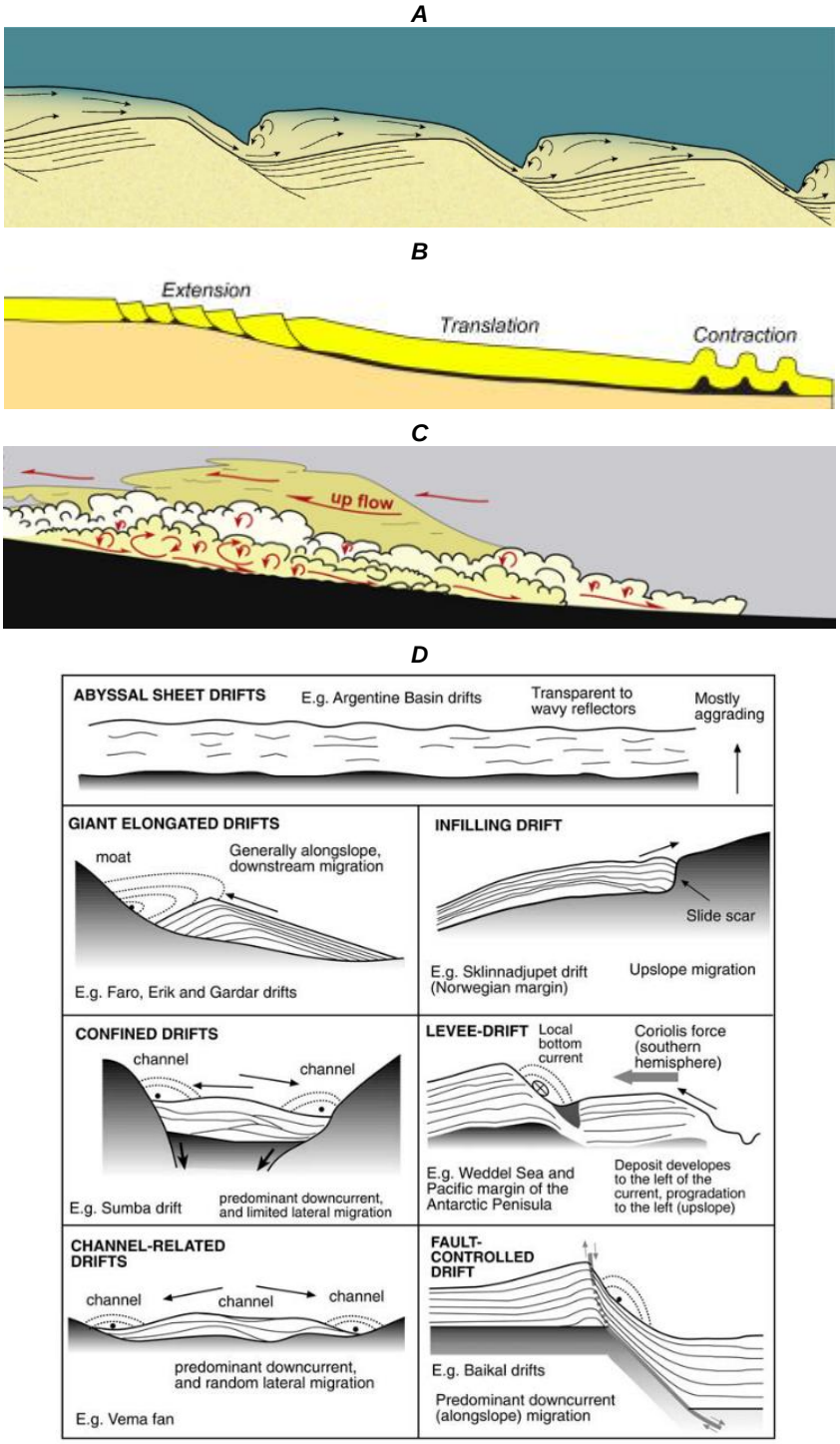


*Fig. 2: A composite figure illustrating the different wave dynamic processes. A) Sketch drawing of downslope asymmetrical cyclic steps beneath a turbidity current, showing the principal of a cyclic step; modified after Cartigny et al. (2011). B) Sketch of a gravity-driven failure dominated by gravity gliding, showing proximal extension, translation and distal contraction; modified after Rowan (2020). C) Sketch of internal waves breaking on a slope creating high turbulence sediment erosion, transportation and redeposition; modified after Pomar et al. (2012). D) A schematic summary of the different types of contourite drifts; after Rebesco and Stow (2001).*

Lastly, an important and complex dynamic for large-scale depositional bedforms are contour currents, which are still poorly understood (Rebesco et al., 2014). These currents move along-slope and can occur on many different depths on the continental slope. Examples are the Atlantic Mediterranean Water contributing to the Le Danois contourite depositional systems (Liu et al., 2020) and the Northern Pacific Deep Water influencing the South China Sea Slope (Gong et al., 2012). The aligned crests usually occur diagonally to the dominant flow direction. There are different contourite drift morphologies that exist with contour currents (Fig. 2D). The sediment waves can migrate upslope as well as downslope (Faugères et al., 2002a). Wave dimensions can vary between a wavelength of 10 km and a wave height of 150 m in fine grained sediments and a wavelength of about 200 m and only a few meters in height in course-grained sediments (Wynn and Stow, 2002).

When such large-scale depositional bedforms are studied, the depositional environment plays a key role in the determination of the dynamic type. Li et al. (2019) studied seafloor undulations at three different dynamic environments. These environmental settings helped the determination, together with the seismic interpretation and/or lithology. Also in the Porcupine Seabight (PSB), offshore Ireland, sediment drifts have been observed that were formed by the along-slope deep-water contour currents present (Stoker, 1997; McDonnell and Shannon, 2001; Stoker et al., 2001). It is also know that internal waves influence the PSB. A permanent pycnocline is observed and is associated with an enhanced energy supply due to the internal waves and tides (Dickson and McCave, 1986; White, 2007; Dullo et al., 2008; White and Dorschel, 2010; Mohn et al., 2014).

In the Porcupine Seabight, cold-water coral (CWC) mounds have been associated with contourite drifts (De Mol et al., 2002; Huvenne et al., 2002; Van Rooij et al., 2003, 2007). Several cold-water coral mound provinces have been discovered in the PSB (Fig. 3B), although the Belgica Mound Province (BMP) is the largest and is clearly influenced by stronger bottom currents (Henriet et al., 1998; De Mol et al., 2002; Huvenne et al., 2002; Van Rooij et al., 2003, 2007). Both the strong currents and the mounds influence each other (Hebbeln et al., 2016). The mounds create obstacles in the bottom topography, inducing stronger bottom currents. But the stronger bottom current also create a better environment for coral growth (Van Rooij et al., 2003). Van Rooij et al. (2003, 2007) inferred a connection with the settlement of some CWC mounds on sigmoidal units observed underneath those mounds (Fig. 4). These depositional bedforms were observed within an interpreted early-middle Miocene unit (Unit P1; Van Rooij et al., 2003; Fig. 4) on the eastern slope of the PSB (Ferdelman et al., 2006a; Van Rooij et al., 2003). However, understanding these depositional bedforms becomes difficult because of the lack of insight in their period of deposition. Even though knowledge about the Miocene Oceanography in the Porcupine Seabight (or Atlantic Ocean in general) is sparse, studying the depositional features is still important.

During the early Miocene, the major intermediate and deep-water masses in the Atlantic and Pacific aged in a northward direction. These water masses had a common source originating around Antarctica (Butzin et al., 2011). Only after the narrowing and/or closure of both the Central American and Tethys seaways, the NADW production intensified starting at around 4.6 Ma (Haug and Tiedemann, 1998). The deepening of the Greenland-Scotland Ridge between 18 Ma and 15.5 Ma, and from 12.5 Ma, could have initiated major deep-water flow from the Nordic Seas into the North Atlantic at 11.5 Ma (Wright and Miller, 1996; Wei and Peleo-Alampay, 1997).

On the eastern slope of the Porcupine several Miocene Isotopic Event stages (Mi-3a, Mi-3b and Mi-4) were recognized in the study of Quaijtaal et al. (2014), which reflect major changes in glaciation (Miller et al., 1991). They concluded that these were associated with the cooling of sea surface waters and a possible drop in relative sea-level. Furthermore, an additional input of nutrients was observed which could have been caused by upwelling due to the possible strengthening of the northerlies (Quaijtaal et al., 2014). At the Atlantic margin the overall Oligocene and Miocene sedimentation also seems to be characterized by along-slope transport caused by a combination of differential basin subsidence and regional sea level and palaeoclimate changes (Ferdelman et al., 2006a). Some of these oceanographic changes will have induced the sigmoidal bedforms and could have also led to the initiation of coral settlement as Van Rooij et al. (2003) suggest.

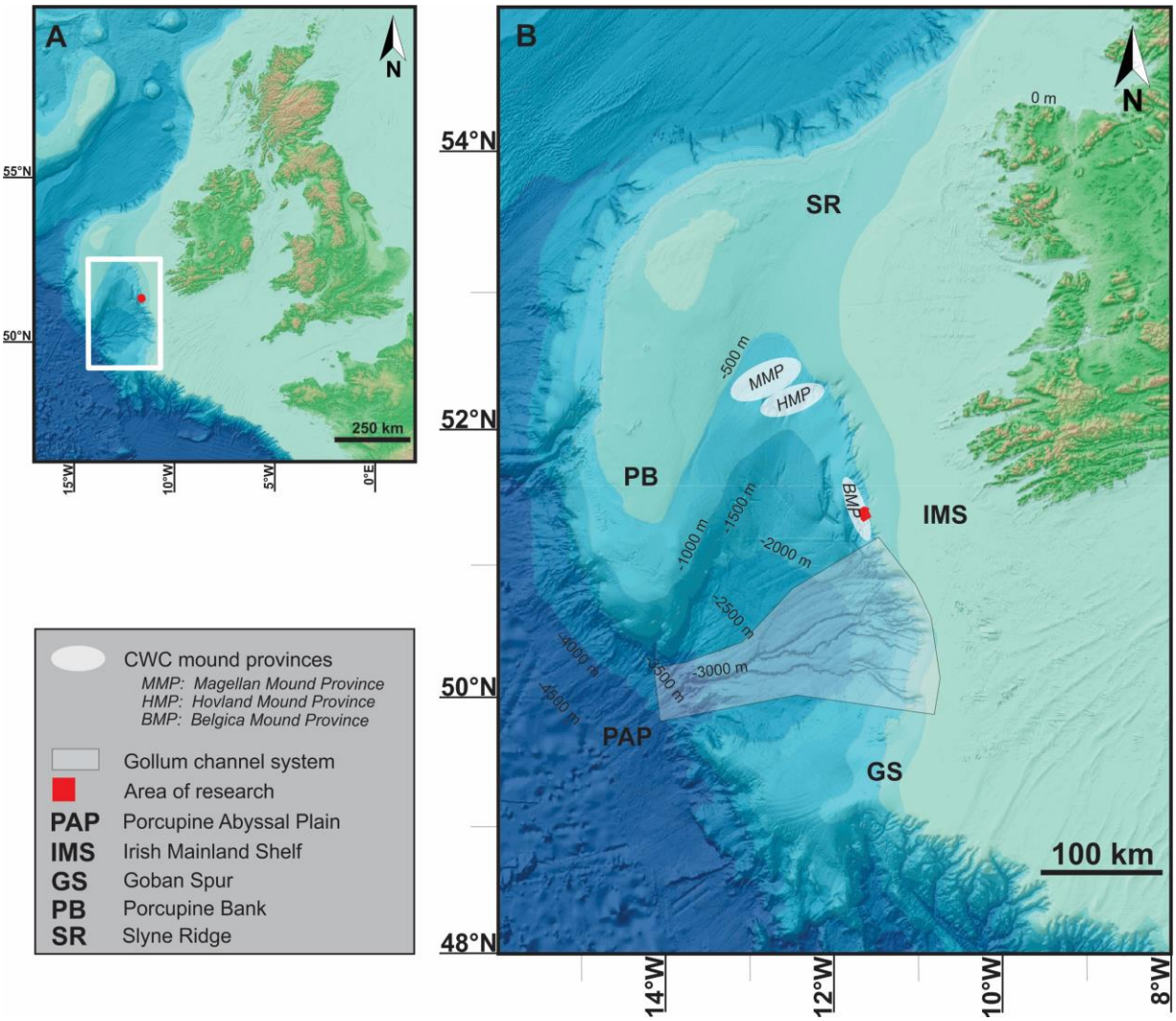


*Fig. 3: A) An overview map indicating the Porcupine Seabight with a white square, B) The Porcupine region with its main morphological structures indicated and contour lines every 500 m. The general bathymetric chart of the Oceans (GEBCO) was used as background image.*

These Miocene bedforms were observed on previous data taken from the BMP. New data may enlighten the dynamics behind the depositions better. This required data was obtained within the scope of the FWO DynaMOD project (*An oceanographic and sediment DYNamic MODelling study of MOunded contourite drifts*; Van Rooij, pers. comm.). This project (2019-2023) aims to study increasing bottom current intensities in the presence of CWC mounds (Van Rooij, pers. comm.). The seismic data within this project yields unique pseudo-3D insight in these sedimentary bedforms. The area of research overlaps with the BMP and is contained between water depths of around 500 m and 800 m (Fig. 3B).

Within this dissertation, there will be attempted to discover the depositional environment of Miocene bedforms only through the study of the spatial and seismic character. This due to the still underexplored Miocene oceanography, which is why the depositional environment cannot be known in advance. Examining these bedforms could lead to an interpretation on oceanographic changes, that might have initiated coral settlement and growth at some locations. Discovering these local oceanographic changes may help the understanding of major palaeoceanographic changes in the North Atlantic. The ultimate goal of this research would be to stimulate further research on palaeo-sedimentary bedforms around the world and, to uncover more information about still unknown local and global palaeoceanography.

Several objectives were established within the framework of this dissertation. First, there will be aimed to document the seismic facies, morphology and geometry to gain a better understanding in how these were formed. Sediment wave dynamics can be discovered by comparing the bedform characteristics with those in literature. A next step will be to discover the relation between the formation of the sedimentary bedforms and the cold-water coral mounds. Thirdly, there will be aimed to look at spatial and temporal changes within (different) sediment wave fields to get an idea about the local palaeoceanographic changes, and there will be assessed how these changes influenced the sediments within the research area. The last aim would be to connect local palaeoceanographic changes to more globally scaled changes within the (North) Atlantic. Eventually, to discover global tectonic or climate changes that induced the major oceanographic changes and broaden our understanding of the Miocene.

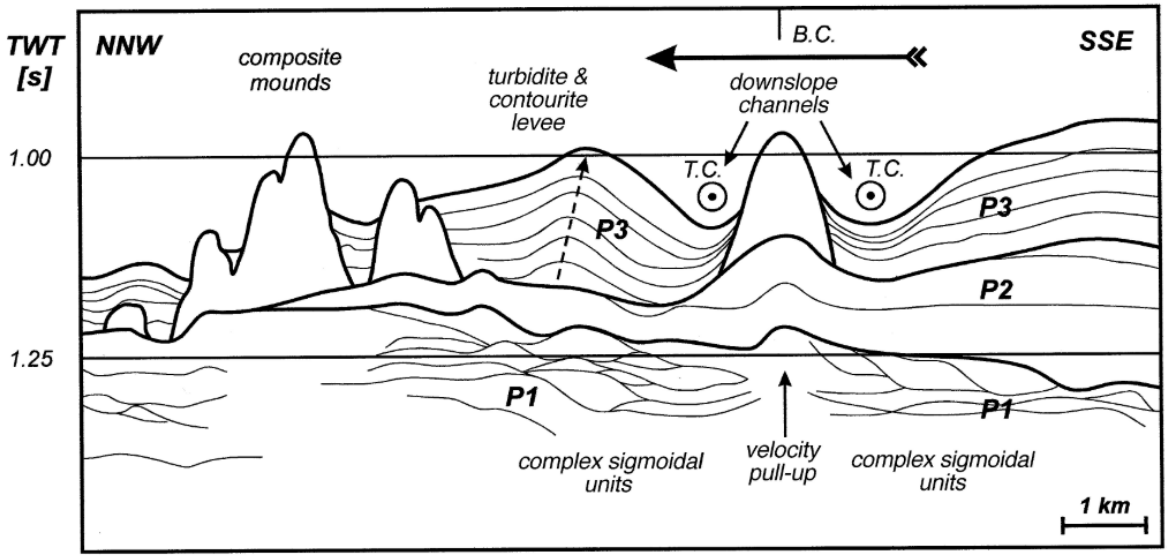


*Fig. 4: Line drawing of P980549 showing the depositional bedforms clearly in the interpreted early-Middle Miocene unit P1; modified after Van Rooij et al. (2003).*

# 7 ENVIRONMENTAL SETTING

## 7.1 Geomorphology

The Porcupine Seabight is a small, amphitheatre-shaped bight along the North Atlantic margin (Van Rooij et al., 2007; Fig. 3A). It is a 50 000 km² large basin, located southwest of the coast of Ireland, with an overall north-south trend (Fig. 3A). The PSB ranges in water depths from 250 m to over 3000 m, respectively from the north to the southwest (Huvenne et al., 2005; Dorschel et al., 2010). In the southwest, the basin evolves into the Porcupine Abyssal Plain (Huvenne et al., 2005). In all other directions, it is enclosed by four shallow platforms consisting of metamorphic Precambrian and Palaeozoic rocks. In the east, it is enclosed by the Irish Mainland Shelf and in the south by the terraced Goban Spur. On the western side, it is bordered by the Porcupine Bank and in the north by the Slyne Ridge (Naylor and Shannon, 1982; Moore and Shannon, 1991; Van Rooij et al., 2003). The bight is unique in many ways and is therefore much investigated (Henriet et al., 1998; De Mol et al., 2002; Van Rooij et al., 2003; Øvrebø et al., 2006; Huvenne et al., 2007; Eisele et al., 2008; Dorschel et al., 2009). The region first gained attention due to the moderate interest of petroleum (Croker and Shannon, 1987). In the course of the petroleum research, the presence of deep-water cold-water coral banks received notice and became the well-known feature of the PSB (Henriet et al., 1998; De Mol et al., 2002; Huvenne et al., 2003). The area of research regarded for this dissertation lies on the eastern slope of the Porcupine Seabight and is about 50 km² in size (Fig. 3B). It is located within 51°19” N and 51°26” N latitude and 11°30” W and 11°45” W longitude.

One of the most prominent morphological features present in the Porcupine Seabight is the Gollum Channel System (Dorschel et al., 2010). It is a meandering feature with a system of levees and channels on the eastern slope of the PSB, first described by Berthois and Brenot (1966). The channel system received its name and was further described by Kenyon et al. (1978). The Gollum channel system extends from the shelf edge through the central Seabight, down to the Porcupine Abyssal Plain (Fig. 3B). Here it left less traces with a poorly present deep-sea fan (Rice et al., 1991; Van Rooij et al., 2003). The poorly developed deep-sea fan can be linked to sediment reworking and redistribution by strong bottom currents (Rice et al., 1991). Some small channels also occur in the north-eastern PSB, where the formation of those is closely related to the presence of cold-water coral mounds (Beyer et al., 2003; Dorschel et al., 2010). The formation of channels on the eastern and central slope of the Porcupine Seabight can be linked with the existence of a gentle slope angle. Furthermore, a small canyon system is present in the southern tip of the PSB, west of the Goban Spur (Dorschel et al., 2010).

Cold-water coral mounds are one of the important marine ecosystems in the North Atlantic Ocean and occur extensively on the upper continental slopes (<1000 m) (Roberts et al., 2006; Wienberg and Titschack, 2017). The heights of the mounds can vary from 50 to 200 m, whereas the diameter is generally between 0.5 and 2 km (White, 2007). The mounds consist of skeletons of cold-water corals, shells of associated fauna, hemipelagic sediments and ice-rafted debris (IRD) or dropstones (De Mol et al., 2002; Dorschel et al., 2005, 2007; Wienberg et al., 2008). Corals prefer a hard substrate for settlement, which explains the presence of IRD within the mound sequence. At first, it was thought that the growth of the cold-water coral mounds was linked to hydrocarbon seepage (Hovland and Thomson, 1997). However, recent data shows that the coral growth is linked to environmental settings such as enhanced ocean currents and water column structure (De Mol et al., 2002; Dorschel et al., 2005, 2007; Wienberg et al., 2008). Along the Irish margin, most carbonate

mounds are also located on an erosional surface, which is probably of late early Pliocene age (Van Rooij et al., 2003; van Weering et al., 2003; Mienis et al., 2006).

Already in 1948, these coral ecosystems were recognized in the Porcupine area by Le Danois (1948). There are three recognized CWC mound provinces in the PSB: the Belgica Mound Province on the eastern slope, the Magellan Mound Province (MMP) and the Hovland Mound Province (HMP) on the northern slope (Eisele et al., 2008). Each province is characterized by its own properties (Wheeler et al., 2007). The small Magellan mounds are almost all buried by hemipelagic sediment and thus do not reach the present-day seabed (Huvenne et al., 2003, 2007). The HMP is characterized by giant carbonate mounds of a conical or elongated form. Nowadays, these mounds are mostly all covered by moderately developed cold-water coral thickets (De Mol et al., 2002; Huvenne et al., 2005; Wheeler et al., 2007). The BMP covers more than 1000 exposed and buried mounds (Wienberg et al., 2020) and is colonized by the best developed and densest coral thickets in the PS (Beyer et al., 2003; Van Rooij et al., 2003; Foubert et al., 2005; De Mol et al., 2007). The mounds in the BMP can reach heights up to 150 m above the seafloor and occur between water depths of 500 and 1100 m (Beyer et al., 2003; Van Rooij et al., 2003; Wheeler et al., 2005). The mounds themselves are conical in shape, can reach heights up to 150 m above the seafloor and laterally spread over several kilometres. The CWC mounds are buried asymmetrically and occur as single mounds or in elongated clusters (Beyer et al., 2003; Van Rooij et al., 2003).

## 7.2 Oceanography

### 7.2.1 Present-day

There are four main water masses currently passing through the Porcupine Seabight. They follow a northward cyclonic flow direction along the Goban Spur, entering the Porcupine and steered by the Shelf Edge Current (SEC), and eventually flowing out along the Porcupine Bank (White, 2007; Fig. 5). At the top of the stratified water column (Fig. 6), below a north-flowing surface current, the East North Atlantic Water (ENAW) can be found between approximately 200 m and 700 m water depth. It comprises of a mixture of subtropical and subpolar gyre waters (Wienberg et al., 2020). The ENAW is part of a southern branch of the North Atlantic Current (NAC), where it flows into the Bay of Biscay (Fig. 5). There it encounters intense deep winter mixing (Pingree, 1993; Van Aken and Becker, 1996).

Below that, the Mediterranean Outflow Water (MOW) stretches up to about 1,200 m water depth (Fig. 6). The MOW is a very saline water originating from the Mediterranean Sea (Millot, 2014). It exits from the Strait of Gibraltar, into the Gulf of Cádiz, flowing north-westward along the Iberian middle slope into the Bay of Biscay and further in the PSB as a notable contour current (Serra et al., 2010; Hernández-Molina et al., 2014). The Labrador Sea Water (LSW) is found below the MOW up to a depth of approximately 1,800 m water depth (Fig. 6). It originates in the Labrador Sea and is transported by the deep NAC. The LSW is a much colder water mass and less saline in comparison with the upper MOW. Lastly, the deepest North East Atlantic Deep Water and Norwegian Sea Water (NEADW, NSW) can be found beneath ~1,800 m (Pingree and Le Cann, 1989, 1990; Rice et al., 1991; Van Aken, 2000; Van Rooij et al., 2007).

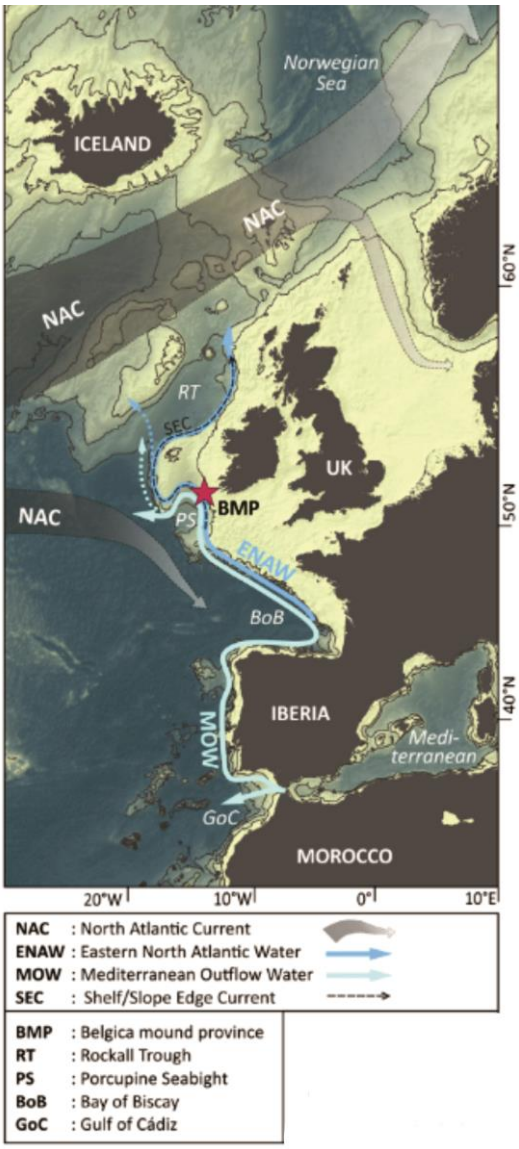


*Fig. 5: An overview map of the North East Atlantic showing the main present-day oceanographic features; modified after Wienberg et al. (2020).*

At the boundary of the ENAW and the MOW a permanent pycnocline has been observed due to the high-density difference (Rice et al., 1991; Fig. 6). At this interface, internal waves can be generated which increases the already present bottom currents. Internal waves provide across-slope sediment movement and can in that way create sediment waves on a 'critical slope angle', where the slope of the ray path of the waves is larger than the slope of the seafloor (Rice et al., 1990, 1991; De Mol et al., 2002; Van Rooij et al., 2007). But also on the bottom boundary of the MOW (with the LSW) a density difference can be recognized and

internal waves can exist. However, the density gradient is lower in this case, thus the internal waves are less pronounced. This is because the 'critical slope angle' is inversely proportional to the density gradient (Sherwin and Taylor, 1987).

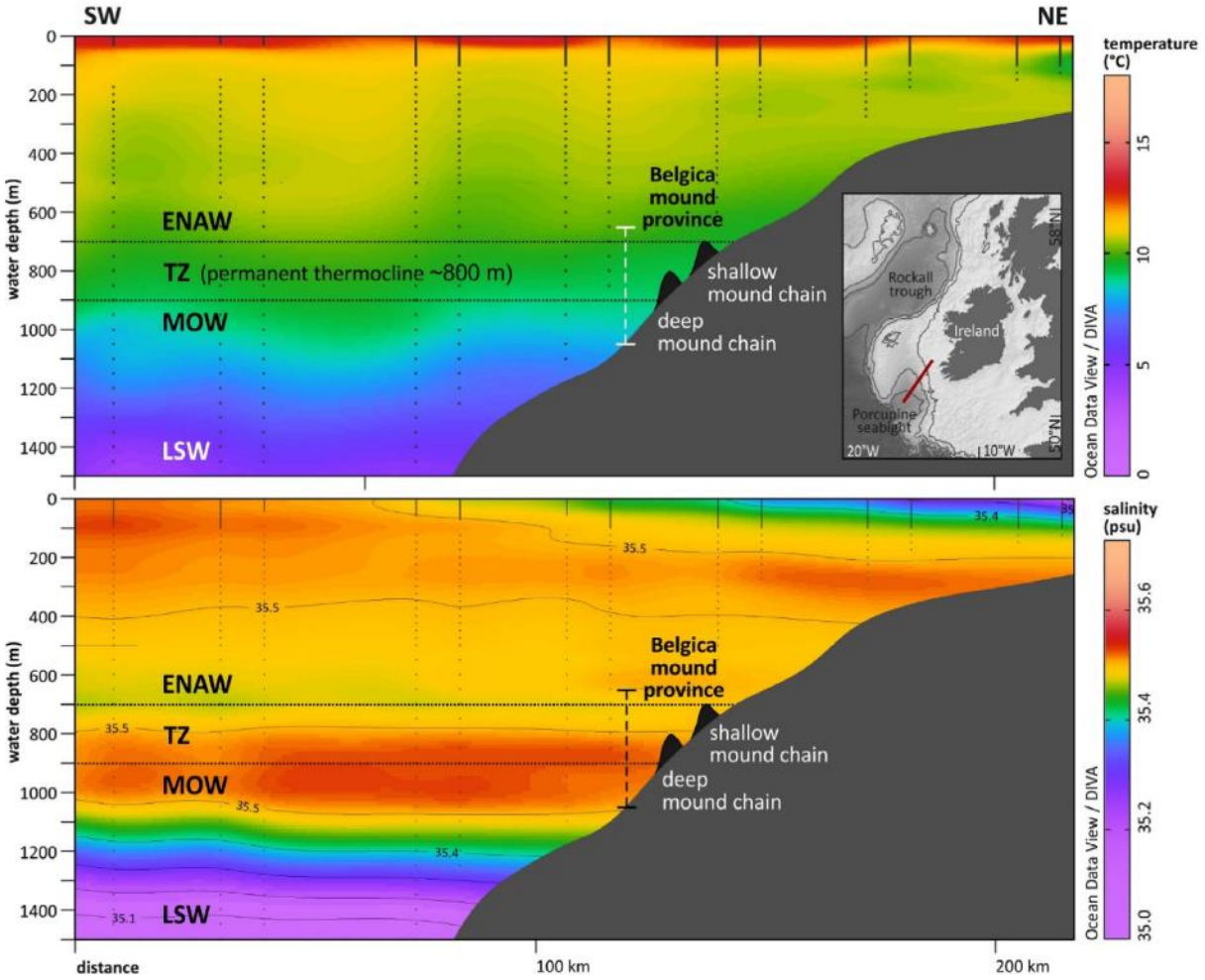


*Fig. 6: Depth-temperature and depth-salinity profile (respectively upper graph and lower graph) along a cross section on the eastern slope of the Porcupine Seabight (which is indicated as a red line on the overview map included in first graph). Both data clearly show the Eastern North Atlantic Water (ENAW), the Mediterranean Outflow Water (MOW) and the Labrador Sea Water (LSW). The transition zone (TZ) between the ENAW and the MOW is rather broad. It comprises water depths between 700 and 900 m. (Wienberg et al., 2020; after Locarnini et al., 2013; Zweng et al., 2013).*

These bottom current enhancements add to the low frequency character and generally weak velocity of the benthic currents (White, 2007). But bottom currents are also strongly steered by bottom topography, which is why these large cold-water coral mounds play a big role in the strength and flow of bottom currents (Pingree and Le Cann, 1989, 1990; Rice et al., 1991; Van Rooij et al., 2003, 2007, 2009). Mean residual bottom currents have been measured between 2 and 5 cm $s^{-1}$, but can go up to 10 cm $s^{-1}$ which is a value measured at 1000 m water depth in the northern part of the Belgica Mound Province (Pingree and Le Cann, 1990; White, 2007). Today, the slope area of the PSB is intensely steered by bottom-current activity. This is

evidenced by the many topographical features surrounding the CWC mounds, as e.g. gravel ridges, barchan dunes, large moats formed by drift sediments and sediment waves (Van Rooij et al., 2003; Foubert et al., 2005; Huvenne et al., 2005; Wheeler et al., 2005; Dorschel et al., 2007).

### 7.2.2 Miocene

The Miocene (23.03 Ma – 5.333 Ma; Cohen et al., 2013, updated) is an epoch characterized by a complex evolution in the Earth's climate and ocean circulation. The continents lay close to their modern position (Fig. 7). The lithosphere plate movements influenced the configuration of interoceanic passages which led to significant changes in ocean circulation (Butzin et al., 2011). Benthic $\delta^{13}C$ records show that interoceanic differences remained small (Billups, 2002; Bickert et al., 2004; Poore et al., 2006). This interconnection was present due to the connection between oceans through the Central American Seaway and the Tethys. The Central American Seaway narrowed from 17 Ma up to its final closure at about 2.7 Ma (Duque-Caro, 1990; Coates et al., 2003; Bartoli et al., 2005; Steph et al., 2006). The Eastern Tethys on the other hand narrowed between 18 Ma and 16 Ma, to finally close around 14 Ma (Rögl, 1991; Meulenkamp and Sissingh, 2003).

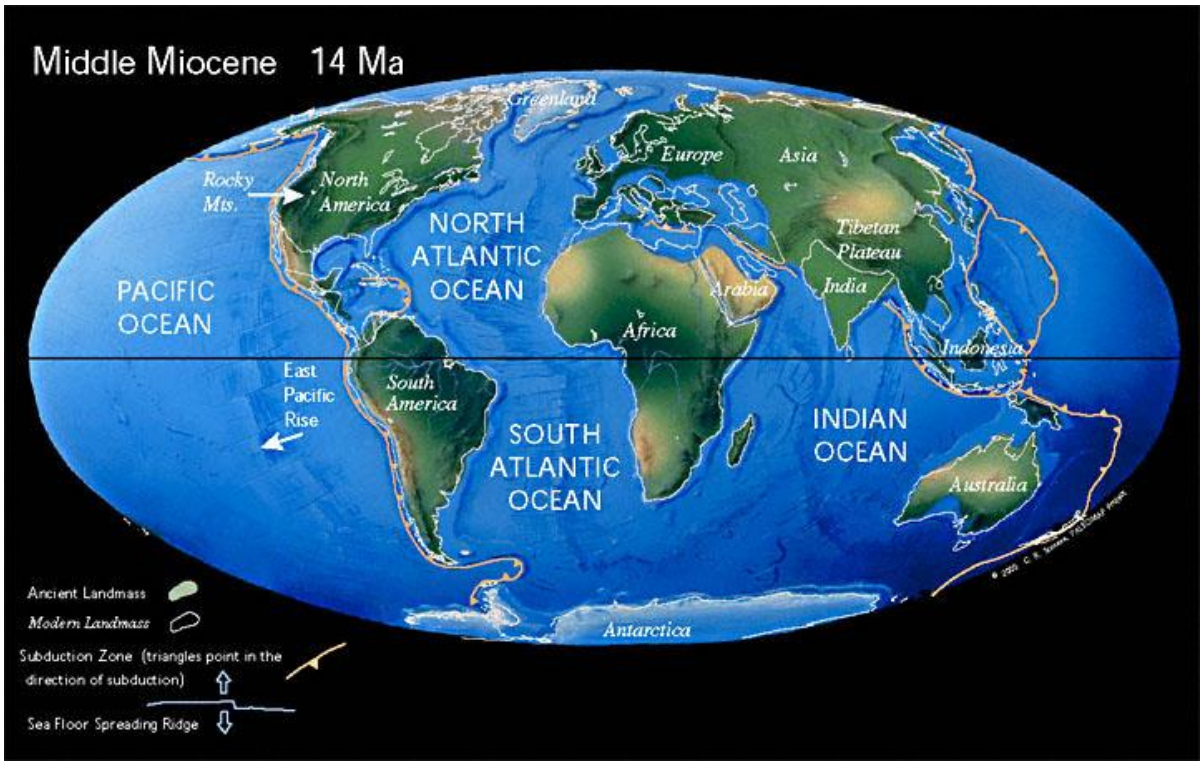


*Fig. 7: A representation of the world during the middle Miocene; after Scotese.*

The temperature changes within the Miocene also influenced some local oceanography. The Oligocene-Miocene transition (~23.1 Ma) marks the termination of the late Oligocene warming trend. The onset of the Miocene is associated with large-amplitude expansion of Antarctic ice sheets (Egger et al., 2018). However, this was followed by the middle Miocene Climatic Optimum (23.03 Ma – 14.5 Ma) and middle Miocene Climatic transition (14.5 Ma -12.5 Ma) (Super et al., 2018). The cooling trend was re-established after around 15 Ma, which was concurrent with the enlargement of the eastern Antarctic Ice sheet and the gradual onset of the modern ocean circulation patterns (Flower and Kennett, 1994).

## 7.3 Geology

The PSB is underlain by the Porcupine basin, which developed as a Middle to Late Jurassic failed rift of the proto-North Atlantic Ocean (Moore and Shannon, 1991; Naylor and Shannon, 1982; Fig. 8). The formation model for this basin is thought to be a general McKenzie (1978) simple shear extensional model (Croker and Shannon, 1987). The basin formed in accordance with a series of rift episodes, each separated by thermal subsidence events (Shannon, 1991). The Late Jurassic differential subsidence episode was responsible for the shallow marine sedimentary environment of the Porcupine basin (Ferdelman et al., 2006a). The failed rift basin is filled with a 10 km thick sediment deposit, acquired during the Mesozoic and Cenozoic (Moore and Shannon, 1991; Fig. 8). The base of the Cretaceous, where marine strata onlap Jurassic sequences, is marked by a undulatory unconformity due to a eustatic sea level fall (Ziegler, 1982; Shannon, 1991; Moore and Shannon, 1995). The Cretaceous sediments vary from offshore sandstones to shelf pelagic carbonates (Ferdelman et al., 2006; Fig. 8). A high-amplitude reflector separates the Mesozoic from the Cenozoic, where the sedimentation changes from carbonate to clastic deposition (Shannon, 1991). The Paleogene postrift sediments are mostly characterized by sandstones and shales with the influence of frequent sea level fluctuations (Ferdelman et al., 2006a).

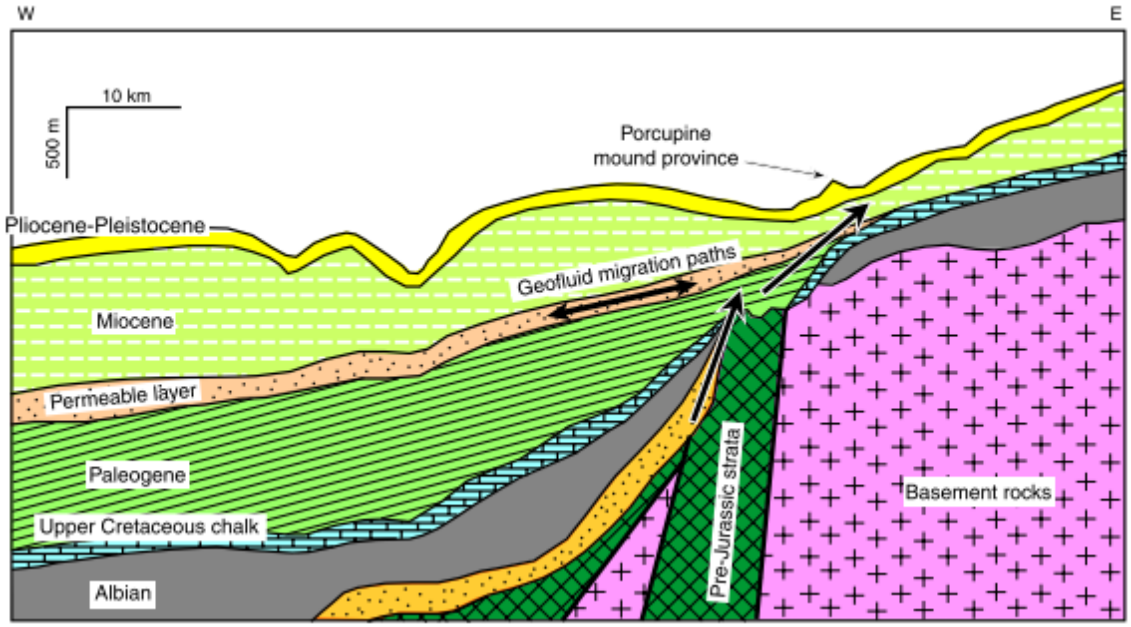


*Fig. 8: A stratigraphy interpretation of the eastern slope of the Porcupine basin (Arrows = modelled pathways of hydrocarbon-rich gases, after Ferdelman et al. (2006) and after Naeth et al. (2005).*

Due to a passive uplift of the Norwegian, British and Irish landmasses during the late Paleogene and Neogene, the present-day Atlantic margin was formed and an enhancement of contour currents was observed (Ferdelman et al., 2006a). Therefore, the Oligocene and Miocene are characterized by local erosion and redeposition leading to the formation of contourite siltstones and mudstones, and hemipelagic-pelagic deep-marine sediments (Ferdelman et al., 2006a). A major shift in sediment transport, downslope to along-slope, was observed at the latest Eocene to earliest Oligocene unconformity (C30; Fig. 9) and marks the start of the contourite dominant Neogene deposits in the PSB (Stoker et al., 2001). Throughout the Neogene, the Porcupine basin remained in deep marine conditions. The only exception is a minor inversion episode (Fig. 9) in the Oligocene accompanied by submarine canyon development (Naylor and Anstey, 1987). The

main sedimentation throughout the Oligocene and Miocene is characterized by transport and redepositional processes yielding mudstones, contourite siltstones and hemipelagic-pelagic deep-marine sediments. A combination of regional sea level and palaeoclimate changes and differential basin subsidence caused the deposition of these sediments (Ferdelman et al., 2006a). The youngest sequences (Miocene to Quaternary) are characterized by the presence of large erosive surfaces (Fig. 9), contourite drifts and a unique existence of cold-water coral mounds (Van Rooij et al., 2003, 2007, 2009). The east-west oriented Gollum Channel is thought to have been the main sediment supplier to the basin. In fact, during glacial periods, the channel system extended downstream from the southern Irish Mainland Shelf (Berthois and Brenot, 1966; Van Rooij et al., 2009). Recent sedimentation is pelagic to hemipelagic, with some foraminiferal sands on the eastern continental margin. Nowadays, the main supply zone seems to be located on the Irish and Celtic shelves (Rice et al., 1991).

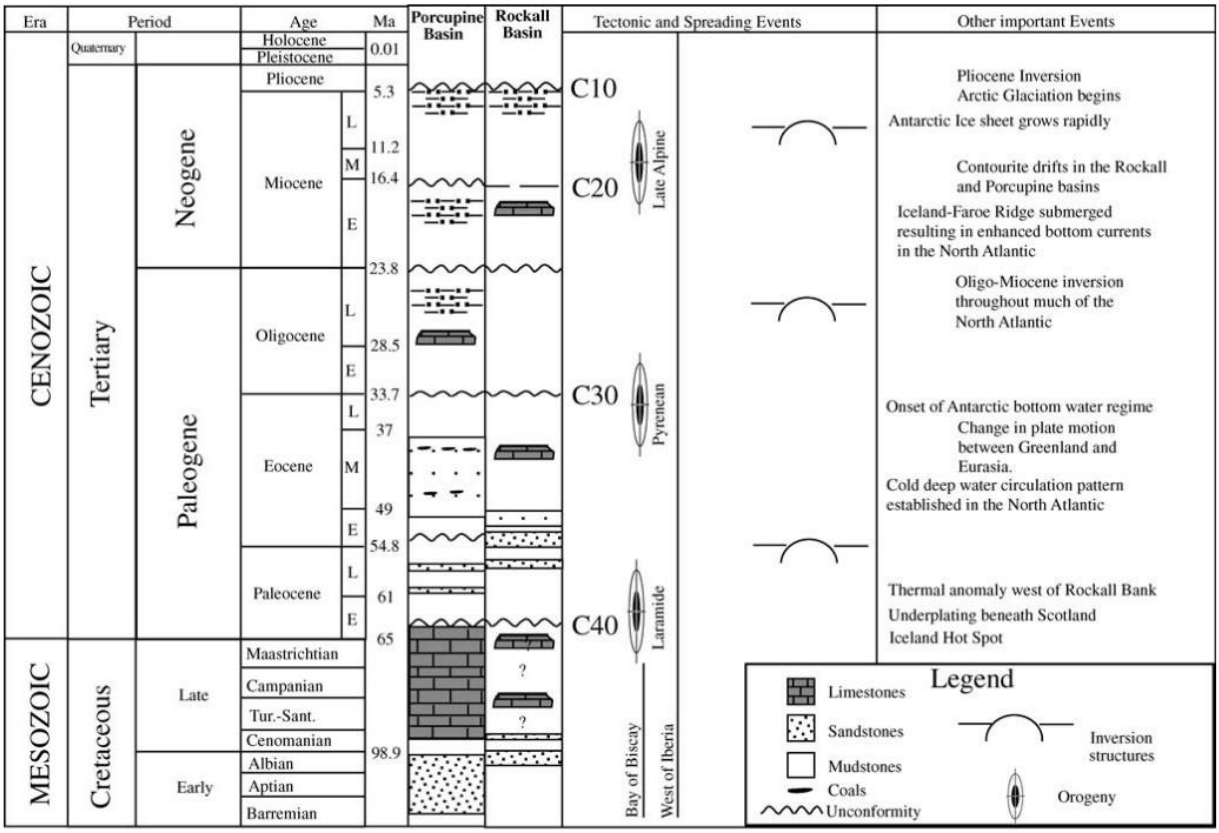


*Fig. 9: A lithostratigraphic column of the Cenozoic successions in the Porcupine and Rockall basins, following the proposed sequence scheme of Stoker et al. (2001); after Shannon et al. (2007).*

The Neogene seismic stratigraphy of the eastern slope of the PSB has been described in detail by Van Rooij et al. (2003) where two major unconformities were recognized (Fig. 10). The first is of early mid-Miocene age (Louwye et al., 2008), defined by Van Rooij et al. (2003) as RD2 unconformity. This unconformity is in accordance with the C20 series unconformities defined by McDonnell and Shannon (2001; Fig. 9), which were formed due to late pulses of the Alpine Orogeny and major plate reorganization. The second unconformity, defined as RD1 by Van Rooij et al. (2003), was linked to the C10 Early Pliocene unconformity observed by Stoker et al. (2001; Fig. 9). The IODP 307 expedition has given the opportunity to perform palynostratigraphic studies (Louwye et al., 2008) and other dating methods could be applied (Kano et al.,

2007). However, due to the inconsistency in dates, the onset of the erosion event is placed at a general Late Miocene age. RD1 represents a large-scale erosional event that must have been induced by a large hydrodynamic regime (Van Rooij et al., 2009). This big oceanographic change could have been the introduction of the MOW in the PSB (Van Rooij et al., 2003). These two unconformities separate three seismic stratigraphic units P3, P2 and P1 (Fig. 10) defined by Van Rooij et al. (2003), but this nomenclature was abandoned in later papers (by Van Rooij et al. (2007) onwards) and U1, U2 and U3 were used instead. The lowermost unit U3 is bound at the top by RD2. This unit is characterized by moderate to locally high amplitude reflectors and continuous parallel strata. Its lithology mainly comprises of sands and silts with some occurrence of clay (Ferdelman et al., 2006a; Fig. 10). A number of sigmoid reflectors are recognized within the unit which are interpreted as migrating drift bodies of Miocene age (De Mol et al., 2007; Van Rooij et al., 2003; Fig. 10). Above U3 lays U2 with its transparent acoustic facies and few high amplitude reflections. Unit U2 is interpreted by De Mol et al. (2002) as a nannofossil ooze of Pliocene age. The uppermost unit, U1, consists of Quaternary drift deposits partly enclosing the mounds that onlap on RD1 (De Mol et al., 2002; Van Rooij et al., 2003). This unit mostly consist of clays with some sands interbedded (Ferdelman et al., 2006a; Fig. 10).

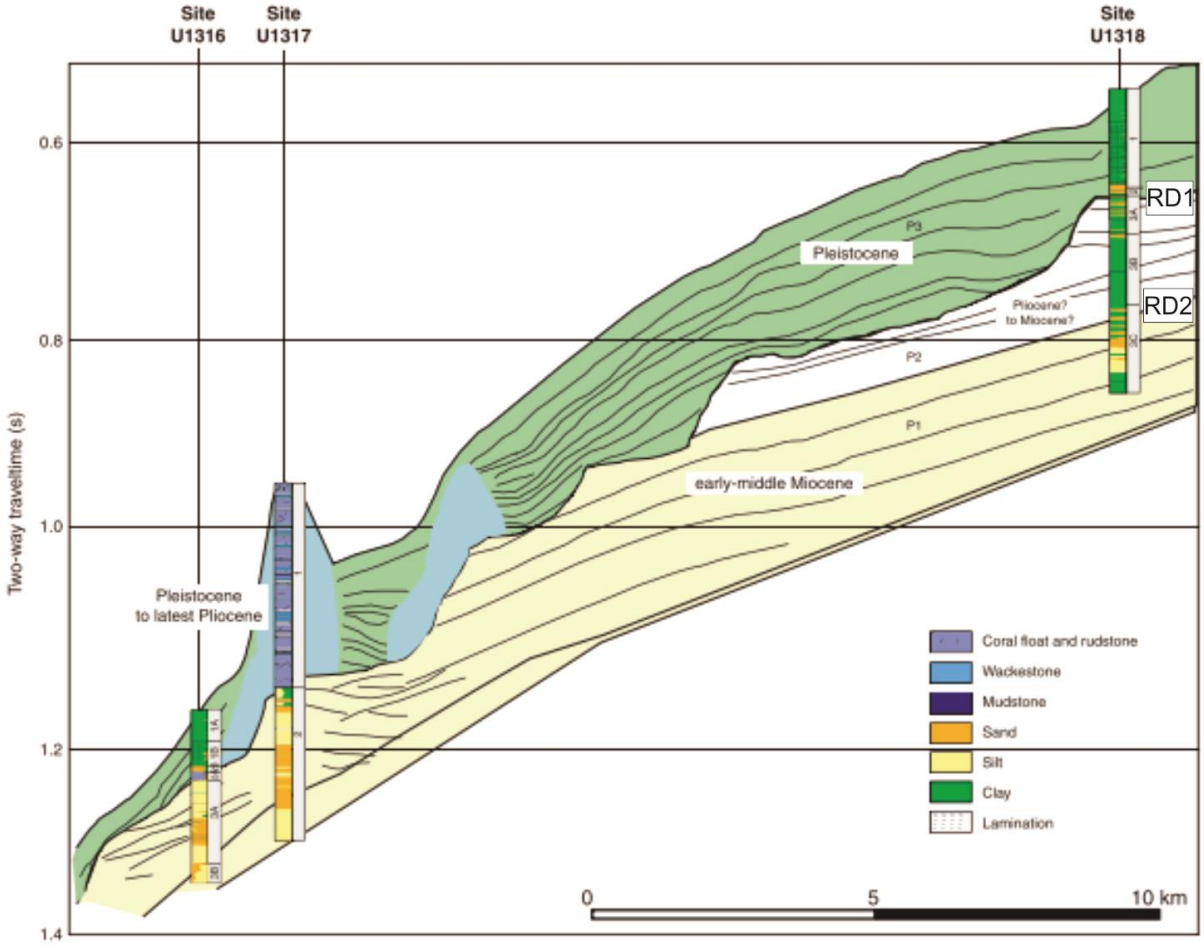


*Fig. 10: An interpretation of a seismic profile with NNW - SSE transect along the eastern slope of the Porcupine Seabight adapted from Van Rooij et al. (2003) with the lithostratigraphy added of all three sites of the 307 IODP expedition; modified after Ferdelman et al. (2006).*

# 8 MATERIAL AND METHODS

## 8.1 Data

This dissertation focusses on the seismic data acquired during the RV Belgica cruise 2019/16 (Van Rooij and Mestdagh, 2019). This cruise was carried out in June 2019 on an attempt to understand and quantify the temporal and spatial variability of the present-day hydrodynamic regime within the Belgica Mound Province, within the scope of the DynaMOD project (Van Rooij and Mestdagh, 2019). This area has been surveyed before, however the density of the seismic grid is exceptional in comparison to previous seismic data (see below). This was one of the reasons why it was opted to only use the most recent seismic data from the RV Belgica cruise 2019/16. Another reason was that the equipment (hydrophones and streamers) has improved over the years and the processing has refined, which lead to an improved dataset. But in particular, better weather circumstances caused an enhanced dataset.

### 8.1.1 Single channel reflection seismic profiling

Single channel reflection seismic profiling uses a single source and single receiver to obtain seismic profiles. This seismic system provides deeper penetration compared to other hydroacoustic systems such as multibeam bathymetry (frequency usually around 12 kHz for deep-water systems; Beyer, 2006) due to the lower frequency used (a frequency of around 3.5 kHz in this case; Van Rooij and Mestdagh, 2019). This makes it possible to view the internal structure of marine sediments and underlying bedrock (Gadallah and Fisher, 2009).

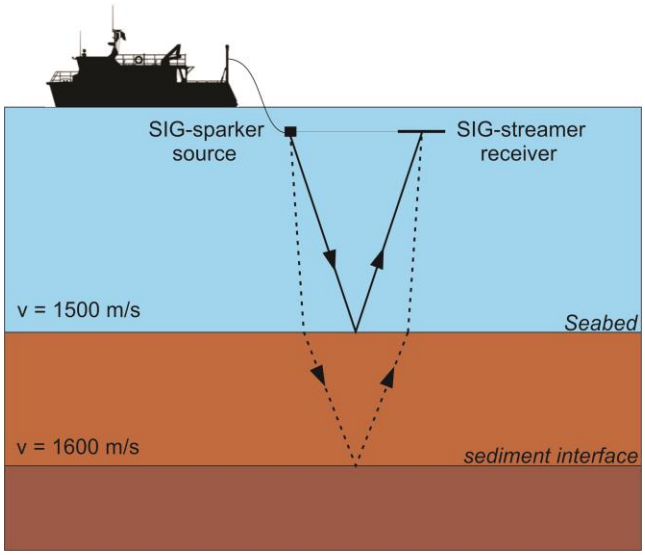


*Fig. 11: Visualization of single channel reflection seismic principle, with a SIG-sparker as source and SIG-streamer as receiver. Two possible pathways of the seismic rays are displayed: one reflecting on the seabed and the second reflecting on an interface in the sediments. The figure also visualizes the principle of TWT. Both estimated velocities of water and sediment are added in the figure.*

Acoustic waves originating from the source will propagate through the water column at a velocity of 1,500 meters per second, which is an averaged estimation of sound velocity in sea water. These waves will reflect at an interface which can be at the seabed, at interfaces in the sediments/bedrock or at an object in the water column. The reflection happens due to a difference in acoustic impedance, which is the product of compressional velocity and density (Onajite, 2014). The reflected signal will be captured by the hydrophone(s) within the streamer, towed at a constant distance from the source (Fig. 11). The measurement made by the system is the time it takes for the signal to go from source to interface to receiver and is called the TWT (two-way travel time) (Fig. 11). The TWT is a measure of depth represented in seconds but can be converted to meters or mbsl (meters below sea level). This can be perceived when the speed of sound in the different media are known. An average of 1,650 meters per seconds for the P-wave velocity in the sediments

was used according to the data of Ferdelman et al. (2006b). For better speed estimation within the water column and sediments, CTD (conductivity, temperature and depth) and core logging analysis can be applied. From the velocity estimations, a depth in metres instead of TWT can be calculated with the following formula:

$$Depth\ (m) = \frac{TWT\ (s) \times V(\frac{m}{s})}{2} \qquad F1.$$

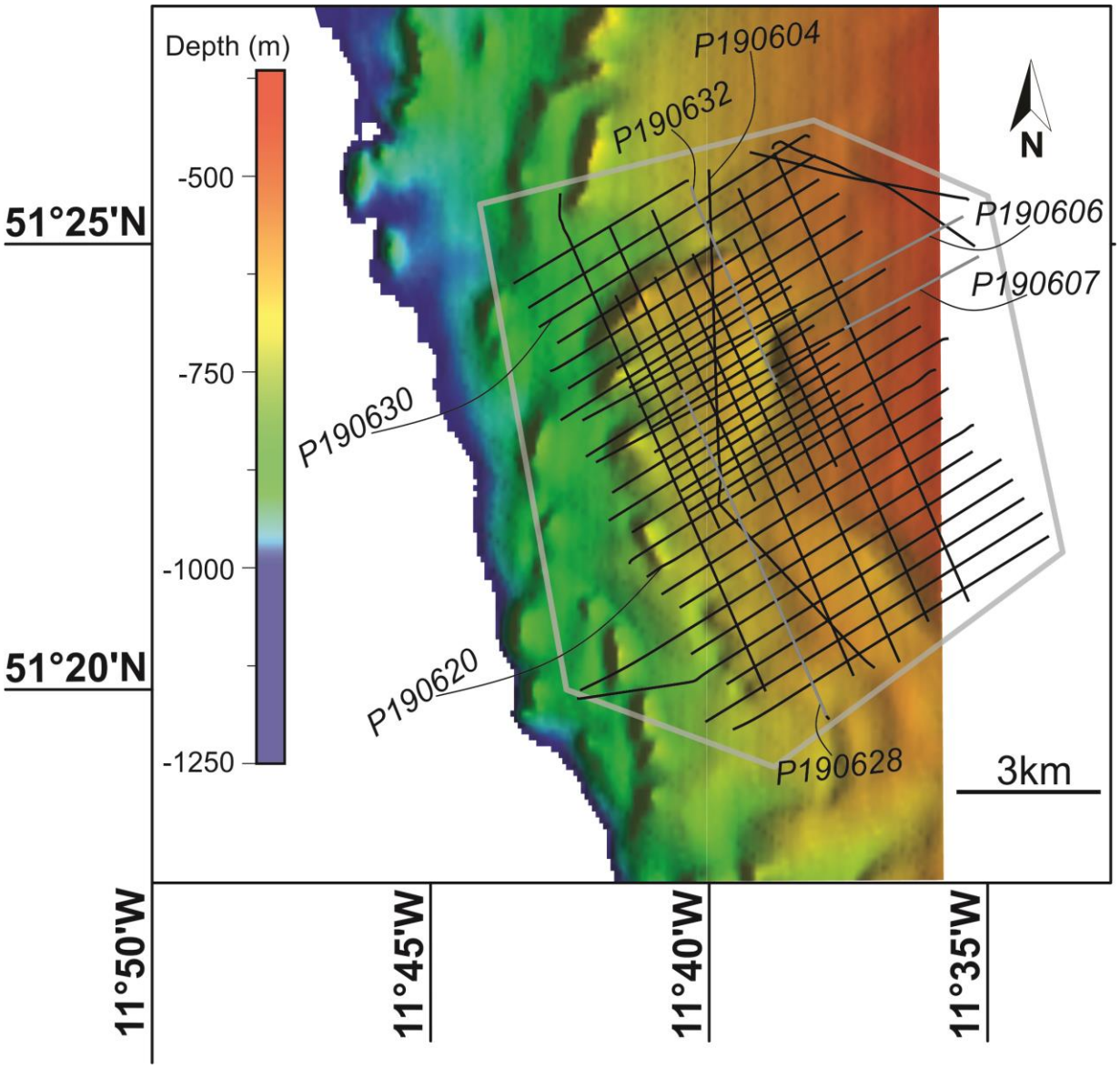


*Fig. 12: A bathymetric map (Beyer et al., 2003) showing the location and orientation of the seismic lines obtained during RV Belgica cruise 2019/16. Seismic lines referred to further in the text, have their name added in this figure. The cropped seismic lines used in further figures are displayed in grey. The grey area represents the survey area.*

During the RV Belgica cruise 2019/16, 44 single channel reflection seismic profiles (average length 68 km) were acquired (Fig. 12). These were obtained with a single channel SIG-streamer receiver and SIG-sparker source (frequency 3.5 kHz). The source was triggered every two seconds with an energy of 600 J. This resulted into an average penetration of 500 ms TWT (400 m). The seismic lines were spread in a grid of approximately 80 km² with water depths ranging from 460 m to 900 m. In NNW-SSE direction the spacing between the lines was 0.25 nautical miles (nm) to 0.5 nm (462.5 m – 925 m), while the lines in WSW-ENE direction were 0.125 nm to 0.25 nm (231,3 m – 462.5 m) spaced from each other. During acquisition, the ships velocity was kept constant at three knots, while using the electrical propulsion. The electrical propulsion is better to use because it generates less noise with respect to a pure diesel propulsion. The data was digitized with an IXblue Delph-system at a sampling frequency of 8 kHz (Van Rooij and Mestdagh, 2019).

Prior to the start of seismic acquisition, a marine mammal survey was carried out for one hour. This is necessary to make sure no marine mammals would suffer from the frequency pulses during seismic acquisition. When no marine mammals were observed, a soft-start procedure was then followed by starting with a lower energy of 200 J, gradually increasing to 600 J over a period of 20 min (Van Rooij and Mestdagh, 2019).

Reflection seismic data are displayed in a seismic profile as a compilation of several seismic traces. A seismic trace is the detected seismic energy received after one shot from the source, often presented as a wiggle line. Similar wiggles can be followed from trace to trace, especially when positive and negative wiggles are represented in a different colour (Onajite, 2014). In this way, reflective surfaces (called reflection when considering only one point, reflector when considering a long traceable interface) become visible, where some show a stronger reflection than others. Some of these strong and distinguishable reflectors can then be defined as a horizon of a specific unit or layer.

## 8.2 Processing

Processing of the data was executed using RadExPro (DECO Geophysical software company, 1992) software. All 44 seismic lines were processed applying the following workflow. First bandpass filtering was applied, which is a filter designed to pass signal and reject noise (Reynolds, 2011). Using the Ormsby bandpass filter, a bandwidth is chosen with a low-cut ramp and high-cut ramp. When choosing the frequencies for the bandwidth, an attempt is made to include the frequencies containing coherent energy (reflections), and exclude the frequencies containing mostly noise (Gadallah and Fisher, 2009). For the purpose of this dissertation, lower frequencies were included to obtain more signal in the deeper parts, where the sediment waves occur. The downside of doing this is that more noise is included in the top layers. The values used for the Ormsby settings were variable from one seismic profile to another, depending on with which values the best amount of noise was rejected. The minimum and maximum values used were: for the lowest value between 100 Hz and 150 Hz, the second value between 200 Hz and 250 Hz, the third value between 700 Hz and 1250 Hz and the last value was set between 1000 Hz and 1500 Hz. The tapering value was left default at 10% of trace length.

The second correction was the burst noise removal, where abnormally high amplitudes randomly occurring through the data were removed, using the default settings. Next an amplitude correction was necessary to correct the gradual amplitude decrease with depth due to spherical spreading and absorption. Doing this, shallow reflections were weakened whereas the deeper amplitudes were strengthened (Reynolds, 2011). On each profile this was applied between the shallowest point of the seafloor to the deepest data point of interest

(usually around 1300 ms TWT, varying between 1080 ms TWT and 1400 ms TWT), using mean trace equalization and the value 2.0 for time raised to power.

Additionally, corrections were carried out to reduce the swell influence. During acquisition, swell can place the source and receiver on a different level. This variation in the reference level is visible in the data and was removed by applying the swell filter. The seafloor location was defined and picked by the functions 'trace header math' and 'first breaks picking' and was adjusted manually in the presence of errors. The swell filter function could then be applied to the newly picked seafloor, with an averaging base of 4 or 5 depending on the seismic profile and a max/min rejection of 30%. Lastly the data above the seafloor was removed with the 'trace editing; top muting' function, using the just picked seafloor as base.

## 8.3 Interpretation procedure

The interpretation of the seismic profiles were carried out in the IHS Kingdom software (IHS Markit, 2019), where all 44 seismic profiles were loaded in. Due to the included coordinate files, all seismic profiles are correctly geographically positioned (WGS84, UTM zone 29N) which makes it possible to obtain reliable geographic and geometric information. This also makes it easier to compare all crossing profiles and compare the interpretations on each one of them.

### 8.3.1 Horizon picking

Horizon interpretation implies picking and tracking of laterally consistent seismic reflectors. A clear horizon shows a transition between two units by having different acoustic and geometric characteristics. Interfaces between units, that can then be defined as horizons, are created due to a difference in acoustic impedance of the sediments. This is influenced by the compression velocity and density of the sediment. A change in either of those will result in a different acoustic impedance. A great difference in acoustic impedance between two sediments will result in a difference in amplitude on the seismic profile (Onajite, 2014). A horizon can also be defined at the transition of different geometric characteristics caused by different geologic facies. Seismic facies can be studied by describing internal seismic reflection patterns that are caused by different depositional environments and related lithofacies. These can show various arrangements of reflectors (e.g., parallel, subparallel, chaotic, divergent…). Reflector terminations and non-conform contacts can also be distinguishing characteristics for defining horizons (Fig. 13). These different components in the sediment bed make it possible to construct a reasoned interpretation (Nanda, 2016).

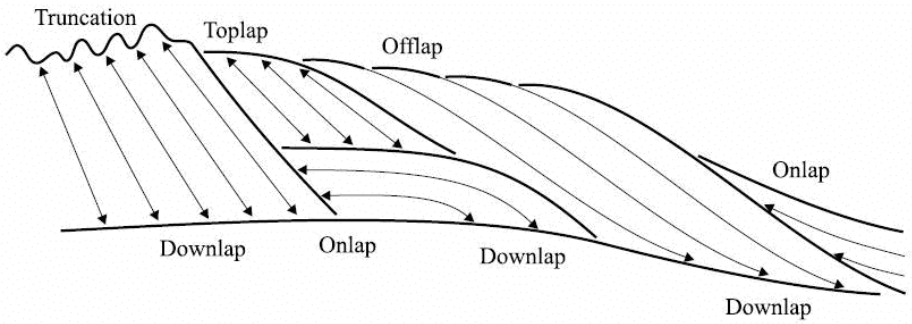


*Fig. 13: Reflector terminations defined within sequence stratigraphy, that can be used to define units in a seismic profile; after Catuneanu (2002).*

### 8.3.2 Describing sedimentary features

Since the objectives of this dissertation deal with clinoforms, sedimentary features such as undulations, convex or concave shapes or clinoform types (Fig. 14) were searched for in the seismic section. If sediment waves were observed, they were described thoroughly through sediment wave characteristics such as: (a)symmetry (Fig. 15A), directionality, thickening upslope/downslope flanks, wave form, shape of through and crest (Fig. 15A), migration wave field (Fig. 15B), wave dimensions, form of the seismic reflections, etc. Sediment waves can also show various types of progradational clinoforms (Fig. 14) which characterize a varied depositional dynamic environment (Nanda, 2016).

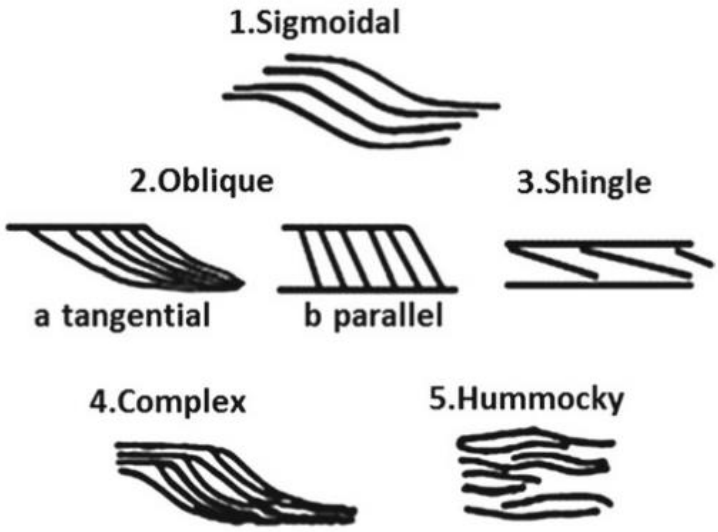


*Fig. 14: A schematic representation of various types of progradational clinoforms; after Mitchum et al. (1977a, b).*

Hereafter, similar features having the same characteristics in different seismic sections were grouped. In that way the large-scale sedimentary bedforms and their spatial arrangement become visible. Comparing the sedimentary features could be done by looking at location and depth-level, to see which of the grouped features were of the same origin. Mapping these depositional bedforms was the next step to further define the groups of features. Individual reflectors within these sedimentary features were picked and tracked (and were termed tracks), to characterize the movement of some of these depositional bedforms. Wavelengths and wave height can then be determined by measuring those in s TWT and converting to meters using F1.

## 8.4 Gridding

A gridding algorithm was used to create relief maps of specific horizons and units in IHS Kingdom (IHS Markit, 2019). The different gridding algorithms available were cubic spline, flex gridding, gradient projection, inverse distance to power and minimum curvature. For this data, my personal confidence level was higher to use flex gridding. The other gridding algorithms gave a less geologically correct image due to the amount of interpolation the algorithm applies and of course the algorithm itself also plays a big role in the geological correctness. An extrapolation limit (convex hull) was applied on top of it to prevent interpolations of horizons where they were not longer visible. The distance limit from the data was set to 400 m, which was chosen so that no holes are created between the seismic lines, but the interpolation is also not stretched too far. Fit to data was set to 0 and the smoothness to 11, other settings were left at default. The image then created is an interpolation that is geologically more correct. Afterwards, isopach maps (thickness maps) could be made by subtracting two horizon grids (deepest – shallowest) from each other.

Relief maps were made from the most important horizons and from the tracks defining the sediment waves (see §8.3.2). Using these, isopach maps could be made for some units or subunits. The isopach maps could

also be used to show the movement of the sediment waves when using the tracks and the slope below. In that way the effect of the slope is diminished and the track movements is better visualised.

A contour can be added to the grid but was in this case not always applied. This because the contours can give a misleading image due to inaccurate interpolation and thus give a geologically incorrect map. A smoothness factor was applied to its maximum and the fit to data was put at its minimum. In that way a smoother transition between the data is obtained, and a better refined map is created. However, this smoothing of the data was not enough to refine the contour lines in some of the maps created and these were left out.

**A.**

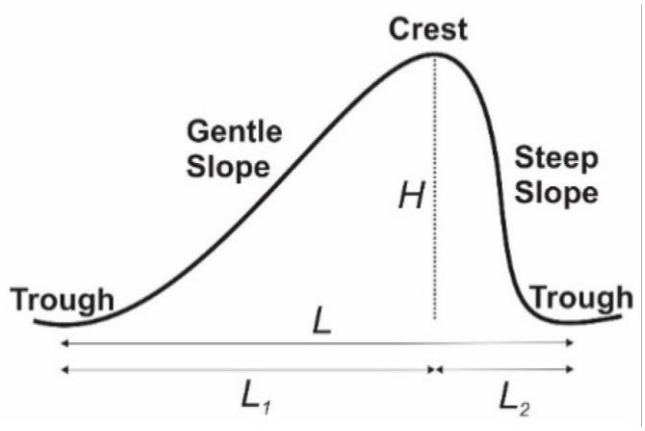


**B.**

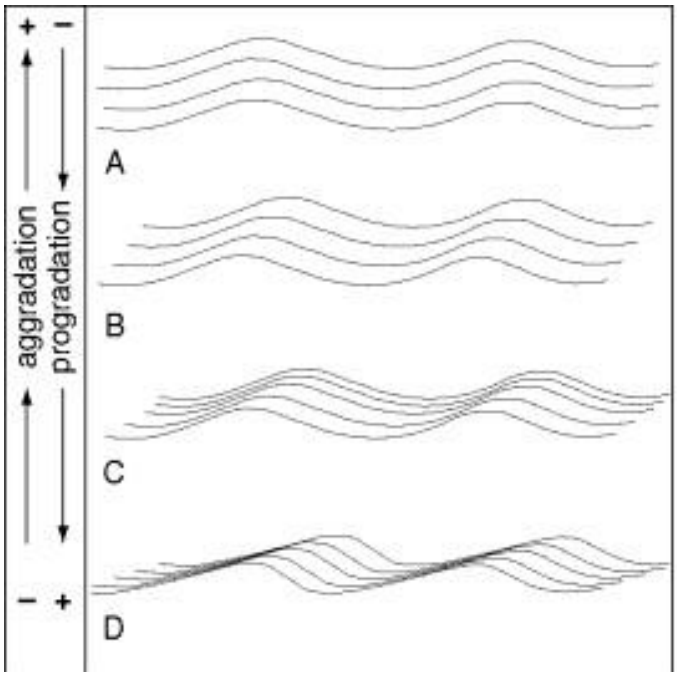


*Fig. 15: A) a schematic representation of a sediment wave, showing the crest and throughs. L represents the wavelength, while H represents the wave height; modified after Cheng et al. (2020). B) A schematic representation of different wave geometries that form due to the dominant process being aggradation or progradation; modified after Faugères and Mulder (2011).*

# 9 RESULTS

In this chapter, the results will be accurately described with regard to the main focus unit of this thesis. Firstly, the general seismic stratigraphy of all units and subdivisions will be given, followed by a thorough seismic characterization of the sedimentary features within unit 3. Lastly, after the seismic description of the sedimentary features, their spatial extend will be elucidated. This spatial characterization will be supported by relief maps of horizons and isopach maps of certain (sub)units.

## 9.1 General seismic stratigraphy

In total, three main units were recognized in the survey area (U1, U2 and U3) on the eastern slope of the Porcupine Seabight. All are separated from each other by erosive surfaces (H1 and H2). In this thesis the main focus is on the third unit, where undulations and various sedimentary features were observed. A brief description will be given for U1 and U2, whereas U3 will be described in more detail. Unit 3 is subdivided in two subunits (sU3.1 and sU3.2) and separated by two horizons (H2.1 and H2.2). However, the lower horizon H2.2 cannot be traced over the complete area. In the latter case, no thickness can be determined for sU3.2, due to the limit of vertical penetration. In case of the presence of H2.2, no unit beneath is defined/described due to the same reason. The seismic profile P190604 (figure 16) is used to describe the general seismic stratigraphy. It is a NNW-SSE profile (Fig. 12) that includes all the units and horizons visible throughout the area. It also contains the main sedimentary structures that will be described in §9.2. The line drawing of figure 16 (and further line drawings) is focussed on sU3.2. This is first of all because, as already mentioned, the main focus within this dissertation lies with unit 3. And second because sU3.1 is more uniform and the sedimentary features lie within sU3.2.

### 9.1.1 Unit 1

The uppermost unit, visible in all profiles within the survey area, is U1 (Fig. 16). It is a unit that varies in thickness from approximately 37 ms TWT (~30.5 m) to 265 ms TWT (~218.5 m). In this unit, there can be distinguished between two components (Fig. 16). One being the large conical feature showing low acoustic amplitude and the comprises of purely sediment.

The sedimentary component comprises of roughly parallel bedding and is characterized by high-amplitude reflections. Some large elongated mounded bedforms, mostly progradational to aggradational features, are visible within the unit (Fig. 16). The unit is bound between the seafloor reflector (SF) and H1, which is defined by truncations (Fig. 16). These truncations are indicative for erosional unconformities, which H1 is. The wavy truncations incise the units below.

The other component, comprising the low amplitude conical features, is acoustically transparent in comparison to the sediments (Fig. 16). These features can be buried by sediment or protrude the SF. Within this survey area, all of these conical features are settled on the erosive surface of H1 (Fig. 16). Most of the conical features leave a velocity pull-up disturbance through the rest of the profile below.

### 9.1.2 Unit 2

In contrast to unit 1, unit 2 is characterized by low amplitude reflections (Fig. 16). It is therefore visible as an acoustically transparent unit on the seismic profiles. The internal reflections are very linearly structured with the occasional high amplitude reflector (for better visualization see §9.2.2 Fig 26). U2 does not extend laterally due to the erosional characteristics of H1. In most cases the unit has been eroded completely, especially in the western part of the survey area. The maximum thickness of the unit within the survey area is roughly 126 ms TWT (~104 m). The lower boundary (H2) is, as H1, also defined by an erosive surface. Although that in the biggest part of the area H1 incises through the erosive surface H2 into the unit below.

### 9.1.3 Unit 3

The lowermost unit (U3) has moderate to high amplitude reflections, which clearly distinguishes it from unit 2. U3 is bound on top by H2 (or H1 where it has eroded to a deeper level than H2) and the lower boundary is not defined due to the limit of vertical penetration (Fig. 16). It is a unit that comprises laterally continuous seismic reflections that are very linearly structured, but at the same time also contains chaotic seismic reflections. This visible contrast can be observed at H2.1, above which a linearly stacked sediment body is located and more disturbed reflections are featured below (Fig. 16). Therefore unit 3 has been subdivided into two subunits, subunit 3.1 (sU3.1) and subunit 3.2 (sU3.2), divided by H2.1. The lower boundary is defined by H2.2, which is a horizon marked by a downlap of reflectors in the northern part of the area (Fig. 16). H2.2 cannot be laterally traced because at a certain point it is consumed by the chaotic reflections in the south-west of the survey area.

Subunit 3.1

Subunit 3.1 is characterized by very linear reflectors, bordered on top by H2 (or H1) and at the bottom by H2.1. It has high amplitude reflections at the top going to moderate amplitude reflections deeper towards H2.1. In the middle part some low-amplitude reflections are observed, creating the image of a unit with a broad variation in amplitudes (Fig. 16). The thickness of the subunit varies and it completely disappears where it is eroded by H1. The maximum thickness of the subunit observed in the survey area is 107 ms TWT (~88 m).

Subunit 3.2

Below the very linearly stacked subunit, a more chaotic reflection pattern is observed in the lowermost subunit, which is sU3.2 (fig. 16). It is bordered on top by H2.1 and on the bottom by H2.2. As mentioned above, H2.2 is only visible in the northern part of the area, where subunit 3.2 is characterized by mainly prograding sigmoidal to complex (Fig. 14) sediment waves. More towards the south H2.2 becomes untraceable due to the presence of chaotic and irregular sedimentary features with poor lateral continuity (Fig. 16). At these locations sU3.2 is thus not (visually) bound by a lower horizon, but it is limited by the end of vertical penetration. In between both the sigmoidal to complex structures in the north and the chaotic features in the south, the reflections are assembled linearly. Both these structures are on the same level of depth, which is shown clearly by reflections that can be continued from the sigmoidal to complex structures into the more southern occurring undulations (Fig. 16). The presence of these sedimentary features in this particular subunit is the reason why only this subunit will be discussed further. In the next section these features will be discussed in a broader sense seismically, but will also be described spatially.

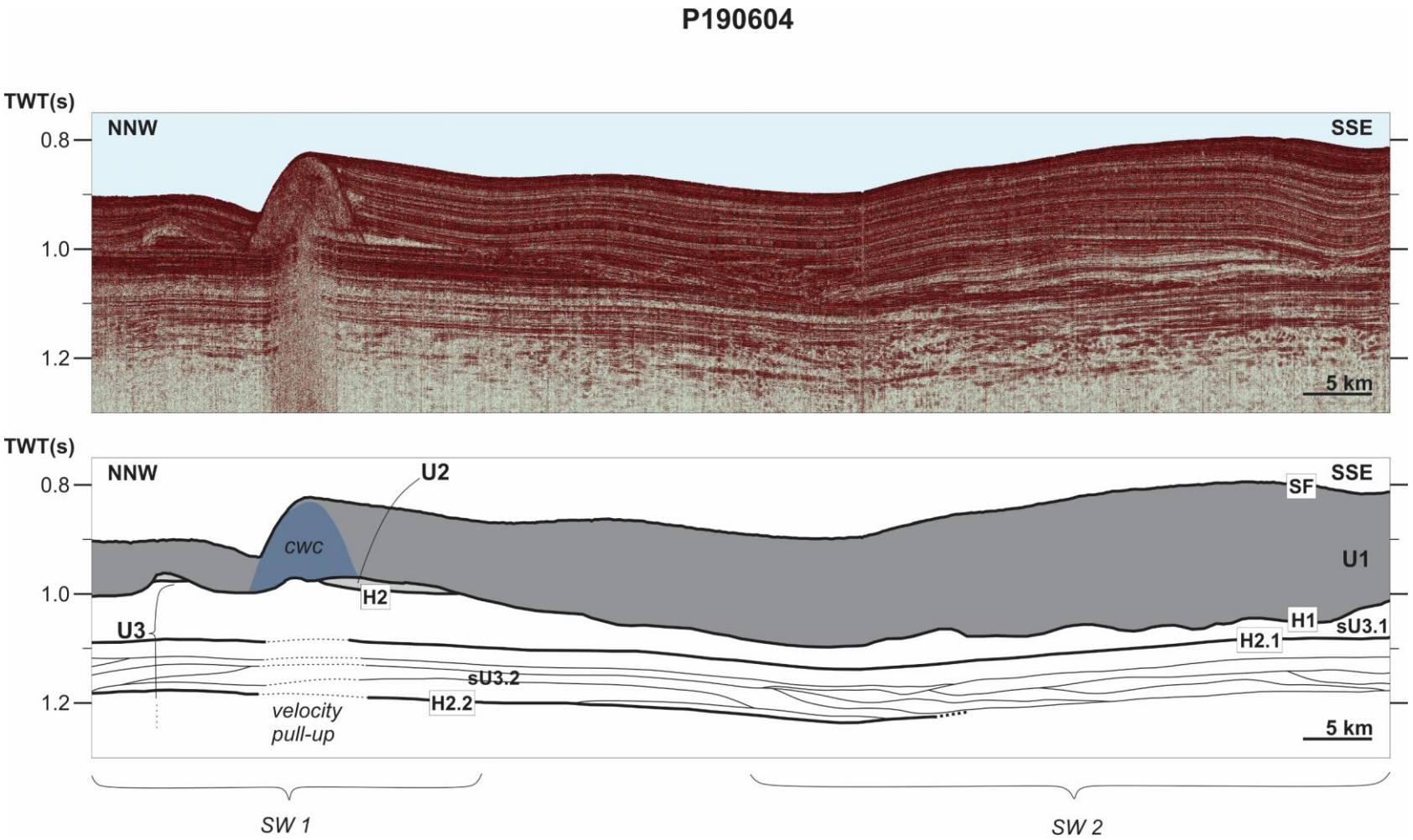


*Fig. 16: P190604 is a seismic profile tracked through the research area in a NNW-SSE direction. The seismic line is represented in the upper part of the figure from 0.75 s to 1.3 s TWT. Within the line drawing, the dark grey area is Unit 1, the light grey area is Unit 2 and everything below is Unit 3 with the thick lines marking the boundaries between the subunits. The (buried) conical features are represented in blue.*

GHENT UNIVERSITY

## 9.2 Seismic and spatial characterization subunit 3.2

When taking into account general sediment feature and internal structure characteristics, three types of features have been recognized within subunit 3.2. As already mentioned in the unit description, sediment waves were distinguished, some located more in the north of the area and others more in the south (Figs. 16, 17). Based on their similar characteristics, the sediment waves could be subdivided in two types and comprise the two main features recognized. The first type of sediment waves, grouped as SW1, are the ones located more to the north. The second type, grouped as SW2, are the ones located more to the south. Both features will be discussed extensively below using two crossing sections per feature (Figs. 18, 19 and Figs. 25, 26), a detail of both sections (Figs. 20, 27) and relief/isopach maps (Figs. 21, 22). The third feature, convex in shape, is recognized on two longer seismic profiles P190606 and P190607 (Figs. 17, 23, 24). It should be mentioned that due to the lack of crossing seismic lines, this feature could only be interpreted from these two lines and is thus not that reliable. More data and research are required. In the view of the foregoing, this third feature will only be discussed briefly together with SW1.

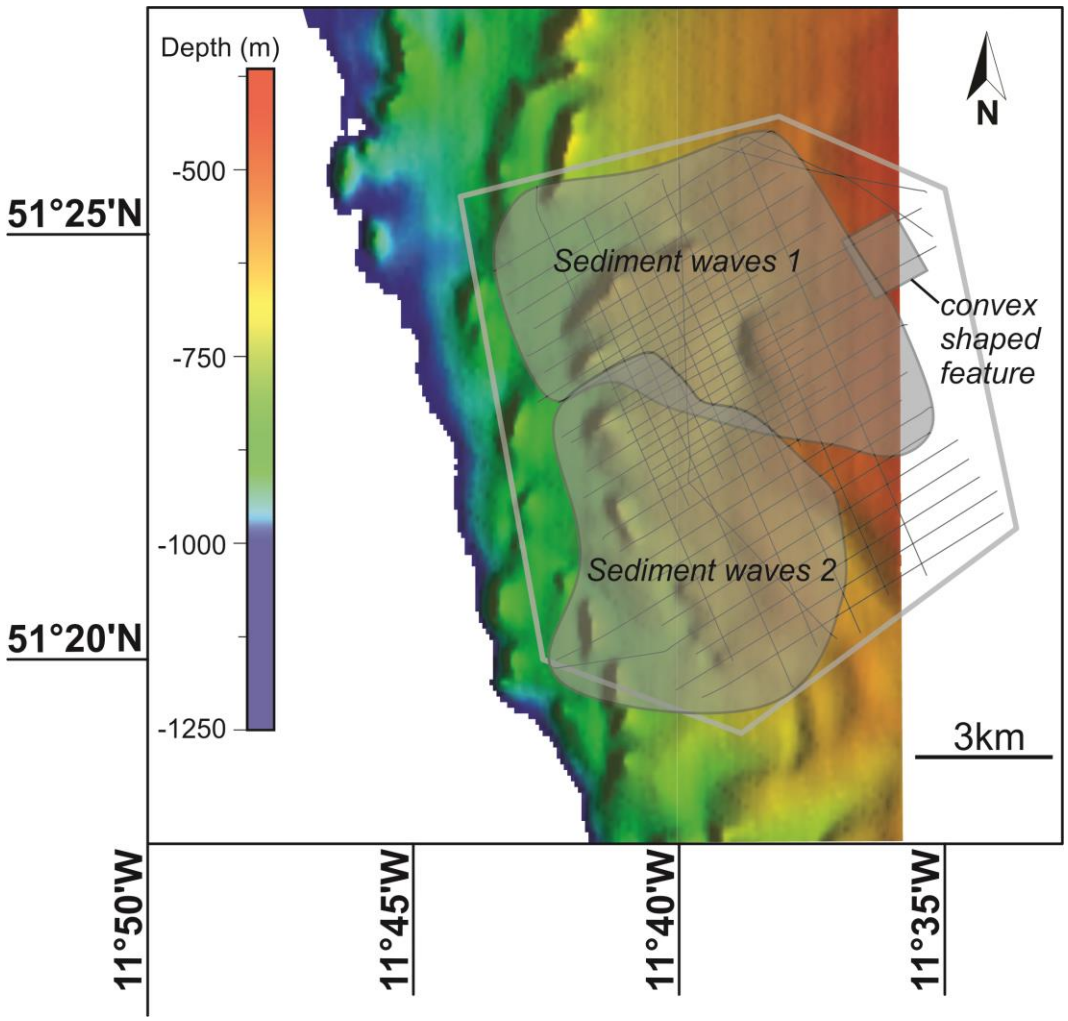


*Fig. 17: A multibeam map (only used to show location, not visible on multibeam because these features are located within sU3.2; Beyer et al., 2003) showing the three distinguished areas where sedimentary features could be determined and grouped. Two types of sediment waves (SW1 and SW2) and a convex shaped feature were distinguished. The grey area represents the survey area.*

Both the top (H2.1) and bottom (H2.2) horizons in which the sediment waves are observed are mapped, to visualize the horizon topography. H2.1 shows a gradual deepening towards the basin (Fig. 21A), following subunit 1 linearly. The slope looks to be slightly less steep (~0.17°) than the present bottom topography (~0.4°) (bathymetry in Fig. 10), especially in the northern part of the survey area. H2.2 also shows a gradual deepening towards the basin (Fig. 21B), but the slope is steeper than H2.1 (~0.2°) (only looking at the area where SW1 occur, because more towards the south H2.2 is influenced by SW2). The difference in slope angle between both horizons can also be observed on the isopach map in figure 22A. A slope upward (north-westward) thinning can be observed of subunit 2.

### 9.2.1 Sediment waves 1

The first set of sediment waves (SW1) is located in the northern part of the area within sU3.2. The sigmoidal/complex (Fig. 14) arrangement of these undulations is visually the most dominant characteristic. This feature is best visible in the WSW-ENE profiles (Fig.18), where the sediment waves migrate upslope. In the NNW-SSE profiles the sigmoidal nature is less explicit. The sediment waves are visible as downlapping northwards along the slope with a gentle angle (Fig. 19). An estimation was made on the average wavelength and wave height being respectively 2-3 km and 30 m.

Within the sigmoid/complex features, a differentiation can be made between two different reflector configurations. Firstly, there are the reflectors that continue laterally throughout the seismic profiles and thus throughout the sediment waves (black lines; Figs. 18, 20). They start with a parallel arrangement towards H2.2 in the WSW. The reflectors will all converge towards H2.2, but not all at once, rather progradational. The transition from parallel arrangement to converging is characterized by the crest (Fig. 20). Afterwards the reflectors will again follow a parallel arrangement to H2.2. Both track 1 and track 2 are such reflectors (Figs. 18, 19). Second, are the internal reflectors (grey lines) that begin or end in toplap or downlap, always between two reflectors of the previously mentioned origin (Fig. 20). Both due to this and due to the converging character, these features lean more towards complex than sigmoid.

In the WSW-ENE profiles (Fig. 18) an upslope thinning of subunit 3.2 can be observed, which is also visible on figure 22A. This could be attributed to the converging character of the reflectors. Another thing that was observed in the WSW-ENE transects is the change in wave dynamic processes. Starting from the WSW the sediment waves follow a progradational geometry. While when moving upwards and towards the ENE through the subunit, the sediment waves start changing towards an aggradational geometry. This shift in dynamic processes is observed with track 1 as boundary. Below track 1 progradation is more prominent. Above track 1 aggradation is more dominant.

Both track 1 (Fig. 21C) and track 2 (Fig. 21D) were mapped. By mapping these, the general directionality and migration could be discovered. Similar maps are observed as in the previously discussed relief map of H2.1 and H2.2, that again show a gradual deepening towards the basin. Track 1 shows a less steep region (~0.05° cf. ~0.21°) between 1.08 s TWT (~850 mbsl) and 1.16 s TWT (~914 mbsl). Track 2 also shows a less steep region (~0.05° cf. ~0.22°), but a bit more towards the southwest between 1.14 s TWT (~898 mbsl) and 1.22 s TWT (~960 mbsl). These regions of gentle slope represent the moment when the specific reflectors that were tracked start converging towards H2.2. Therefore, a line was added on both maps to illustrate where the crest (Fig. 17) of that track is located and is interpolated to cross all seismic lines (Figs. 22 C, D; Figs. 23 B, C).

A better visualization of the pathway of track 1 and track 2 was realised by creating isopach maps, where the thickness between both tracks and H2.2 was visualized (respectively Fig. 24B and Fig. 24C). In that way, the sediment waves are also straightened to remove the influence of the slope (as represented in the sketch on figure 20) and the converging character of the sediment waves becomes visible. On both isopach maps the general upslope thinning is clearly visible, with the steep converging feature prominent. For track 1 this feature manifests between a thickness of 20 ms TWT (~16.5 m) and 50 ms TWT (~41 m). The feature for track 2 manifests more to the southwest between a thickness of 10 ms TWT (~8 m) and 45 ms TWT (~37 m). The directionality of this converging feature seams to follow a NW-SE transect.

Another aspect recognized within sU3.2 is a convex shaped feature visible in the east on profiles P190606 (Fig. 23) and P190607 (Fig. 24). These are two WSW-ENE transect profiles that extend a little bit further towards the northeast in comparison to the other profiles. There should be taken into account that this structure is only observed in these two lines at the border of the research area and could not be recognized in other sections. This feature occurs at the end of SW1, where they start to show an aggradational trend. The feature is not recognized as a part of SW1 because the reflections start going upward towards the ENE side of the feature.

The convex shaped feature itself seems to move upslope on section P190606 (Fig.23), however it does not seem to move much on P190607 (Fig. 24). On the latter section, the feature is also smaller. Comparing both seismic profiles spatially, it seems that the feature has a NW-SE directionality. However, it should be mentioned that this is based on only two seismic lines, whereof interpreting spatial directionality is something to be vigilant about.

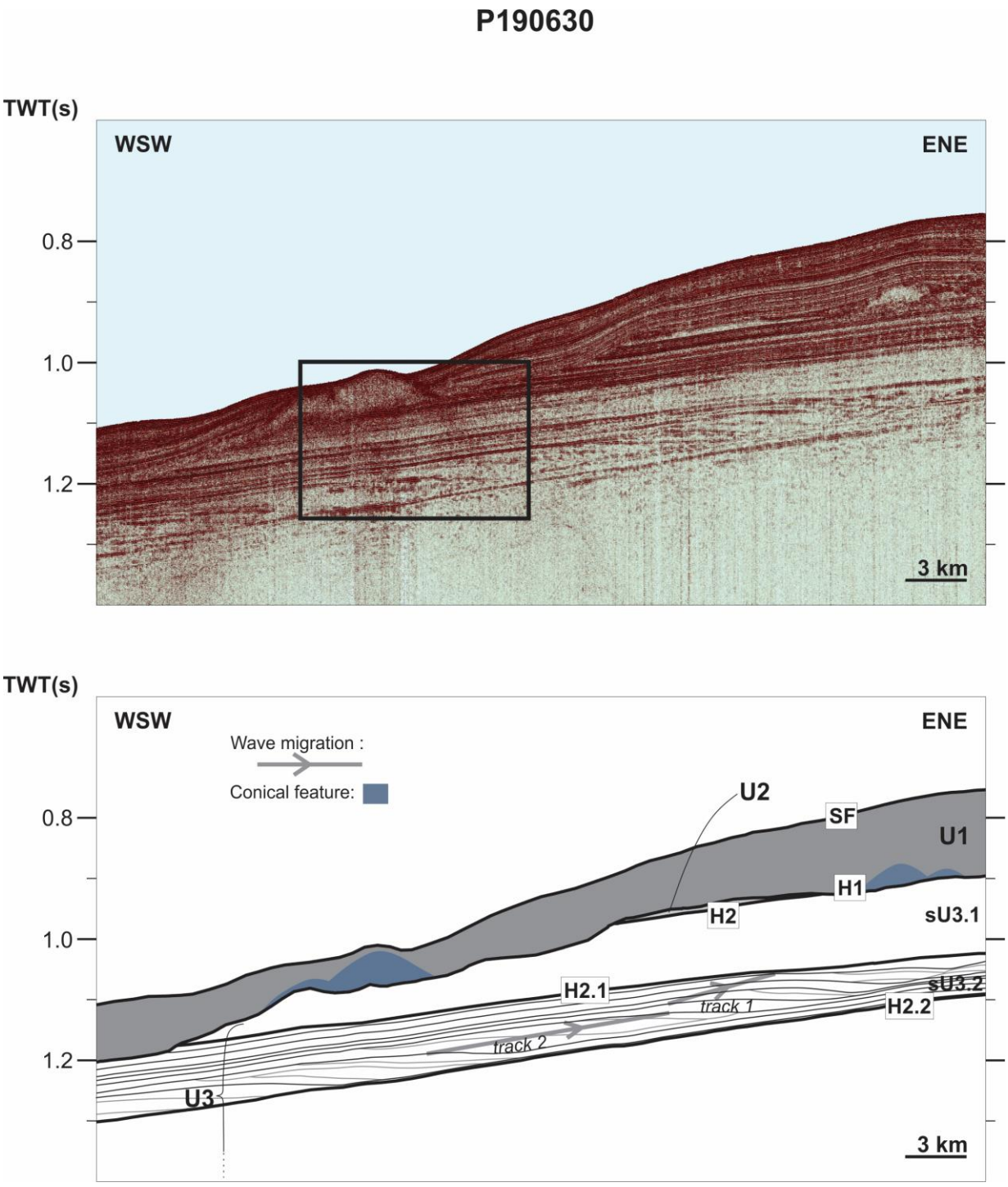


*Fig. 18: P190630 is a seismic profile tracked in the northern part of the research area in a WSW-ENE direction. In the upper image the full seismic line is represented from 0.6 s to 1.4 s TWT. A differentiation is made between horizons (thick black lines), reflectors (black) including the tracks and internal reflectors (grey). The (buried) conical features are represented in blue. The black box indicates the area taken for the detail image (Fig. 20).*

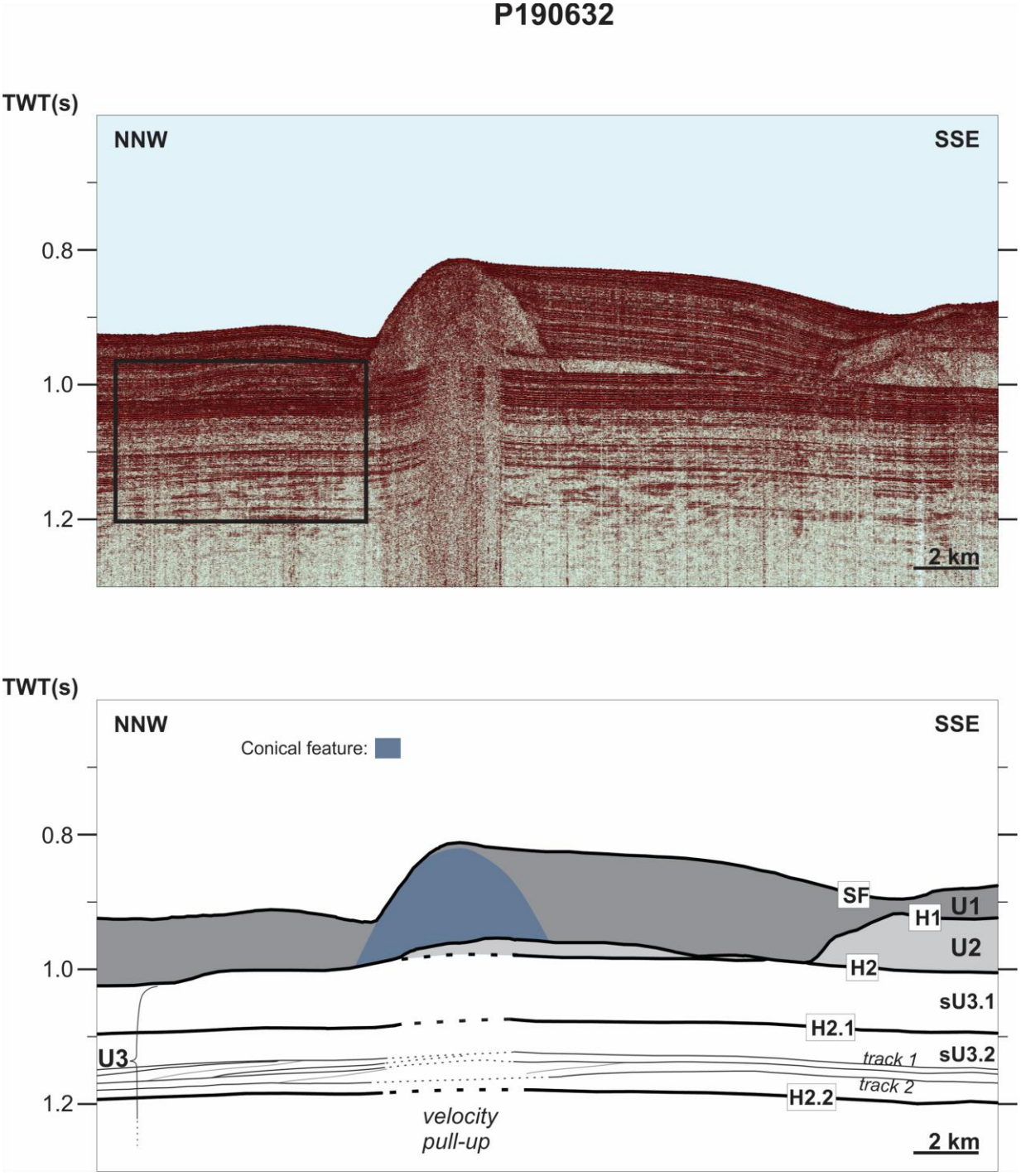


*Fig. 19: P190632 is a seismic profile tracked through the centre of the research area in a NNW-SSE direction. The seismic line is represented in the upper part of the figure, but only partly from shotpoint 1 to 1050 and from 0.6 s to 1.3 s TWT (Fig. 12). A differentiation is made between horizons (thick black lines), reflectors (black) including the tracks and internal reflectors (grey). The (buried) conical features are represented in blue. The black box indicates the area taken for the detail image (Fig. 20).*

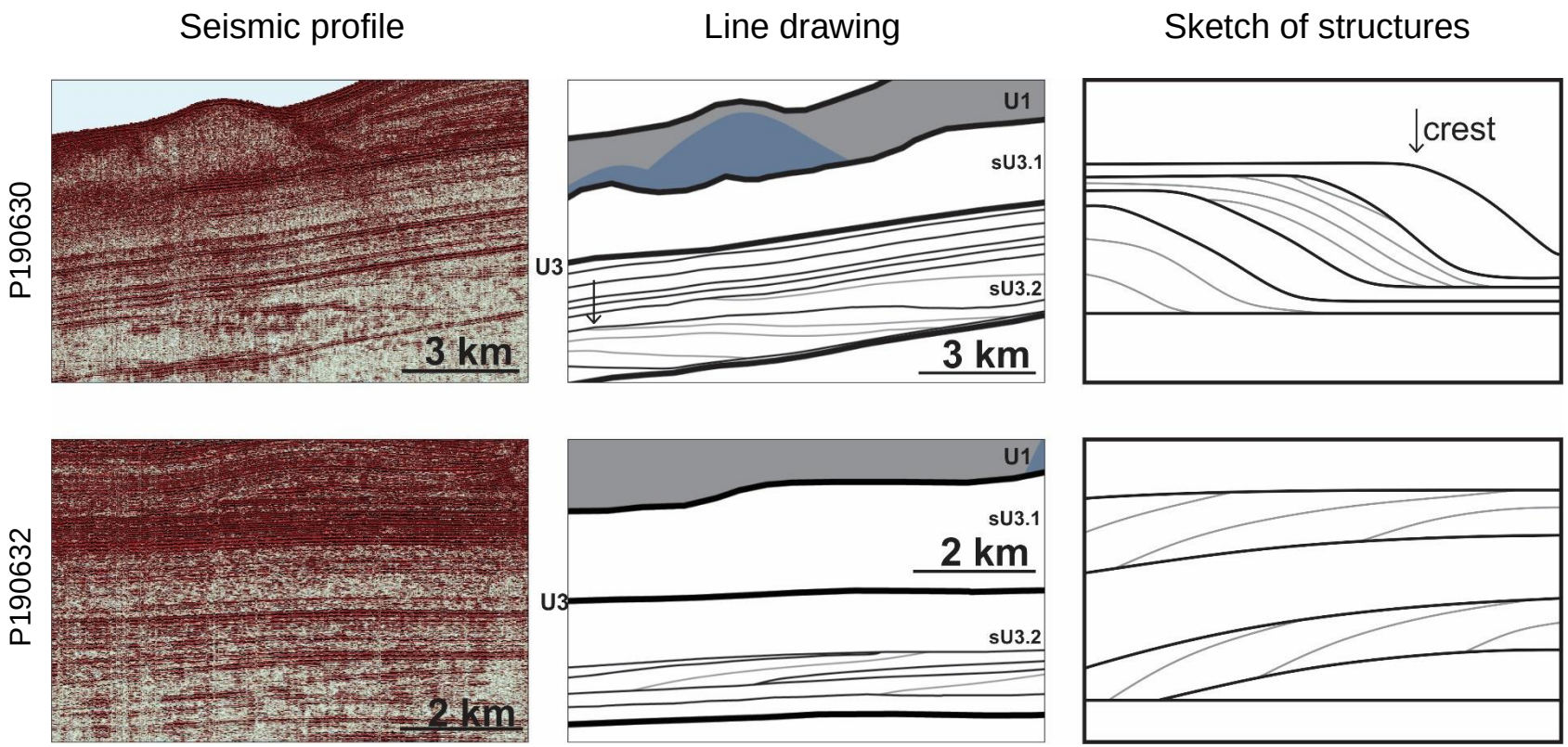


*Fig. 20: A more detailed view of the seismic profiles and line drawings from figures 17 and 19. A Sketch of the structures within subunit 2 was added to clarify the architecture of the sediment waves, and was based on all profiles combined. In the sketch the slope was rotated to a horizontal for additional clarity. The crest of the reflections is indicated on one reflector, both in the line drawing and sketch, with an arrow.*

GHENT UNIVERSITY

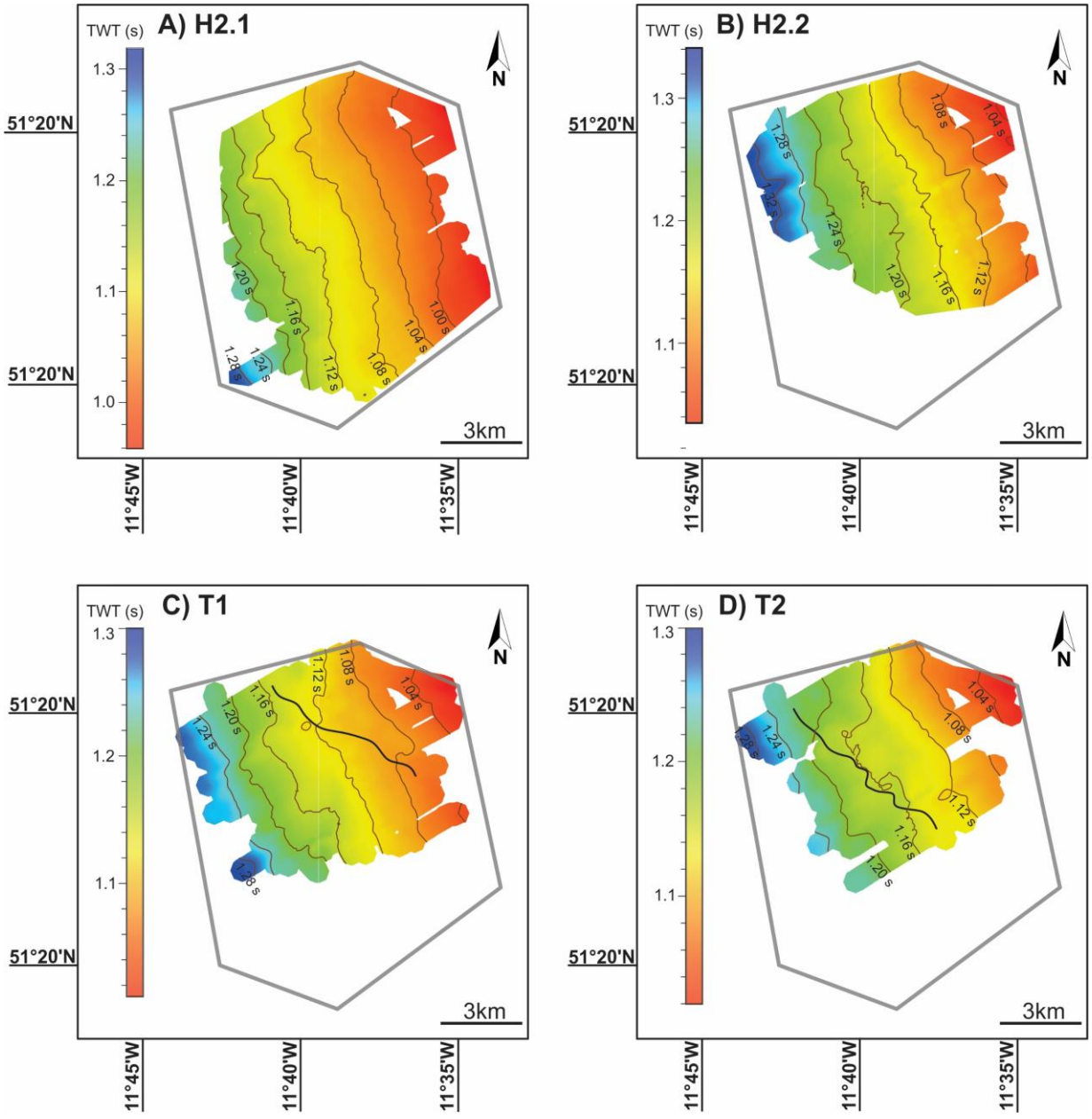


*Fig.21: Relief maps of horizons H2.1 (A) and H2.2 (B), and of tracks T1 (C) and T2 (D) with a contour every 0.04 s TWT (~30 m). The grey area shows the survey area as displayed in figures 12 and 17. In image C and D the black line represents the alignment of the crests of both wave tracks.*

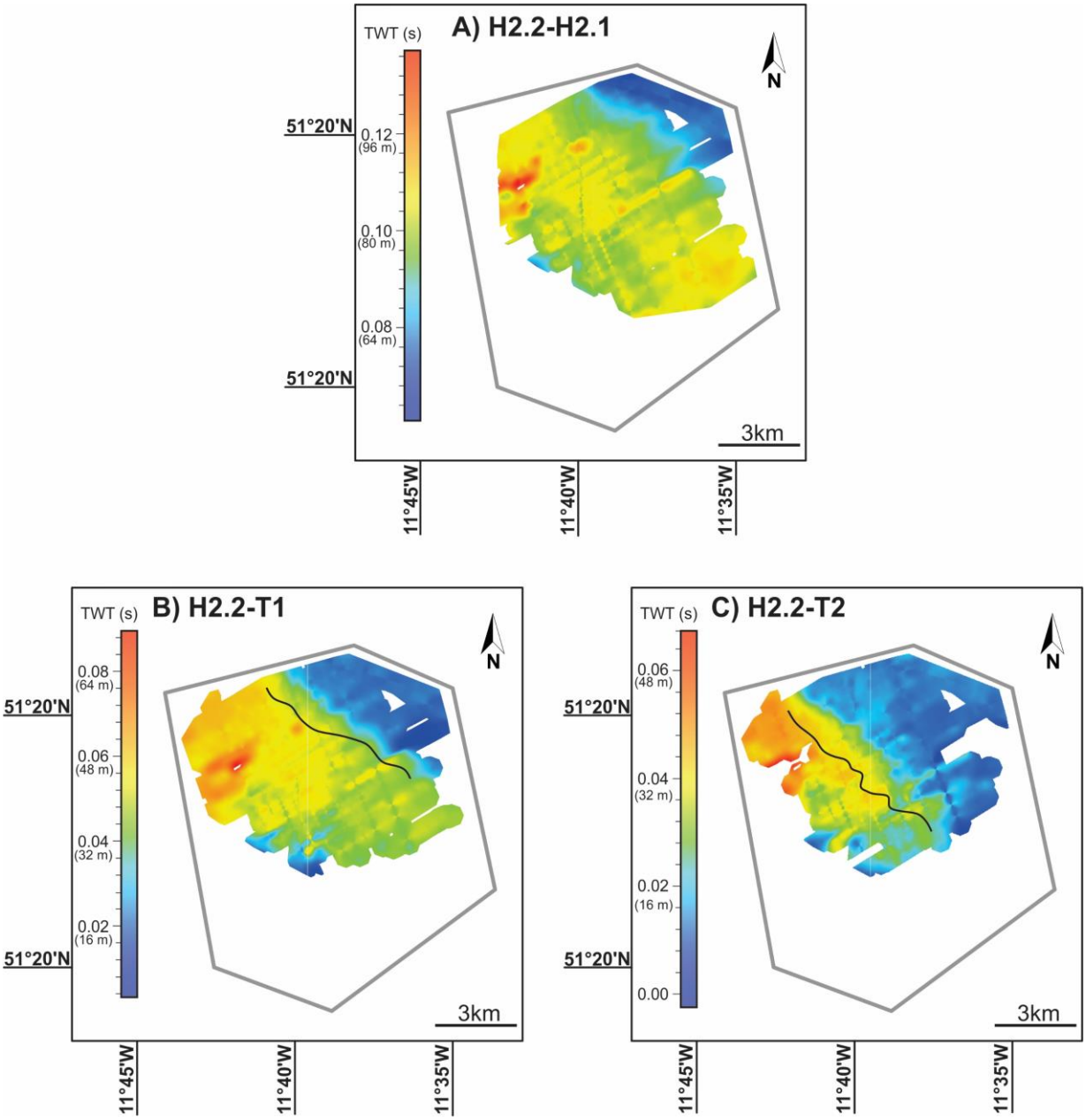


*Fig. 22: Isopach maps from A) subunit 3.2; B) Track 1 to H2.2; C) Track 2 to H2.2. The grey area shows the survey area as displayed in figures 12 and 17. In image B and C the black line represents the alignment of the crests of both wave tracks.*

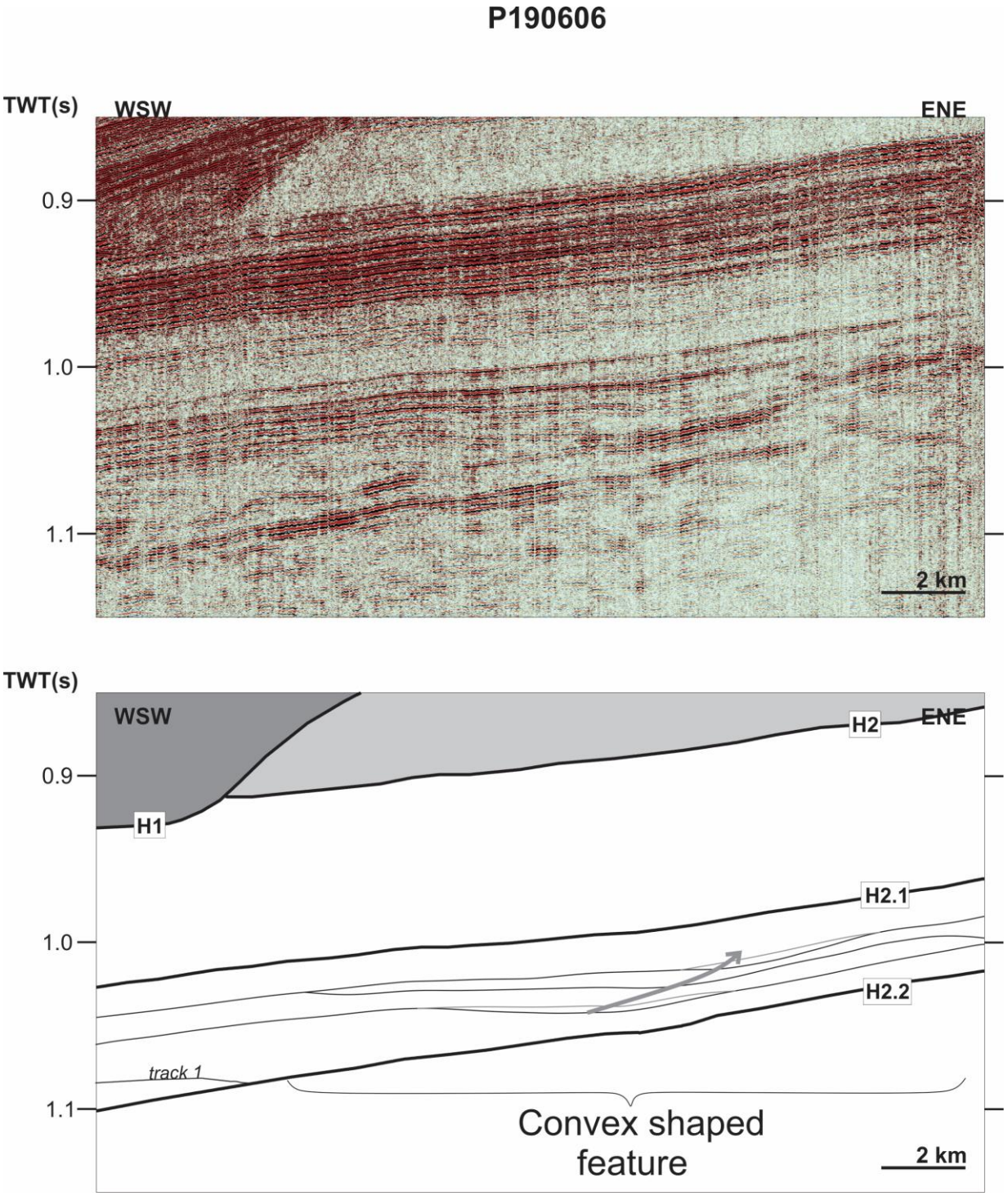


*Fig. 23: P190606 is a seismic profile tracked in the north-western part of the research area in a WSW-ENE direction. The seismic line is partly represented in the upper part of the figure, from shotpoint 1 to 800 and from 0.85 s to 1.15 s TWT (Fig. 12). A differentiation is made between horizons (thick black lines), reflectors (black) including the tracks and internal reflectors (grey). The arrow marks the movement of the channel.*

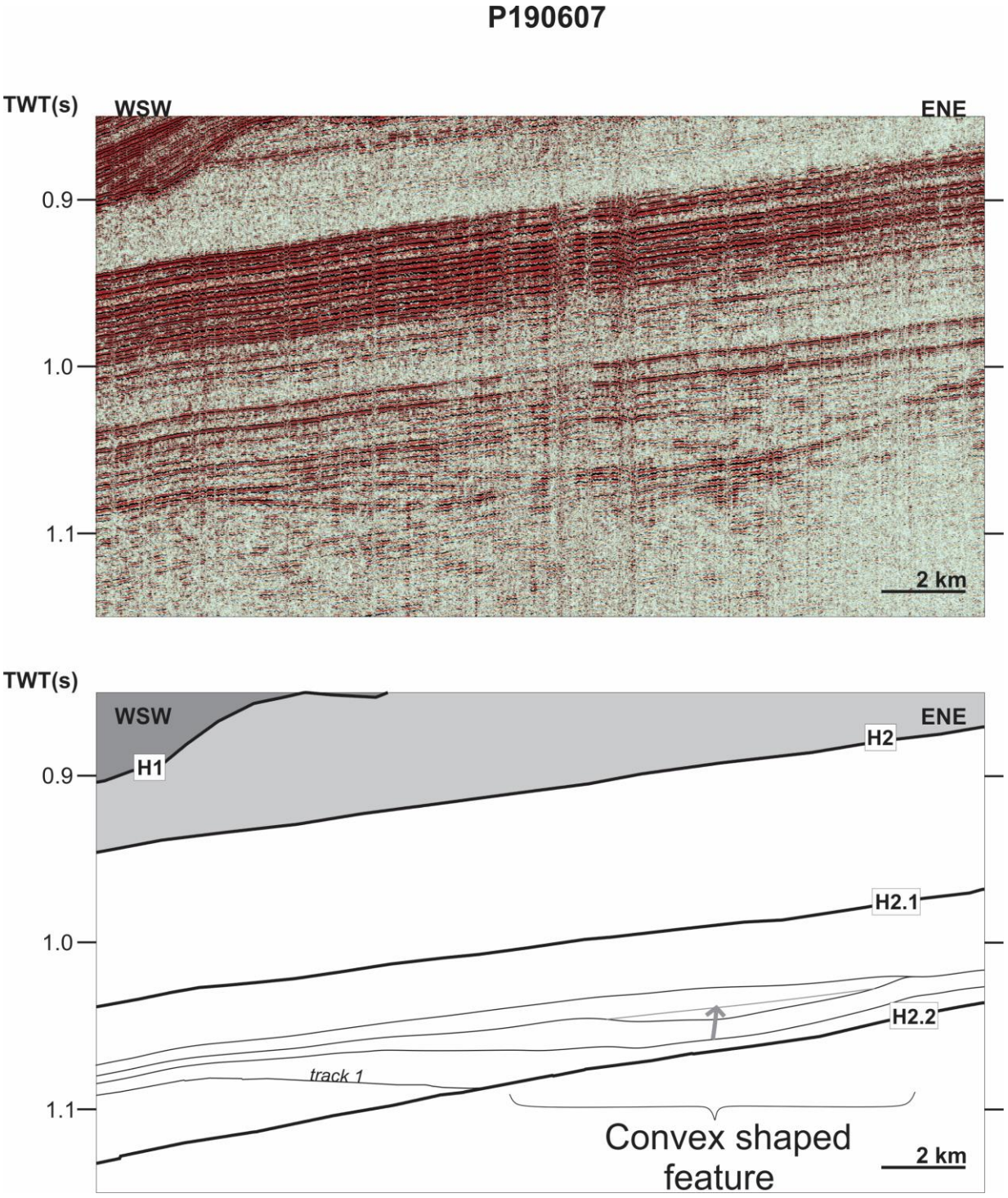


*Fig. 24: P190607 is a seismic profile tracked in the north-western part of the research area in a WSW-ENE direction. The seismic line is partly represented in the upper part of the figure, from shotpoint 1554 to 2354 and from 0.85 s to 1.15 s TWT (Fig. 12). A differentiation is made between horizons (thick black lines), reflectors (black) including the tracks and internal reflectors (grey). The arrow marks the movement of the channel.*

### 9.2.2 Sediment waves 2

The second set of sediment waves (SW2) are observed in the southwestern part of the study area. These undulations are much less a model example of sediment waves. The characteristics, migration pattern and directionality were much harder to distinguish due to its irregularity and poor lateral continuity. In some parts in the centre of the survey area the sediment waves can slightly overlap SW1 (Fig. 17). Both NNW-SSE (Fig. 25) and WSW-ENE (Fig. 26) profiles show a chaotic character and hummocky (Fig. 14) undulations. However, the undulations in the WSW-ENE transects are slightly less chaotic than those on the NNW-SSE transects. An average estimation was made of the wavelength being ~700 m and of the wave height being ~20 m.

Once more, two types of reflector configurations were recognized in figures 25, 26 and 27. Firstly, there are the reflectors that continue over a larger part of the section and eventually downlap or toplap other reflectors (black lines; Figs. 25, 26 and 27). In contrast to the previous type of configuration, the second type of reflectors is expressed on a smaller scale. The second type of reflectors can be regarded as internal reflectors (grey lines; Figs. 25,26 and 27) downlapping or toplapping within the first set of reflectors.

The hummocky character, best observed in the NNW-SSE profiles, comes from the erosion on one flank and the redeposition on the other flank (Fig. 27). In this case the erosion flank of all the undulations switches between upslope and downslope flank easily, but it is occurring more on the downslope flank.

The track visualization was also attempted with the second set of sediment waves (SW2), but failed due to the lack of lateral continuity. Reflectors could not be mapped well throughout the different profiles. Therefore, no relief maps nor isopach maps could be realized to observe directionality and migration pattern.

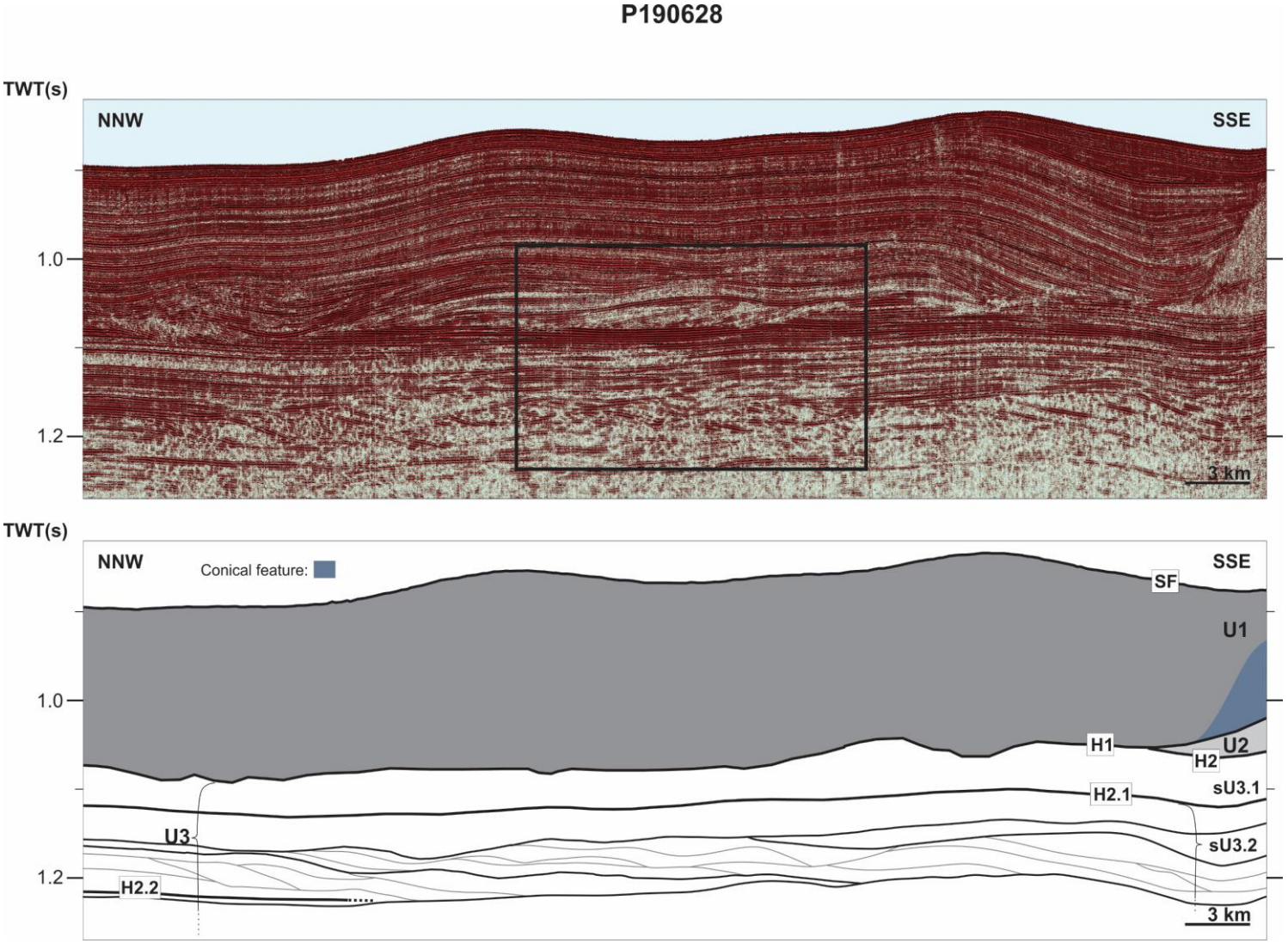


*Fig. 25: P190628 is a seismic profile tracked through the western part of the research area in a NNW-SSE direction. The seismic line is partly represented in the upper part of the figure, from shotpoint 50 to 2050 and from 0.82 s to 1.27 s TWT (Fig. 12). A differentiation is made between horizons (thick black lines), reflectors (black) including the tracks and internal reflectors (grey). The (buried) conical features are represented in blue. The black box indicates the area taken for the detail image (Fig. 27).*

GHENT UNIVERSITY

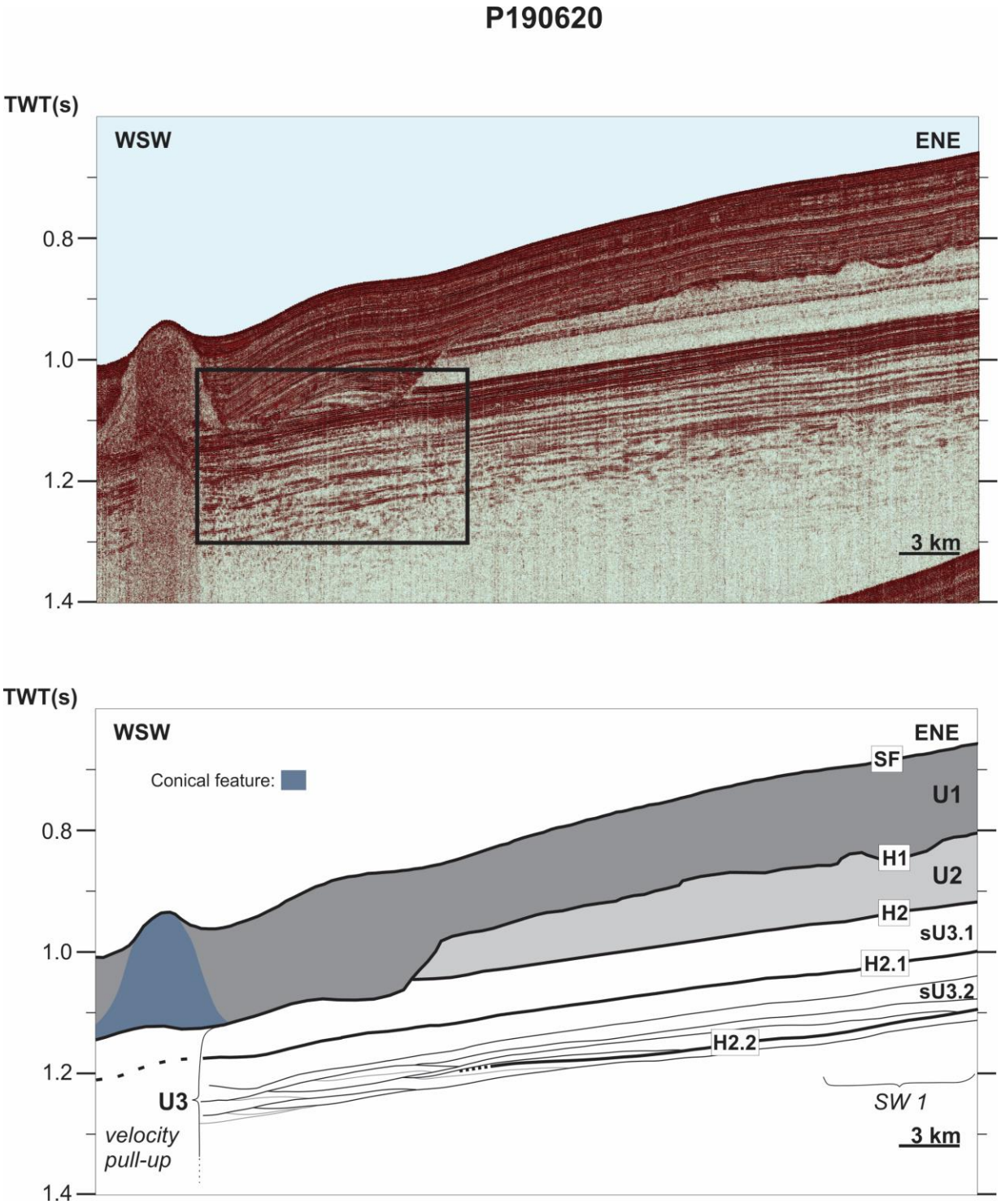


*Fig. 26: P190620 is a seismic profile tracked in the southern part of the research area in a WSW-ENE direction. The seismic line is fully represented in the upper part of the figure from 0.6 s to 1.4 s TWT. A differentiation is made between horizons (thick black lines), reflectors (black) including the tracks and internal reflectors (grey). The (buried) conical features are represented in blue. The black box indicates the area taken for the detail image (Fig. 27).*

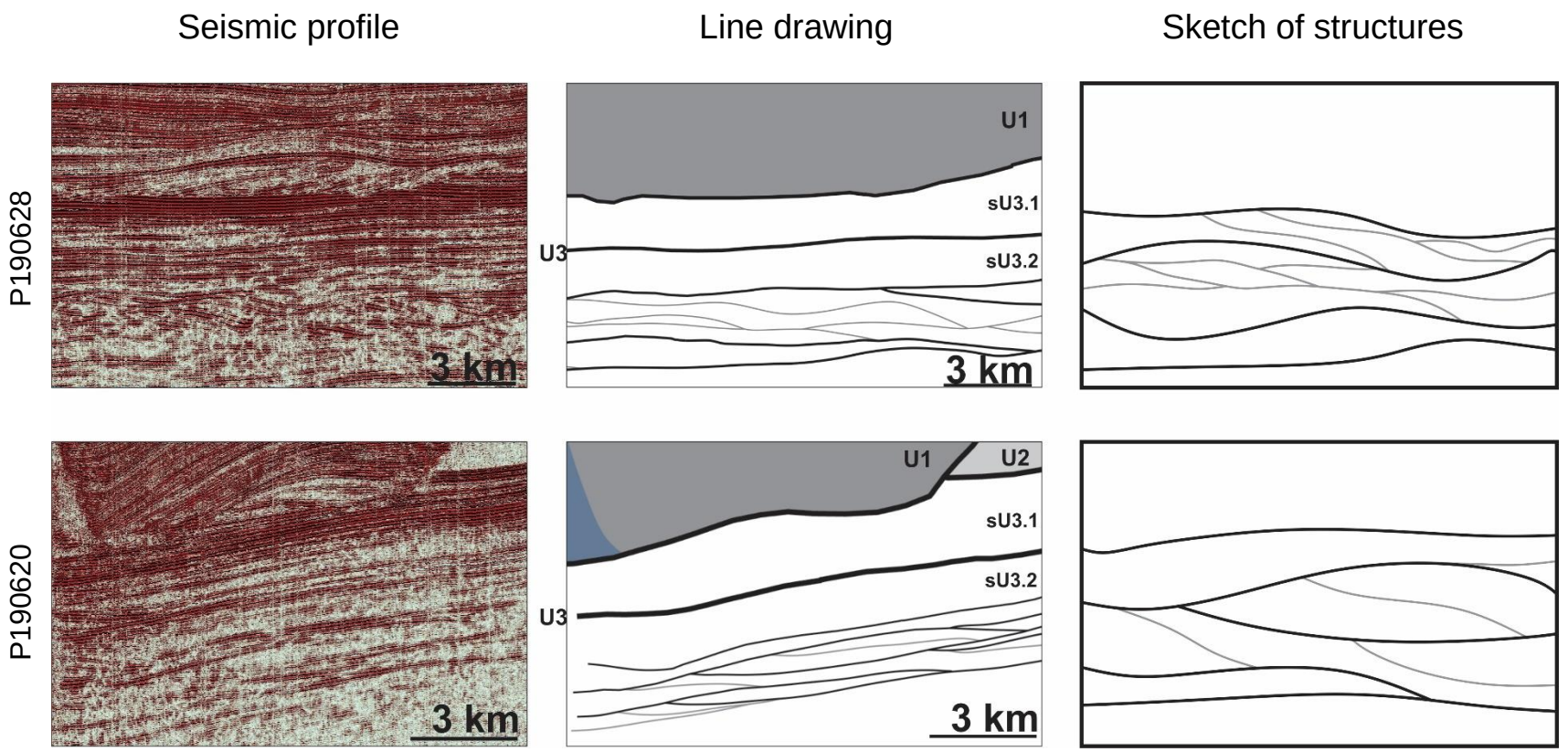


*Fig. 27: A more detailed view of the seismic profiles and line drawings from figures 25 and 27. A Sketch of the structures within subunit 2 was added to clarify the construction of the sediment waves, and was based on all profiles.*

GHENT UNIVERSITY

# 10 DISCUSSION

## 10.1 Seismic stratigraphy

The Neogene stratigraphy within this study area has been examined extensively by Van Rooij et al. (2003, 2007) and Huvenne et al. (2009). Their studies will be compared with the data obtained in this dissertation (Fig. 28). This will elucidate on the formation history of the corresponding units and horizons. The nomenclature used by Van Rooij et al. (2007) will be applied where possible, and will be used for further discussion.

The lowermost unit U3, separated in two subunits sU3.2 and sU3.1, is characterised by seismic facies for both calm and less calm depositional environments. Complex/sigmoidal (SW1) and hummocky (SW2) sediment configurations were recognized within sU3.2, where they occur on the same depth level within the seismic profiles and thus were formed at roughly the same time. sU3.1 represents the sedimentation during a calm depositional environment with its linearly stacked reflectors. This unit has no lower boundary due to the limit of vertical penetration. Unit 3 is described by Van Rooij et al. (2007) but shows a lower boundary in the case of the presence of downlapping sigmoidal features and a 4th unit U4 is defined beneath (Fig. 28). This horizon defining the boundary between U3 and U4, seems to coincide with H2.2. However, H2.2 is not defined by the downlapping of these structures. It seems that the horizon defined by Van Rooij et al. (2007) crosses reflectors through the structure of SW1. Also H2.2 is a horizon that becomes untraceable in the chaotic seismic facies of SW2, which is why it was not considered as a horizon dividing two units, but rather two subunits. No subunits were described in literature, which is why the nomenclature for these two is maintained, together with both their horizons. U3 is bound on top by RD2. This horizon coincides with H2 in this research (Van Rooij et al., 2003; Fig. 28). RD2 is thought to be of early mid-Miocene age (Louwye et al., 2008). It is assumed to be related to late pulses of the Alpine Orogeny and major plate reorganization (McDonnell and Shannon, 2001) and could be linked to bottom currents introduced by the initiation of Norwegian Sea water in the Nord Atlantic (de Graçiansky et al., 1985). The associated hiatus is thought to be of minor magnitude because it is not reflected as a clear break in the palynological record (Louwye et al., 2008).

The middle unit U2, bound on top by the erosive horizon H1, is an acoustic transparent unit containing the occasional high amplitude reflector. This unit was also defined by Van Rooij et al. (2007). The horizon H1 is equal to RD1 defined by Van Rooij et al. (2003; Fig. 28). The erosional event that RD1 defines, eroded most part of U2 and also some of U3. Data from Kano et al. (2007) and Louwye et al. (2008) infer that RD1 represents a long hiatus between the late Miocene and late Pliocene. The oceanographic change that induced such large erosive event must have been of great scale (Van Rooij et al., 2009). Van Rooij et al. (2003) proposed the introduction of the MOW as a possible onset for this erosive event.

The low-amplitude conical features observed within the uppermost unit (fig. 28) are interpreted as cold-water coral mounds (De Mol et al., 2002). These CWC mounds are in this survey area only settled on RD1, which is an erosive surface that marks the onset of the glacial and inter-glacial cycles and with that also the onset of the modern oceanographic regime (Van Rooij et al., 2003). This means that in this survey area no coral mounds were settled on the sediment waves. Van Rooij et al. (2003) suggested that there could be a connection between both, but this is thus not the case within this research area. It is considered that by the

late Pliocene the corals have successfully colonized the appealing environment of this erosional event that RD1 represents (Ferdelman et al., 2006c).

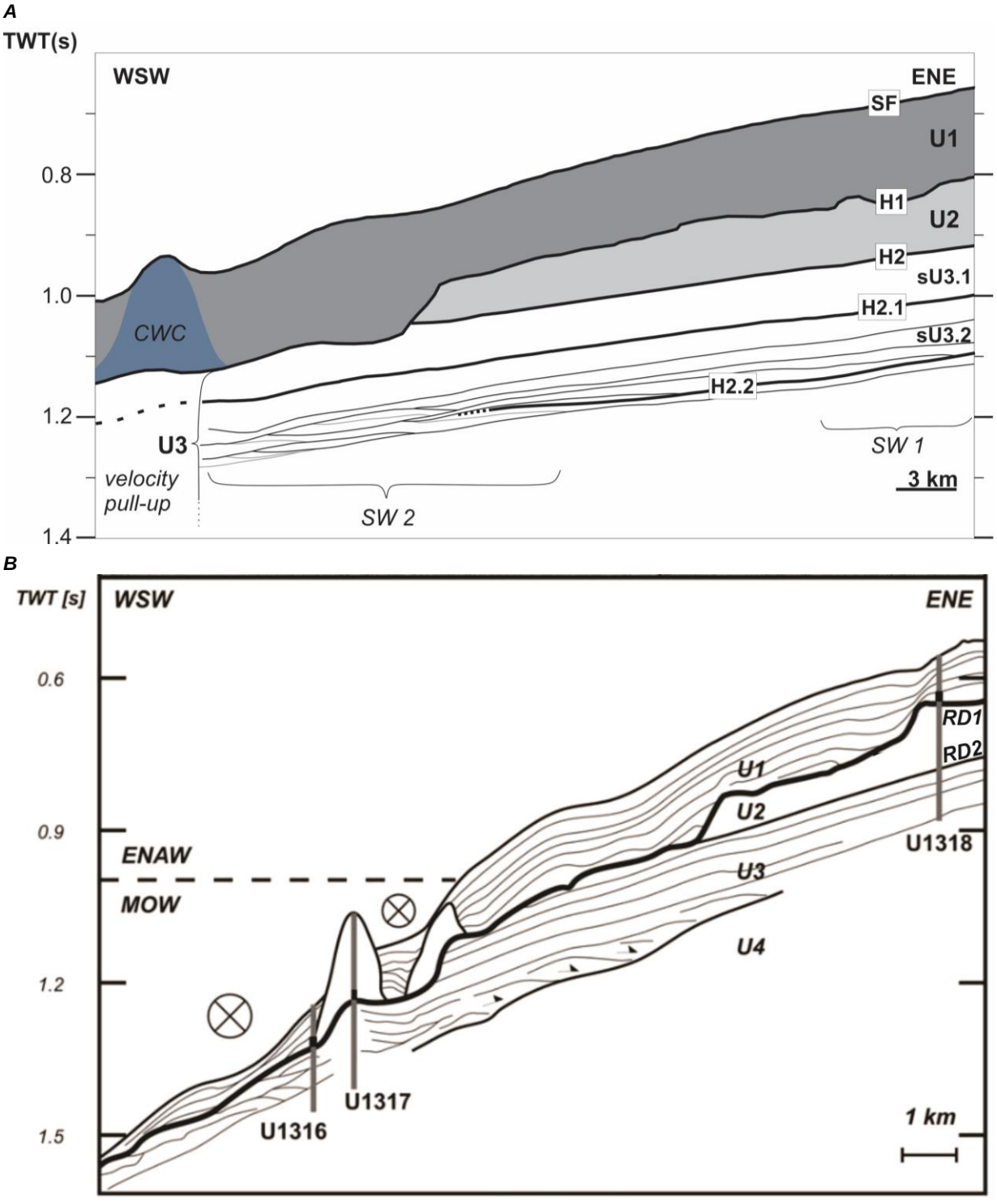


*Fig. 28: Comparison of the seismic stratigraphy with literature A) line drawing of P190620 showing both SW1 and SW2; B) line drawing of a seismic profile showing the three drill sites with seismic units U1 through U4 marked (Van Rooij et al., 2007) and the depth of the interface between the MOW and ENAW; modified after Huvenne et al. (2009).*

The uppermost unit (U1) comprises of parallel bedding with some elongate mounded packages close to the CWC mounds. This unit is the same as U1 defined by Van Rooij et al. (2007; Fig. 28). The mostly progradational feature within this unit are elongate sediment drifts that are part of the current contourite regime oceanography within this area. Wherein, the CWC mounds play a big role in the bottom topography and thereby influencing the bottom currents (Van Rooij et al., 2003). This drift sedimentation is thought to have started later than the settlement of the CWC mounds, namely from the middle early Pleistocene (Kano et al., 2007; Van Rooij et al., 2007).

## 10.2 Uncovering the sediment wave dynamics

Both types of sediment waves will be discussed separately in this section since they display different geometries and localities. Based on the sediment facies and geometries of the sediment waves, the genetic processes can be assessed. Afterwards both will be compared spatially with each other to determine the local oceanographic processes.

### 10.2.1 Sediment waves 1

The first set of sediment waves have a complex/sigmoidal architecture (Fig. 20) and were formed on a slope of about ~0.2°. They show a general asymmetrical geometry with their crests closer upslope (Fig 20). The sediment waves show a progradational to aggradational migration pattern (Fig. 18). Sigmoidal clinoforms showing aggradation usually suggest a high rate of sediment supply (Nanda, 2016). This could indicate that these sediment waves started with a low rate of sediment supply and changed to a higher rate of sediment supply. Their crests are aligned along-slope, slightly diagonally (~21° cf. isobaths in horizontal plane) with a NW directionality (Fig. 22B, C). Internally the sediment waves show a downlapping seismic facies (Fig. 20). The wave dimensions were estimated with the wavelength and wave height, respectively at 2-3 km and 30 m.

Sediment waves formed by turbidity currents occur most of the time close to canyon or channel systems (Lee et al., 2002). Taking into account that no major downslope channel or canyon features were observed within the present-day bathymetry, it seems less likely that these sediment waves could have been formed by turbidity currents. On the other hand, the crest are more or less aligned perpendicular to the slope, which also occurs in turbidity formed sediment waves (Wynn and Stow, 2002; Fig. 22B,C). However, the undulating, climbing bedforms (Cartigny et al., 2011) are not recognized in SW1, where a more progradational migration without cyclic steps is observed (Fig. 20). For these reasons, it seems not likely that turbidity currents were related with the formation of SW1.

Gravity-driven mass transport usually occurs on a steep slope, which is generally taken at >10°, but can in some cases also occur on less steep slopes (Faugères et al., 2002a). But still, because of the low slope angle this system is less likely to have formed the sediment waves. Also no extensional or compressional characteristic elements were observed within sU3.2 (Fig. 20), but they could also just not be visible. However, sediment waves formed by deformation do not show lateral migration, but rather a random scatter of dimensions (Wynn and Stow, 2002). SW1 have a migration pattern and also internally show downlapping in one specific dimension, namely upslope towards the ENE (Figs. 18, 20). For these reasons there was concluded that SW1 are not related to gravity-driven mass transport.

The sediment movement with internal waves is generally bidirectional in deep-water environments. However they can have a net downslope component (Hotchkiss and Wunsch, 1982; Karl et al., 1986; Pomar et al., 2012). This creates crests aligned to the slope isobaths (Ma et al., 2016), which is the case with the crests of SW1 (Fig. 22B, C). Large-scale sediment waves have diagnostic approximate sinusoidal curves (He et al., 2008). This cannot be observed in the sediment waves in this survey area (Figs. 18, 19, 20). Internal waves can occur very locally and can have a very variable intensity (Pomar et al., 2012). However, internal-wave deposits are very variable and definitive criteria are still underdeveloped (Pomar et al., 2012; Ribó et al., 2016b). This is why there cannot be concluded with certainty if internal waves are related to the formation of the sediment waves or not.

Contour currents are along-slope currents, where the sediment wave crests are formed usually diagonally to the dominant flow (Wynn and Stow, 2002). This is the case with these sediment waves. Contour currents usually flow over long distances and are generally strong (Masson et al., 2002). Due to the many varieties within contourite drift deposits (Fig. 2D), this dynamic system could be an option when considering it as the formation dynamic for SW1. If so, the most likely contourite drift system would be an elongated drift, because of the internal downlapping seismic facies (Fig. 20). The contour current could have moved upslope through time to form these prograding bedforms (Fig. 18). The convex feature recognized in the northeastern side of the area (Figs. 23, 24) could be the moat where this contour current flowed through. But the wave dimensions are on the smaller side, especially the wave height when comparing to the dimensions defined for this type of dynamic process. Fine grained contourites can have wavelengths up to 10 km and wave heights up to 150 m.

In a study by Roveri (2002, P67) of the Corsica Channel contourites in the Tyrrhenian Sea, similar sediment wave configurations were recognized. Figure 1D shows an upslope migration of an elongate drift and can be compared with the sediment waves observed in the WSW-ENE transects (Fig. 20). The sediment drifts of the Corsica Channel show a more aggradational wave geometry in comparison to those presented in figure 18. However, at the eastern end of SW1 in the WSW-ENE transects a transition was observed from progradation to aggradation. These sediment waves with a more aggradational character (Fig. 18) show better similarities to the sediment waves in the Corsica Channel (Fig. 1D). If SW1 are considered elongate drifts, it is likely that the more progradational character was formed due to an upslope movement of the along-slope flow.

### 10.2.2 Sediment waves 2

The other sediment waves located more to the southwest of the area (Fig. 17) are characterized by chaotic seismic facies and hummocky undulations (Fig. 27). No migration pattern or other dimensions could be determined due to the poor lateral continuity of these sediment waves. The internal reflectors show downlapping and toplapping facies (Fig. 27). An average estimation of the wavelength and wave height are respectively ~700 m and ~20 m.

Turbidity formed sediment waves also seem less likely to have formed SW2, for the same reason as for SW1 that no major downslope channel or canyon features were recognized. However, the crest alignment or migration pattern, respectively perpendicular to slope and upslope for turbidites, were of no use to determine these sediment waves due to their poor lateral continuity. But the lack of crest alignment and migration pattern is also a determining factor to discard the relationship of turbidity currents with these sediment waves.

For gravity-driven mass transport, the same applies as with SW1. The slope was not that steep and no extensional nor compressional elements were observed. However, sediment waves formed by deformation do not show lateral migration, but rather a random scatter of dimensions (Wynn and Stow, 2002). The chaotic and random character of SW2 could thus be related to gravity-driven mass transport, but the slope angle is too small for that (~0.2°).

Due to the poor lateral continuity with these sediment waves, there is a lack of information on the crest alignment or migration pattern of SW2. With internal wave deposits, crests are aligned parallel to the isobaths of the slope (Ma et al., 2016). According to Pomar et al. (2012) a hummocky character can be caused by internal wave dynamics. However, the general characteristics of internal wave deposits are still underdeveloped (Pomar et al., 2012; Ribó et al., 2016b). Thus internal waves may have formed these sediment waves.

Also for contour currents the crest alignment cannot tell everything. The estimated wave height and wavelength seem a bit too low for the waves to be contourites. Wave dimensions in fine grained sediments can go up to a wavelength of 10 km and a wave height of 150m (Wynn and Stow, 2002). However, contourite deposits are very diverse in morphology (Fig. 2D), which is why this dynamic system cannot be excluded, together with internal waves. A channel related contourite drift (Fig. 2D) usually shows random lateral migration and hummocky configurations (Rebesco and Stow, 2001), which SW2 also shows. Nonetheless, these channel related contourite drifts are formed in confined basins or channels (Rebesco et al., 2014), but this is not the case with SW2. So according to the general model for contourite morphologies (Fig. 2D), these sediment waves could not have been formed by contour currents.

In any case, it is clear that these sediment waves have been formed in a high-energy depositional area. Their chaotic character alone indicates a link to a high-energy deposition (Nanda, 2016). Turbidity currents can definitely be excluded together with gravity-driven mass transport and there is a high probability for the sediment waves to be related to internal waves. They could also be related to a combination of multiple dynamic systems, which could explain the chaotic character, the lack of lateral continuity and the inability to map these features. An example could be a combination of contour currents and internal wave dynamics (Rebesco et al., 2014). These would create the existence of an along-slope component together with a bidirectional upslope and downslope component.

### 10.2.3 Spatial comparison of the sedimentary waves and their dynamics

The hydrodynamic processes behind both sediment wave types may be related to either contour currents or to internal waves action. The interpreted sediment waves are located at more or less the same level and can thus be spatially and stratigraphically related to each other. This is visible on figure 16 where both sediment waves are present and reflectors are laterally continued from the first set of sediment waves to the other. Hence, the sediment waves are situated on the same level and should have been deposited at more or less the same time. This leads to think that the dynamic systems that formed both sediment waves were related to one another.

Nevertheless, the first set of sediment waves seems to be best related to contour currents. With the crest aligned slightly diagonally to the slope and thus flow direction. Their internal downlapping facies leading to think about elongate drift depositions. The progradation trend could then be explained by an upslope

movement of the current causing the deposition of the elongate drift also to move upslope (Fig. 29). On the other hand, the second set of sediment waves seems to be most likely formed by internal waves. With their hummocky undulations and random lateral migration, all other processes could be excluded. Of course, a multi-dynamic system with the influence of both internal waves and contour currents could also explain the chaotic character. This means that also SW1 might have been influenced or formed by internal waves.

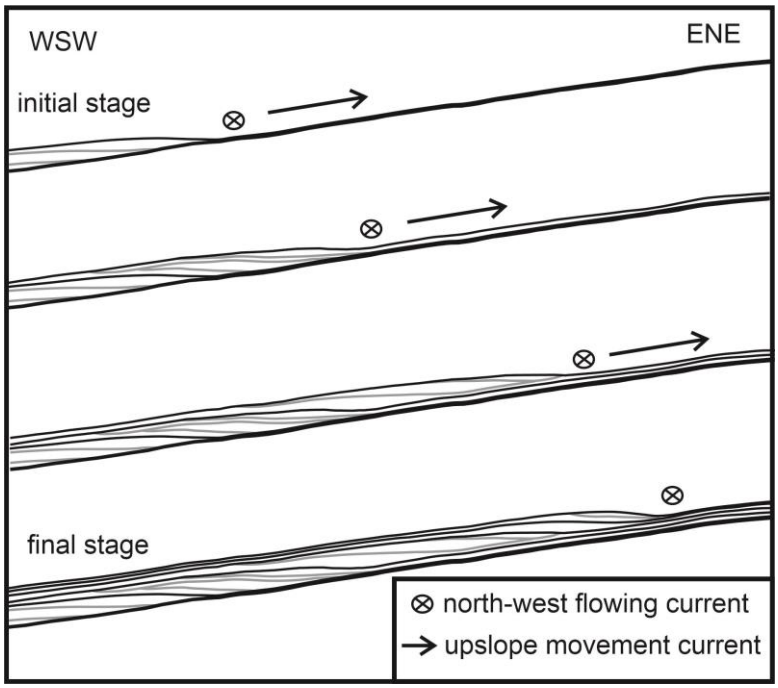


*Fig. 29: A representation of SW1 formed by an upslope moving contour current.*

Figure 30 visualizes a formation model where both sediment-waves were influenced by a combination of internal waves and contour currents. Here it is considered that the first set of sediment waves were formed mostly by contour current influence and a minor influence of internal waves. While the second set of sediment waves were less influenced by the contour current and more by the internal waves. In an initial stage the influence of internal waves would have been larger then at a later stage. This change of major to minor influence may be explained by changes in sea level that can cause weakening or strengthening in the energy of the internal waves (He et al., 2008; Zhenzhong et al., 2013). The formation model presented here is only one possible interpretation. There are still other options. Both could be formed by internal waves or both may be formed by contour currents. It could also be that this formation model is too simple and a more complex situation occurred.

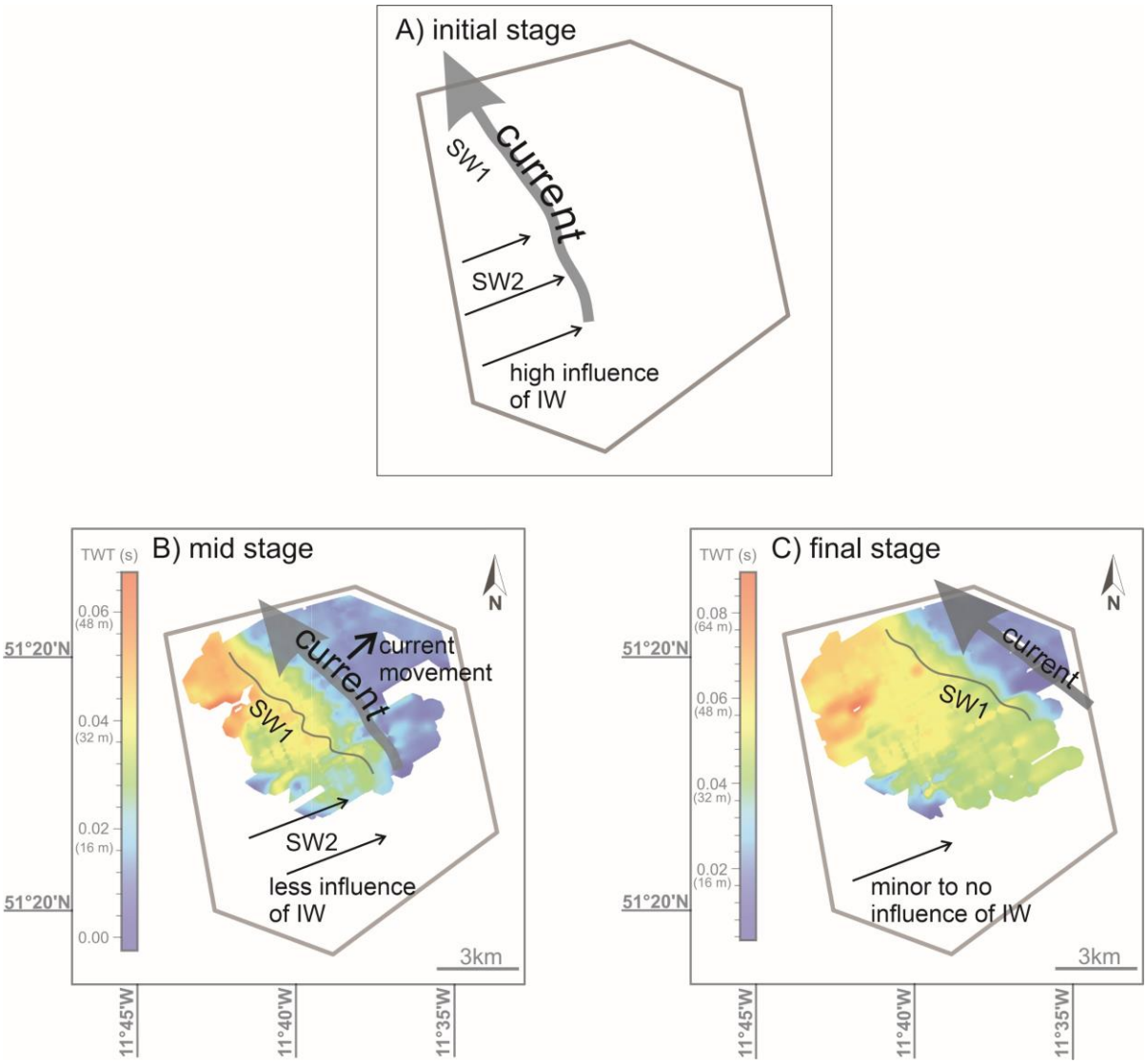


*Fig. 30: A formation model of SW1 and SW2 influenced by both a contour current and internal waves (IW). The influence of internal waves is stronger in the initial stage and diminishes towards a later stage. It was chosen to visualize this representation of the mid and final stage on top of the isopach maps (Fig. 22B C), because these show the sediment wave architecture very well at two different moments in time.*

## 10.3 Origin of the oceanographic changes

For contour currents to have formed the sediment waves, in the research area on the eastern slope of the Porcupine Seabight, an along-slope deep-water current arising from thermohaline circulation needs to be present. For determining sediment waves formed by internal waves, the oceanographic setting is a very important factor. However, this is rather difficult in this case considering these are palaeo-sediment waves that formed somewhere before the early-middle Miocene. The presence of internal waves requires an interface between two water masses with a high contrast in density and temperature (Cullen and Ivanov, 2020).

Due to the sparse knowledge about the Miocene palaeoceanography, it becomes difficult to form an interpretation on the origin and flow direction of the contour current that flowed through the PSB, or the water masses present in the PSB. The NADW was still underdeveloped during the Miocene and only started intensifying around 4.6 Ma (Haug and Tiedemann, 1998). Due to a deepening of the Greenland-Scotland Ridge a major deep-water flow could have been initiated around 11.5 Ma from the Nordic Seas into the North Atlantic (Wright and Miller, 1996; Wei and Peleo-Alampay, 1997). Quaijtaal et al. (2014) interpreted a possible strengthening of the northerlies within the Porcupine Seabight during the middle Miocene. These several possible flow origins leave the interpretation of the flow direction in the PSB open for discussion. Considering these possible intensifying currents, a contour current could have shaped the eastern slope of the PSB. For internal waves on the other hand, there is less evidence concerning a water-mass with a high density or temperature contrast. The influence of MOW seems unlikely because the closure of the Eastern Tethys only occurred from the middle Miocene and thus a connection between the Southern Ocean was still established (Butzin et al., 2011). A strong Labrador current has been suggested to be present from 46 Ma onwards in the western North Atlantic and could have caused a density/temperature difference due to its very cold and low salinity characteristics (Egger et al., 2018). A first onset of LSW deep-convection is thought to be the cause of the deep-water stratification change in the Atlantic between 10.6 Ma and 7.3 Ma (Thomas and Via, 2007; Butzin et al., 2011). From the latest Oligocene, bottom water temperature increased while the extend of the Antarctic ice sheets reduced. This warming continued up to the Middle Miocene Climatic Optimum. Hereafter, from 14.5 Ma, a cooling phase was initiated (Zachos et al., 2001; Böhme, 2003). These warm bottom waters together with early cold LSW pulses may have caused an interface where internal waves may have occurred.

It is remarkable that the sedimentary features only occur within sU3.2. In sU3.1 bottom current influence is nowhere to be seen. It looks like a certain flow strengthened suddenly, but later faded or disappeared. The duration of deposition for these sediment waves can be estimated comparing to data from the IODP expedition (Ferdelman et al., 2006a). In core U1316 a lithological subunit 3A is defined with an age of 15.6-18.3 Ma (Ferdelman et al., 2006c; Fig. 10). This youngest age was reassessed with strontium isotope dating ($^{87}Sr/^{86}Sr$) at 16.58 Ma (Kano et al., 2007). The lithological unit was correlated to the seismic profile (Fig. 10) and seems to coincide with the average thickness of the package of sediment waves (Figs. 18, 26) being 0.1 s TWT (~82.5 m). This core was taken more to the WSW of the profiles in this research and consequently caution should be taken when correlating and extrapolating. There can thus be estimated that the sediments were deposited over a period of about 2 Ma, considering a continuous sedimentation rate equal to the one at site U1316. This may have been a short pulse/strengthening before the real onset of the Norwegian Sea water into the North Atlantic, which is represented by H2 (de Graçiansky et al., 1985), or it could have been a strengthening pulse in the NADW. In conclusion, other options cannot be totally excluded to declare this short but strong pulse that created the sediment waves.

# 11 CONCLUSIONS

Previous seismic data taken from the eastern slope of the Porcupine Seabight revealed sediment structures in a unit (P1; defined by Van Rooij et al., 2003) beneath the cold-water coral mounds of the Belgica Mound Province. Dating clarified that this unit and thus also the sedimentary features are at least of early-middle Miocene age (Ferdelman et al., 2006a; Louwye et al., 2008). Van Rooij et al. (2003) suggested that these sedimentary features could have something to do with the settlement of some of the CWC mounds. With new data acquired of this specific area during the DynaMOD project, better understanding of these sedimentary bedforms could be realised. Within the framework of this dissertation, there was aimed to document the seismic facies, geometry and morphology to obtain information about their formation processes. In that way the relation between the sedimentary bedforms and the CWC mounds was assessed and information about the local palaeoceanography was obtained. Two different sediment wave fields were recognized and were compared based on spatial and temporal changes. An attempt was made to discover information or clues to the palaeoceanography and global changes that induced the formation of those sediment waves. However, this was not easy to obtain due to the lack of information on Miocene oceanography.

A first set of sediment waves were found to be located in the northeastern part of the survey area within sU3.2. These sediment waves are prograding sigmoidal to complex features that show internal downlapping facies. They were formed on a slope of about 0.2°. Both internal waves as contour currents have been found to be likely formation processes for these sediment waves. Nevertheless, the formation by contour currents showed a better agreement with the characteristics. Their crests are aligned slightly diagonally to the slope and thus also to the flow direction in the case of the presence contour current. The internal downlapping facies and sigmoidal to complex architecture could be formed as an elongate drift. The progradational trend could then be explained by an upslope movement of the flow. The second set of sediment waves, located in the south-western part of the research area, was very different to the first. They show a very chaotic and random lateral migration. They also reveal a hummocky architecture. Mainly because of this chaotic feature, several formation processes could be excluded. Except for internal wave dynamics, these may show a hummocky character according to Pomar et al. (2012).

However, both sediment wave fields occur on the same level, which means that they are spatially related to each other and were deposited around the same time. This suggests a shared hydrodynamic formation system. This leads to think that both internal waves and contour currents influenced both sediment wave fields. This multi-dynamic system would then cause for the existence of an along-slope component together with a bidirectional upslope and downslope component. An initial stage where the influence of internal waves was more prominent, followed by a change to a more contour current controlled environment was used as a formation model. The change in wave dynamics may then explain the two very different sediment wave fields. There is evidence of sea-level changes in the Miocene (Quaijtaal et al., 2014), which could explain the change in wave dynamics.

For the existence of internal waves and contour currents, specific oceanographic criteria need to be fulfilled. Contour currents require a deep-water flow through the Porcupine Seabight to establish drift sedimentation. Internal waves on the other hand, need an interface between two water-masses where a high contrast in density or temperature exists. The presence of the latter is more difficult to interpret due to the sparse

knowledge on the Miocene palaeoceanography. Nonetheless, this study might have evidence for the presence of these criteria, but further research is needed to elaborate on that. Better 3D insight, in both sediment wave fields and especially SW2, would already be one thing that could clarify the formation of the sediment waves. Deeper penetration would also be an asset in future data acquirement, but this would result in a loss of resolution which would be disadvantageous in this case.

Further research is a necessity to discover the true local palaeoceanography, not only by studying the sediment waves that were discussed in this dissertation but also to broaden the general knowledge about the different wave dynamic systems and their definitive criteria. A denser seismic grid or even 3D seismic acquisition would be a strong benefit in studying the sediment waves in this area. Additionally, coring through the sediment wave fields would be beneficial to discover the lithology but especially an asset to the age constraints that could elaborate on the duration of high-energy deposition. Coring would also give insight on the palaeoecology, which not only helps dating but may also elucidate on the water-masses that contributed to the formation of the sediment waves. Further research on the dynamic systems and their diagnostic criteria is also a necessity. In this way it might be possible to typify the sediment waves better without knowledge about their depositional environment. Especially further research on depositions caused by internal waves is essential, because their knowledge is rather sparse. A classifying system, as those that exist with contour currents (Fig. 2D), could be beneficial and would in that way help the identification of the diagnostic criteria. Future research on palaeo-sediment waves around the world, like the research presented here, would be very interesting to learn about their local palaeoceanography. These could eventually be compared to other studies to obtain insight on the global palaeoceanography.

# 12 BIBLIOGRAPHY


Baldwin, K.E., Mountain, G.S., Rosenthal, Y., 2017. Sediment waves in the Caroline Basin suggest evidence for Miocene shifts in bottom water flow in the western equatorial Pacific. Marine Geology 393, 194–202.

Bartoli, G., Samthein, M., Weinel, M., Erlenkeuser, H., Garbe-Schoneberg, D., Lea, D.W., 2005. Final closure of Panama and the onset of Northern Hemisphere glaciation. Earth and Planetary Science Letters 237, 33–44.

Belde, J., Reuning, L., Back, S., 2017. Bottom currents and sediment waves on a shallow carbonate shelf, Northern Carnarvon Basin, Australia. Continental Shelf Research 138, 142–153.

Berthois, L., Brenot, R., 1966. Existence d'une flexure continentale parcourue par un réseau hydrographique, au Sud-Ouest de l'Irlande. Comptes Rendus de l'Académie des Sciences Paris Sér IIa 263, 1297–1299.

Beyer, A., Schenke, H.W., Klenke, M., Niederjasper, F., 2003. High resolution bathymetry of the eastern slope of the Porcupine Seabight. Marine Geology 198, 27–54.

Beyer, A., 2006. Seafloor analysis based on multibeam bathymetry and backscatter data. Ber. Polarforsch. Meeresforsch 540.

Bickert, T., Haug, G.H., Tiedemann, R., 2004. Late Neogene benthic stable isotope record of Ocean Drilling Program Site 999: Implications for Caribbean paleoceanography, organic carbon burial, and the Messinian Salinity Crisis. Palaeogeography, Palaeoclimatology, Palaeoecology 19, PAI 023.

Billups, K., 2002. Late Miocene through early Pliocene deep water circulation and climate change viewed from the sub-Antarctic South Atlantic. Palaeogeography, Palaeoclimatology, Palaeoecology 185, 287–307.

Bogucki, D.J., Redekopp, L.G., 1999. A mechanism for sediment resuspension by internal solitary waves. Geophysical Research Letters 26, 1317–1320.

Böhme, M., 2003. The Miocene Climatic Optimum: evidence from ectothermic vertebrates of Central Europe. Palaeogeography, Palaeoclimatology, Palaeoecology 195, 389–401.

Butzin, M., Lohmann, I.G., Bickertl, T., 2011. Miocene ocean circulation inferred from marine carbon cycle modeling combined with benthic isotope records. Paleoceanography 26, 1–19.

Cartigny, M.J.B., Postma, G., van den Berg, J.H., Mastbergen, D.R., 2011. A comparative study of sediment waves and cyclic steps based on geometries, internal structures and numerical modeling. Marine Geology 280, 40–56.

Catuneanu, O., 2002. Sequence stratigraphy of clastic systems: concepts, merits, and pitfalls. Journal of African Earth Sciences 35, 1–43.

Cheng, C.H., Soetaert, K., Borsje, B.W., 2020. Sediment Characteristics over Asymmetrical Tidal Sand Waves in the Dutch North Sea. Journal of Marine Science and Engineering 8, 409.

Coates, A.G., Aubry, M.-P., Berggren, W.A., Collins, L.S., Kunk, M., 2003. Early Neogene history of the Central American arc from Bocas del Toro, western Panama. Geological Society of America Bulletin 115, 271–287.

Cohen, K.M., Harper, D.A.T., Gibbard, P.L., Fan, J.-X., 2013, updated. Internaltional Chronostratigraphic Chart. Episodes 36, 199–204.

Croker, P.F., Shannon, P.M., 1987. The evolution and hydrocarbon prospectivity of the Porcupine Basin, offshore Ireland, in: Brooks, J., Glennie, K. (Eds.), Petroleum Geology of North West Europe. Graham & Trotman, London, pp. 633–642.

Cullen, J., Ivanov, R., 2020. On the intermediate long wave propagation for internal waves in the presence of currents. European Journal of Mechanics, B/Fluids 84, 325–333.

de Graçiansky, P.C., Poag, C.W., Cunningham, R., Loubere, P., Masson, D.G., Mazzullo, J.M., Montadert, L., Müller, C., Otsuka, K., Reynolds, L.A., Singal, J., Snyder, S.W., Townsend, H.A., Vaos, S.P., Waples, D., 1985. The Goban Spur transect: Geologic evolution of a sediment-starved passive continental margin. Geological Society of America Bulletin 96, 58–76.

De Mol, B., Van Rensbergen, P., Pillen, S., Van Herreweghe, K., Van Rooij, D., McDonnell, A., Huvenne, V., Ivanov, M., Swennen, R., Henriet, J.P., 2002. Large deep-water coral banks in the Porcupine

Basin, southwest of Ireland. Marine Geology 188, 193–231.
De Mol, B., Kozachenko, M., Wheeler, A.J., Alvares, H., Henriet, J.-P., Roy, K., 2007. Thérèse Mound: a case study of coral bank development in the Belgica Mound Province, Porcupine Seabight. International Journal of Earth Sciences 96, 103–120.
DECO Geophysical software company, 1992. RadExPro.
Dickson, R.R., McCave, I.N., 1986. Nepheloid layers on the continental slope west of Porcupine Bank. Deep Sea Research Part A, Oceanographic Research Papers 33, 791–818.
Dorschel, B., Hebbeln, D., Ruggeberg, A., Dullo, W.C., Freiwald, A., 2005. Growth and erosion of a cold-water coral covered carbonate mound in the Northeast Atlantic during the Late Pleistocene and Holocene. Earth and Planetary Science Letters 233, 33–44.
Dorschel, B., Hebbeln, D., Foubert, A., White, M., Wheeler, A.J., 2007. Hydrodynamics and cold-water coral facies distribution related to recent sedimentary processes at Galway Mound west of Ireland. Marine Geology 244, 184–195.
Dorschel, B., Wheeler, A.J., Huvenne, V.A.I., de Haas, H., 2009. Cold-water coral mounds in an erosive environmental setting: TOBI side-scan sonar data and ROV video footage from the northwest Porcupine Bank, NE Atlantic. Marine Geology 264, 218–229.
Dorschel, B., Wheeler, A.J., Monteys, X., Verbruggen, K., 2010. Atlas of the Deep-Water Seabed: Ireland. Springer Netherlands, Dordrecht.
Dullo, W.C., Flögel, S., Rüggeberg, A., 2008. Cold-water coral growth in relation to the hydrography of the Celtic and Nordic European continental margin. Marine Ecology Progress Series 371, 165–176.
Duque-Caro, H., 1990. Neogene stratigraphy, paleoceanography and paleobiogeography in northwest South America and the evolution of the Panama Seaway. Palaeogeography, Palaeoclimatology, Palaeoecology 77, 203–234.
Egger, L.M., Bahr, A., Friedrich, O., Wilson, P.A., Norris, R.D., van Peer, T.E., Lippert, P.C., Liebrand, D., Pross, J., 2018. Sea-level and surface-water change in the western North Atlantic across the Oligocene–Miocene Transition: A palynological perspective from IODP Site U1406 (Newfoundland margin). Marine Micropaleontology 139, 57–71.
Eisele, M., Hebbeln, D., Wienberg, C., 2008. Growth history of a cold-water coral covered carbonate mound - Galway Mound, Porcupine Seabight, NE-Atlantic. Marine Geology 253, 160–169.
Faugères, J.-C., Mulder, T., 2011. Contour Currents and Contourite Drifts, in: HüNeke, H., Mulder, T. (Eds.), Deep-Sea Sediments. Elsevier, pp. 149–214.
Faugères, J.C., Gonthier, E., Mulder, T., Kenyon, N., Cirac, P., Griboulard, R., Berné, S., Lesuavé, R., 2002a. Multi-process generated sediment waves on the Landes Plateau (Bay of Biscay, North Atlantic). Marine Geology 182, 279–302. https://doi.org/10.1016/S0025-3227(01)00242-0
Faugères, J.C., Gonthier, E., Mulder, T., Kenyon, N., Cirac, P., Griboulard, R., Berné, S., Lesuavé, R., 2002b. Multi-process generated sediment waves on the Landes Plateau (Bay of Biscay, North Atlantic). Marine Geology 182, 279–302.
Ferdelman, T.G., Kano, A., Williams, T., Henriet, J.-P., Expedition 307 Scientists, 2006a. Expedition 307 summary. Proceedings of the IODP, 307 307, 34.
Ferdelman, T.G., Kano, A., Williams, T., Henriet, J.-P., Scientists, E. 307, 2006b. Site U1318, in: Proceedings of the IODP, 307. Integrated Ocean Drilling Program, p. 57.
Ferdelman, T.G., Kano, A., Williams, T., Henriet, J.-P., Expedition 307 Scientists, 2006c. Site U1317. Proceedings of the IODP, 307 307, 65.
Ferdelman, T.G., Kano, A., Williams, T., Henriet, J.-P., Expedition 307 Scientists, 2006d. Site U1316. Proceedings of the IODP, 307 307.
Flower, B.P., Kennett, J.P., 1994. The Middle Miocene climatic transition: East Antarctic ice sheet development, deep ocean circulation and global carbon cycling. Palaeogeography, Palaeoclimatology, Palaeoecology 108, 537–555.
Foubert, A., Beck, T., Wheeler, A.J., Opderbecke, J., Grehan, A., Klages, M., Thiede, J., Henriet, J.-P., 2005. New view of the Belgica Mounds, Porcupine, NE Atlantic: preliminary results from the Polarstern ARK-XIX/3a ROV cruise, in: Freiwald, A., Roberts, J.M. (Eds.), Cold-Water Corals and Ecosystems. Springer, Berlin, pp. 403–415.
Gadallah, M.R., Fisher, R., 2009. Exploration Geophysics. Springer Berlin Heidelberg, Berlin, Heidelberg.

Gong, C., Wang, Y., Peng, X., Li, W., Qiu, Y., Xu, S., 2012. Sediment waves on the South China Sea Slope off southwestern Taiwan: Implications for the intrusion of the Northern Pacific Deep Water into the South China Sea. Marine and Petroleum Geology 32, 95–109.
Gonthier, E., Faugères, J.C., Gervais, A., Ercilla, G., Alonso, B., Baraza, J., 2002. Quaternary sedimentation and origin of the Orinoco sediment-wave field on the Demerara continental rise (NE margin of South America). Marine Geology 192, 189–214.
Haug, G.H., Tiedemann, R., 1998. Effect of the formation of the Isthmus of Panama on Atlantic Ocean thermohaline circulation. Nature 393, 673–676.
He, Y., Gao, Z., Luo, J., Luo, S., Liu, X., 2008. Characteristics of internal-wave and internal-tide deposits and their hydrocarbon potential. Petroleum Science 5, 37–44.
Hebbeln, D., Van Rooij, D., Wienberg, C., 2016. Good neighbours shaped by vigorous currents: Cold-water coral mounds and contourites in the North Atlantic. Marine Geology 378, 171–185.
Henriet, J.-P., De Mol, B., Pillen, S., Vanneste, M., Van Rooij, D., Versteeg, W., Croker, P.F., Shannon, P.M., Unnithan, V., Bouriak, S., Chachkine, P., The Porcupine-Belgica 97 Shipboard party, 1998. Gas hydrate crystals may help build reefs. Nature 391, 648–649.
Hernández-Molina, F.J., Llave, E., Preu, B., Ercilla, G., Fontan, A., Bruno, M., Serra, N., Gomiz, J.J., Brackenridge, R.E., Sierro, F.J., Stow, D.A.V., García, M., Juan, C., Sandoval, N., Arnaiz, A., 2014. Contourite processes associated with the mediterranean outflow water after its exit from the Strait of Gibraltar: global and conceptual implications. Geology 42, 227–230.
Hotchkiss, F.S., Wunsch, C., 1982. Internal waves in Hudson Canyon with possible geological implications. Deep Sea Research Part A, Oceanographic Research Papers 29, 415–442.
Hovland, M., Thomson, E., 1997. Cold-water corals—are they hydrocarbon seep related? Marine Geology 137, 159–164.
Huvenne, V.A.I., Blondel, P., Henriet, J.P., 2002. Textural analyses of sidescan sonar imagery from two mound provinces in the Porcupine Seabight. Marine Geology 189, 323–341.
Huvenne, V.A.I., De Mol, B., Henriet, J.P., 2003. A 3D seismic study of the morphology and spatial distribution of buried coral banks in the Porcupine Basin, SW of Ireland. Marine Geology 198, 5–25.
Huvenne, V.A.I., Beyer, A., de Haas, H., Dekindt, K., Henriet, J.-P., Kozachenko, M., Olu-Le Roy, K., Wheeler, A.J., 2005. The seabed appearance of different coral bank provinces in the Porcupine Seabight, NE Atlantic: results from sidescan sonar and ROV seabed mapping, in: Cold Water Corals and Ecosystems. Springer, Berlin, pp. 535–569.
Huvenne, V.A.I., Bailey, W.R., Shannon, P.M., Naeth, J., di Primio, R., Henriet, J.-P., Horsfield, B., de Haas, H., Wheeler, A.J., Roy, K., 2007. The Magellan mound province in the Porcupine Basin. International Journal of Earth Sciences 96, 85–101.
Huvenne, V.A.I., Van Rooij, D., De Mol, B., Thierens, M., O'Donnell, R., Foubert, A., 2009. Sediment dynamics and palaeo-environmental context at key stages in the Challenger cold-water coral mound formation: Clues from sediment deposits at the mound base. Deep-Sea Research Part I: Oceanographic Research Papers 56, 2263–2280.
IHS Markit, 2019. Kingdom.
Kano, A., Ferdelman, T.G., Williams, T., Henriet, J.P., Ishikawa, T., Kawagoe, N., Takashima, C., Kakizaki, Y., Abe, K., Sakai, S., Browing, E.L., Li, X., Andres, M.S., Bjerager, M., Cragg, B.A., De Mol, B., Dorschel, B., Foubert, A., Frank, T.D., Fuwa, Y., Gaillot, P., Gharib, J.J., Gregg, J.M., Huvenne, V.A.I., Léonide, P., Mangelsdorf, K., Monteys, X., Novosel, I., O'Donnell, R., Rüggeberg, A., Samarkin, V., Sasaki, K., Spivack, A.J., Tanaka, A., Titschack, J., van Rooij, D., Wheeler, A., 2007. Age constraints on the origin and growth history of a deep-water coral mound in the northeast Atlantic drilled during Integrated Ocean Drilling Program Expedition 307. Geology 35, 1051–1054.
Karl, H.A., Cacchione, D.A., Carlson, P.R., 1986. Internal-wave currents as a mechanism to account for large sand waves in Navarinsky Canyon head, Bering Sea. Journal of sedimentary petrology 56, 706–714.
Kenyon, N.H., Belderson, R.H., Stride, A.H., 1978. Channels, canyons and slump folds between South-West Ireland and Spain. Oceanologica Acta 1, 369–380.
Le Danois, E., 1948. Les profondeurs de la mer. Payot, Paris.
Lee, H.J., Syvitski, J.P.M., Parker, G., Orange, D., Locat, J., Hutton, E.W.H., Imran, J., 2002. Distinguishing

sediment waves from slope failure deposits: Field examples, including the ‘humboldt slide’, and modelling results. Marine Geology 192, 79–104.
Li, J., Li, W., Alves, T.M., Rebesco, M., Zhan, W., Sun, J., Mitchell, N.C., Wu, S., 2019. Different origins of seafloor undulations in a submarine canyon system, northern South China Sea, based on their seismic character and relative location. Marine Geology 413, 99–111.
Liu, S., Hernández-Molina, F.J., Ercilla, G., Van Rooij, D., 2020. Sedimentary evolution of the Le Danois contourite drift systems (southern Bay of Biscay, NE Atlantic): A reconstruction of the Atlantic Mediterranean Water circulation since the Pliocene. Marine Geology 427, 106217. https://doi.org/10.1016/j.margeo.2020.106217
Locarnini, R.A., Mishonov, A.V., Antonov, J.I., Boyer, T.P., Garcia, H.E., Baranova, O.K., Zweng, M.M., Paver, C.R., Reagan, J.R., Johnson, D.R., Hamilton, M., Seidov, D., Levitus, S., 2013. World ocean Atlas 2013. In: Levitus, S., Mishonov, A. (Eds.), NOAA Atlas NESDIS 74. National Oceanographic Data Center, Ocean Climate Laboratory United States, National Environmental Sat- ellite Data Information Service.
Louwye, S., Foubert, A., Mertens, K., Van Rooij, D., 2008. Integrated stratigraphy and palaeoecology of the Lower and Middle Miocene of the Porcupine Basin. Geological Magazine 145, 321–344.
Ma, X.C., Yan, J., Hou, Y.J., Lin, F.L., Zheng, X.F., 2016. Footprints of obliquely incident internal solitary waves and internal tides near the shelf break in the northern South China Sea. Journal of Geophysical Research: Oceans 121, 8706–8719.
Masson, D.G., Howe, J.A., Stoker, M.S., 2002. Bottom-current sediment waves, sediment drifts and contourites in the northern Rockall Trough. Marine Geology 192, 215–237.
McDonnell, A., Shannon, P. M., 2001. Comparative tertiary stratigraphic evolution of the Porcupine and Rockall basins, in: Shannon, Patrick M., Haughton, P.D.W., Corcoran, D.V. (Eds.), The Petroleum Exploration of Ireland’s Offshore Basins. Geological Society, London, pp. 323–344.
McKenzie, D.P., 1978. Some remarks on the development of sedimentary basins. Earth and Planetary Science Letters 66, 182–202.
Meulenkamp, J.E., Sissingh, W., 2003. Tertiary palaeogeography and tectonostratigraphic evolution of the Northern and Southern PeriTethys platforms and the intermediate domains of the African Eurasian convergent plate boundary zone. Palaeogeography, Palaeoclimatology, Palaeoecology 196, 209–228.
Mienis, F., van Weering, T.C.E., de Haas, H., de Stigter, H.C., Huvenne, V.A.I., Wheeler, A.J., 2006. Carbonate mound development at the SW Rockall Through margin based on high resolution TOBI and seismic recording. Marine Geology 233, 1–19.
Miller, K.G., Wright, J.D., Fairbanks, R.G., 1991. Unlocking the Ice House: Oligocene-Miocene oxygen isotopes, eustasy, and margin erosion. Journal of Geophysical Research: Solid Earth 96, 6829–6848.
Millot, C., 2014. Heterogeneities of in- and out-flows in the Mediterranean Sea. Progress in Oceanography 120, 254–278.
Mitchum, R.M.J., Vail, P.R., Thompson, S.I., 1977a. Seismic stratigraphy and global changes of sea level: part 2, The depositional sequence as a basic unit for stratigraphic analysis. AAPG memoir 26, 53–62.
Mitchum, R.M.J., Vail, P.R., Sangree, J.B., 1977b. Seismic stratigraphy and global changes of sea level: part 6, Stratigraphic interpretation of seismic refl ection patterns in depositional sequences. AAPG memoir 26, 117–133.
Mohn, C., Rengstrof, A., White, M., Duineveld, G., Mienis, F., Soetaert, K., Grehan, A., 2014. Linking benthic hydrodynamics and cold-water coral occurrences: a high- resolution model study at three cold-water coral provinces in the NE Atlantic. Progress in Oceanography 122, 92–104.
Moore, J.G., Shannon, P.M., 1991. Slump structures in the Late Tertiary of the Porcupine Basin, offshore Ireland. Marine and Petroleum Geology 8, 184–197.
Moore, J.G., Shannon, P.M., 1995. The Cretaceous succession in the Porcupine Basin, offshore Ireland: faxies distribution and hydrocarbon potential, in: Croker, P.F., Shannon, P.M. (Eds.), The Petroleum Geology of Ireland’s offshore basins. Geological Society Special Publication 93, 345–370.
Naeth, J., di Primio, R., Horsfield, B., Schaefer, R.G., Shannon, P.M., Bailey, W.R., Henriet, J.-P., 2005. Hydro-carbon seepage and carbonate mound formation: a basin modelling study from the Porcupine basin (off- shore Ireland). journal of petroleum geology 28, 147–166.

Nanda, N.C., 2016. Seismic Data Interpretation and Evaluation for Hydrocarbon Exploration and Production, Seismic Data Interpretation and Evaluation for Hydrocarbon Exploration and Production.
Naylor, D., Shannon, P.M., 1982. Geology of Offshore Ireland and West Britain. Graham & Trotman Limited, Sterling House, London.
Naylor, D., Anstey, N.A., 1987. A reflection seismic study of the Porcupine basin, offshore west Ireland. Irish Journal of Earth Sciences 8, 187–210.
Normark, W.R., Hess, G.R., Stow, D.A.V., Bowen, A.J., 1980. Sediment waves on the monterey fan levee: A preliminary physical interpretation. Marine Geology 37, 1–18.
Onajite, E., 2014. Understanding Seismic Interpretation Methodology, in: Seismic Data Analysis Techniques in Hydrocarbon Exploration. Elsevier, pp. 177–211.
Øvrebø, L.K., Haughton, P.D.W., Shannon, P.M., 2006. A record of fluctuating bottom currents on the slopes west of the Porcupine Bank, offshore Ireland - Implications for Late Quaternary climate forcing. Marine Geology 225, 279–309.
Perez-Hernandez, S., Comas, M.C., Escutia, C., 2014. Morphology of turbidite systems within an active continental margin (the Palomares Margin, western Mediterranean). Geomorphology 219, 10–26.
Pingree, R.D., Le Cann, B., 1989. Celtic and Armorican slope and shelf residual currents. Progress in Oceanography 23, 303–338.
Pingree, R.D., Le Cann, B., 1990. Structure, strength and seasonality of the slope currents in the Bay of Biscay region. Journal of Marine Biological Association of the United Kingdom 70, 857–885.
Pingree, R.D., 1993. Flow of surface waters to the west of the British Isles and in the Bay of Biscay. Deep-Sea Research Part II 40, 369–388.
Pomar, L., Morsilli, M., Hallock, P., Bádenas, B., 2012. Internal waves, an under-explored source of turbulence events in the sedimentary record. Earth-Science Reviews 111, 56–81.
Poore, H.R., Samworth, R., White, N.J., Jones, S.M., McCave, I.N., 2006. Neogene overflow of Northern Component Water at the Greenland-Scotland Ridge. Geochemistry, Geophysics, Geosystems 7, Q06010.
Pope, E.L., Jutzeler, M., Cartigny, M.J.B., Shreeve, J., Talling, P.J., Wright, I.C., Wysoczanski, R.J., 2018. Origin of spectacular fields of submarine sediment waves around volcanic islands. Earth and Planetary Science Letters 493, 12–24.
Quaijtaal, W., Donders, T.H., Persico, D., Louwye, S., 2014. Characterising the middle Miocene Mi-events in the Eastern North Atlantic realm: A first high-resolution marine palynological record from the Porcupine Basin. Palaeogeography, Palaeoclimatology, Palaeoecology 399, 140–159.
Rebesco, M., Stow, D.A.V., 2001. Seismic expression of contourites and related deposits: A preface. Marine Geophysical Researches 22, 303–308.
Rebesco, M., Hernández-Molina, F.J., Van Rooij, D., Wåhlin, A., 2014. Contourites and associated sediments controlled by deep-water circulation processes: State-of-the-art and future considerations. Marine Geology 352, 111–154.
Reeder, D.B., Ma, B.B., Yang, Y.J., 2011. Very large subaqueous sand dunes on the upper continental slope in the South China Sea generated by episodic, shoaling deep-water internal solitary waves. Marine Geology 279, 12–18.
Reynolds, J.M., 2011. An introduction to applied and environmental geophysics, second. ed. John Wiley & Sons, Ltd. (Wiley-Blackwell).
Ribbe, J., Holloway, P.E., 2001. A model of suspended sediment transport by internal tides. Continental Shelf Research 21, 395–422.
Ribó, M., Puig, P., Muñoz, A., Lo Iacono, C., Masqué, P., Palanques, A., Acosta, J., Guillén, J., Gómez Ballesteros, M., 2016a. Morphobathymetric analysis of the large fine-grained sediment waves over the Gulf of Valencia continental slope (NW Mediterranean). Geomorphology 253, 22–37.
Ribó, M., Puig, P., Urgeles, R., Van Rooij, D., Muñoz, A., 2016b. Spatio-temporal evolution of sediment waves developed on the Gulf of Valencia margin (NW Mediterranean) during the Plio-Quaternary. Marine Geology 378, 276–291.
Ribó, M., Durán, R., Puig, P., Van Rooij, D., Guillén, J., Masqué, P., 2018. Large sediment waves over the Gulf of Roses upper continental slope (NW Mediterranean). Marine Geology 399, 84–96.
Rice, A.L., Thurston, M.H., New, A.L., 1990. Dense aggregations of a hexactinellid sponge, Pheronema

carpenteri, in the Porcupine Seabight (notheast Atlantic Ocean), and possible causes. Progress in Oceanography 24, 179–196.
Rice, A.L., Billet, D.S.M., Thurston, M.H., Lampitt, R.S., 1991. The Institute of Oceanographic Sciences Biology programme in the Porcupine Seabight: background and general introduction. Journal of Marine Biological Association of the United Kingdom 71, 281–310.
Roberts, J.M., Wheeler, A.J., Freiwald, A., 2006. Reefs of the deep: The biology and geology of cold-water coral ecosystems. Science 312, 543–547.
Rögl, F., 1991. Mediterranean and Paratethys. Facts and hypotheses of an Oligocene to Miocene Paleogeography (short overview). Geological Carpathica 20, 339–349.
Roveri, M., 2002. Sediment drifts of the Corsica Channel, northern Tyrrhenian Sea. Geological Society Memoir 22, 191–208.
Rowan, M.G., 2020. Salt- and shale-detached gravity-driven failure of continental margins, in: Scarselli, N., Adam, J., Chiarella, D., Roberts, D.G., Bally, A.W. (Eds.), Regional Geology and Tectonics: Principles of Geologic Analysis. Elsevier, pp. 205–234.
Scotese, C.R., n.d. Paleomap Earth History: Middle Miocene [WWW Document]. URL http://www.scotese.com/miocene.htm (accessed 5.6.21).
Serra, N., Ambar, I., Boutov, D., 2010. Surface expression of Mediterranean Water dipoles and their contributions to the shelf/slope - open ocean exchange. Ocean Science 6, 191–209.
Shannon, P.M., 1991. The development of Irish offshore sedimentary basins. Journal of the Geological Society of London 148, 181–189.
Shannon, P.M., McDonnell, A., Bailey, W.R., 2007. The evolution of the porcupine and rockall basins, offshore Ireland: The geological template for carbonate mound development. International Journal of Earth Sciences 96, 21–35.
Sherwin, T.J., Taylor, N.K., 1987. Modelling internal tide processes around the North-west European shelf edge. Advances in Underwater Technology, Ocean Science and Offshore Engineering 12, 263–278.
Steph, S., Tiedemann, R., Prange, M., Groeneveld, J., Niimberg, D., Reuning, L., Schulz, M., Haug, G.H., 2006. Changes in Caribbean surface hydrography during the Pliocene shoaling of the Central American Seaway. Paleoceanography 21, PA4221.
Stoker, M.S., 1997. Mid-to late Cenozoic sedimentation on the continental margin off NW Britain. Journal of the Geological Society, London 154, 509–515.
Stoker, M.S., van Weering, T.C.E., Svaerdborg, T., 2001. A mid- to late Cenozoic tectonostratigraphic framework for the Rockall Trough, in: Shannon P.M., Houghton, P, Corcoran, D. (Eds.), Petroleum exploration of Ireland's offshore basins. Geological Society London Special Publication 188, 441–438.
Super, J.R., Thomas, E., Pagani, M., Huber, M., O'Brien, C., Hull, P.M., 2018. North Atlantic temperature and pCO2 coupling in the early-middle Miocene. Geology 46, 519–522.
Symons, W.O., Sumner, E.J., Talling, P.J., Cartigny, M.J.B., Clare, M.A., 2016. Large-scale sediment waves and scours on the modern seafloor and their implications for the prevalence of supercritical flows. Marine Geology 371, 130–148.
Thomas, D.J., Via, R.K., 2007. Neogene evolution of Atlantic thermohaline circulation: Perspective from Walvis Ridge, southeastern Atlantic Ocean. Paleoceanography PA22, 12.
Van Aken, H.M., Becker, G., 1996. Hydrography and through-flow in the north-eastern North Atlantic Ocean: The NANSEN project. Progress in Oceanography 38, 297–346.
Van Aken, H.M., 2000. The hydrography of the mid-latitude Northeast Atlantic Ocean II: The intermediate water masses, Deep-Sea Research Part I: Oceanographic Research Papers.
Van Rooij, D., De Mol, B., Huvenne, V., Ivanov, M., Henriet, J.P., 2003. Seismic evidence of current-controlled sedimentation in the Belgica mound province, upper Porcupine slope, southwest of Ireland. Marine Geology 195, 31–53.
Van Rooij, D., Blamart, D., Kozachenko, M., Henriet, J.P., 2007. Small mounded contourite drifts associated with deep-water coral banks, Porcupine Seabight, NE Atlantic Ocean. Geological Society Special Publication 276, 225–244.
Van Rooij, D., Huvenne, V.A.I., Blamart, D., Henriet, J.-P., Wheeler, A., de Haas, H., 2009. The Enya mounds: a lost mound-drift competition. International Journal of Earth Sciences 98, 849–863.
Van Rooij, D., Mestdagh, T., 2019. RV Belgica cruise 2019/16 – cruise report. Royal Belgian Institute of

Natural Sciences (BELSPO).
van Weering, T.C.E., de Haas, H., de Stigter, H.C., Lykke-Andersen, H., Kouvaev, I., 2003. Structure and development of giant carbonate mounds at the SW and SE Rockall Trough margins, NE Atlantic Ocean. Marine Geology 198, 67–81.
Wei, W., Peleo-Alampay, A., 1997. Onset of North Atlantic Deep Water 11 .5 million years ago triggered by climate cooling. Proceedings international Geological Congress 30th 13, 57–64.
Wheeler, A.J., Kozachenko, M., Beyer, A., Foubert, A., Huvenne, V.A.I., Klages, M., Masson, D.G., Olu-Le Roy, K., Thiede, J., 2005. Sedimentary processes and carbonate mounds in the Belgica Mound province, Porcupine Seabight, NE Atlantic, in: Freiwald, A., Roberts, J.M. (Eds.), Cold-Water Corals and Ecosystems. Springer Berlin Heidelberg, Berlin, Heidelberg, pp. 571–603.
Wheeler, A.J., Beyer, A., de Haas, H., Huvenne, V.A.I., Kozachenko, M., Olu-Le Roy, K., Opderbecke, J., 2007. Morphology and environment of cold-water coral carbonate mounds on the NW European margin. International Journal of Earth Sciences 96, 37–56.
White, M., 2007. Benthic dynamics at the carbonate mound regions of the Porcupine Sea Bight continental margin. International Journal of Earth Sciences 96, 1–9.
White, M., Dorschel, B., 2010. The importance of the permanent thermocline to the cold water coral carbonate mound distribution in the NE Atlantic. Earth and Planetary letters 296, 395–402.
Wienberg, C., Beuck, L., Heidkamp, S., Hebbeln, D., Freiwald, A., Pfannkuche, O., Monteys, X., 2008. Franken Mound: facies and biocoenoses on a newly-discovered “carbonate mound” on the western Rockall Bank, NE Atlantic. Facies 54, 1–24.
Wienberg, C., Titschack, J., 2017. Framework-Forming Scleractinian Cold-Water Corals Through Space and Time: A Late Quaternary North Atlantic Perspective, in: Rossi S., Bramani L., Gori A., Orejas C. (Eds) Marine Animal Forests. pp. 699–732.
Wienberg, C., Titschack, J., Frank, N., De Pol-Holz, R., Fietzke, J., Eisele, M., Kremer, A., Hebbeln, D., 2020. Deglacial upslope shift of NE Atlantic intermediate waters controlled slope erosion and cold-water coral mound formation (Porcupine Seabight, Irish margin). Quaternary Science Reviews 237, 106310.
Wright, J.D., Miller, K.G., 1996. Control of North Atlantic Deep Water circulation by the Greenland-Scotland Ridge. Paleoceanography 11, 157–169.
Wynn, R.B., Stow, D.A.V., 2002. Classification and characterisation of deep-water sediment waves. Marine Geology 192, 7–22.
Yuan, C., Wang, Z., Chen, X., 2020. The derivation of an isotropic model for internal waves and its application to wave generation. Ocean Modelling 153, 101663.
Zachos, J., Pagani, M., Sloan, L., Thomas, E., Billups, K., 2001. Trends, rhythms, and aberrations in global climate 65 Ma to present. Science 292, 686–693.
Zhenzhong, G., Youbin, H., Xiangdong, L., Taizhong, D., Yuan, W., Min, L., 2013. Review of research in internal-wave and internal-tide deposits of China. Journal of Palaeogeography 2, 56–65.
Ziegler, P.A., 1982. Geological Atlas of Western and Central Europe. Elsevier.
Zweng, M.M., Reagan, J.R., Antonov, J.I., Locarnini, R.A., Mishonov, A.V., Boyer, T.P., Garcia, H.E., Baranova, O.K., Johnson, D.R., Seidov, D., Biddle, M.M., Levitus, S., 2013. World ocean Atlas 2013. In: Levitus, S., Mishonov, A. (Eds.), NOAA Atlas NESDIS 74. National Oceanographic Data Center, Ocean Climate Laboratory United States, National Environmental Satellite Data Infor- mation Service 2, 39.